Local translation of actin-binding proteins in the healthy and diseased central nervous system

Von der Fakultät für Lebenswissenschaften

der Technischen Universität Carolo-Wilhelmina zu Braunschweig

zur Erlangung des Grades eines

Doktors der Naturwissenschaften

(Dr.rer.nat.)

genehmigte

D i s s e r t a t i o n

von Jonas Feuge
aus Braunschweig

1. Referent: Professor Dr. Martin Korte
2. Referent: Professor Dr. Reinhard Köster
3. Referent: Professor Dr. Marco Rust
eingereicht am: 12.08.2019
mündliche Prüfung (Disputation) am: 20.12.2019

Druckjahr 2020

Vorveröffentlichungen der Dissertation

Teilergebnisse aus dieser Arbeit wurden mit Genehmigung der Fakultät für Lebenswissenschaften, vertreten durch den Mentor der Arbeit, in folgenden Beiträgen vorab veröffentlicht:

Publikationen

Feuge J.*, Scharkowski F.*, Michaelsen-Preusse K., Korte M. (2019) FMRP mediates spine plasticity by regulating the localization and local translation of cofilin1 mRNA. *Cerebral Cortex* bhz059, https://doi.org/10.1093/cercor/bhz059 (*equal contribution)

Michaelsen-Preusse K., **Feuge J.**, Korte M. (2018) Imbalance of synaptic actin dynamics as a key to fragile X syndrome? *The Journal of Physiology 596(14):2773-2782*

Michaelsen-Preusse K., Zessin S., Grigoryan G., Scharkowski F., **Feuge J.**, Remus A., Korte M. (2016) Neuronal profilins in health and disease: Relevance for spine plasticity and Fragile X syndrome. *Proceedings of the National Acadamy of Science of the United States of America 113(12):3365-3370*

Tagungsbeiträge

Feuge J., Korte M., Michaelsen-Preusse K.: mRNA dynamics and local translation of actin-binding proteins in the CNS *1st Brainswick Meeting*, *Braunschweig* (2016)

Posterbeiträge

Feuge J., Scharkowski F., Korte M., Michaelsen-Preusse K.: Activity-dependent dysregulation of cofilin in the Fragile X Syndrome *13th Meeting of the German Neuroscience Society*, Göttingen (2019)

Feuge J., Scharkowski F., Korte M., Michaelsen-Preusse K.: Activity-dependent dysregulation of cofilin in the Fragile X Syndrome *10th FENS Forum of Neuroscience,* Berlin (2018)

Feuge J., Korte M., Michaelsen-Preusse K.: Local translation of actin-binding proteins in the CNS *12th Meeting of the German Neuroscience Society*, Göttingen (2017)

Feuge J., Korte M., Michaelsen-Preusse K.: Local translation of actin-binding proteins in the CNS *2nd Brainswick Symposium,* Braunschweig (2017)

Contents

1 Abstract

Long-lasting modifications of synaptic efficacy of single synapses are believed to represent the cellular correlates of learning and memory formation and depend on the global and local translation of pre-existing mRNAs. These local translation events allow synapses to autonomously and specifically change their structural and functional properties on a rapid time scale, a phenomenon that crucially depends on a fast remodeling of the actin cytoskeleton mediated by actin-binding proteins (ABPs). In the Fragile X Syndrome (FXS), where the Fragile X mental retardation protein 1 (FMRP) as a regulator of mRNA transport and local translation is absent, alterations in synapse structure and function indeed point towards dysregulated actin dynamics. Therefore, this study aimed at analyzing the role of dynamic actin and ABPs as an underlying cause of synapse pathology in FXS.

In experiments involving NMDAR-dependent long-term potentiation (LTP; glycine-mediated) or mGluR-dependent long-term depression (LTD; DHPG-mediated) combined with Fluorescence *in situ* Hybridization, this work provides first evidence that the mRNAs of the ABPs Profilin 1 (Pfn1), Profilin 2a (Pfn2a) and Cofilin 1 (Cof1) are not only localized in dendrites of hippocampal neurons but moreover that ABP mRNA localization is mediated in an activity-dependent manner. In addition, Fluorescence Recovery after Photobleaching of membrane-targeted eGFP fused to the 3'UTR of Cof1 revealed that the local translation of Cof1 is modulated in an activity-dependent manner as well. Intriguingly, this study shows that in the mouse model of FXS (*fmr1* KO), these activity-dependent modulations of ABP mRNAs are absent and in case of NMDAR-dependent LTP, these defects are additionally accompanied by a complete loss of structural plasticity. Most importantly, this structural plasticity defect could be rescued by mimicking Cof1 modulation of WT neurons, thereby directly attributing plasticity deficits in FXS to a dysregulation of ABPs.

In summary, this work shows for the first time that the local translation of ABPs is mediated in an activity-dependent manner, a modulation that appears to be crucial for the proper induction of NMDAR-dependent LTP as well as mGluR-dependent LTD in hippocampal neurons. In addition, this study proposes a causal relationship between dysregulated actin dynamics, derived from alterations in the modulation of local ABP synthesis and local ABP mRNA availability, and synapse pathologies as well as learning deficits in the mouse model of FXS.

2 Zusammenfassung

Neuronale Korrelate von Lern- und Gedächtnisvorgängen beruhen auf Veränderungen an Synapsen, die sich Input-spezifisch verstärken oder abschwächen. Um diese Spezifität zu wahren, müssen Synapsen individuell regulierbar sein. Dies bedingt, dass synaptische Plastizität abhängig ist von einer globalen als auch lokalen Translation von prä-existierenden mRNAs, die es Synapsen ermöglicht schnell und autonom ihre Struktur als auch ihre Funktion anzupassen. Diese Regulationen beruhen auf einer schnellen Umstrukturierung des Aktin-Zytoskeletts durch Aktin-bindende Proteine (ABPs). Im Fragilen X Syndrom (FXS), in dem das Fragile X mental retardation Protein nicht mehr exprimiert wird, welches sowohl den Transport als auch die lokale Translation von mRNAs reguliert, kommt es zu Veränderungen in der Struktur als auch Funktion von Synapsen. Diese Phänotypen deuten auf eine Fehlregulation von synaptischen Aktindynamiken hin, weshalb im Rahmen dieser Arbeit die Rolle von dynamischem Aktin und ABPs als potentielle Ursache für synaptische Phänotypen im FXS untersucht wurde. In Experimenten, in denen die NMDA-Rezeptor abhängige Langzeitpotenzierung (LTP; chemisch induziert mit Glycin) als auch die mGluR-Rezeptor abhängige Langzeitdepression (LTD; DHPG-mediiert) mit Fluoreszenz *in situ* Hybridisierungen kombiniert wurde, konnte diese Arbeit zum allerersten Mal zeigen, dass die mRNAs von den ABPs Profilin 1, Profilin 2a und Cofilin 1 (Cof1) in Dendriten von hippokampalen Neuronen lokalisiert sind und das die Lokalisation von ABP mRNAs aktivitätsabhängig reguliert ist. Zusätzlich konnte über Fluorescence Recovery after Photobleaching von Membran-gebundenem eGFP, welches an die 3' untranslatierte Region von Cof1 fusioniert wurde, die aktivitätsabhängige lokale Translation von Cof1 nachgewiesen werden. Weiterhin konnte diese Studie zeigen, dass diese aktivitätsabhängigen Regulationen im Mausmodell für FXS (*fmr1* KO) nicht stattfinden und dass diese Defekte im Falle von NMDAR-abhängigem LTP von einem Verlust der strukturellen Plastizität von Synapsen begleitet werden. Interessanterweise konnte dieser strukturelle Plastizitätsverlust in *fmr1* KO Neuronen gerettet werden, indem die aktivitätsabhängige Regulation von Cof1, die in Wildtyp Neuronen nachgewiesen werden konnte, nachgeahmt wurde, wodurch Plastizitätsdefekte im FXS direkt der Fehlregulation von ABPs zugeordnet werden konnten.

Zusammenfassend konnte diese Arbeit Belege dafür finden, dass die lokale Translation von ABPs aktivitätsabhängig reguliert ist und das diese Modulationen für die korrekte Induktion von NMDA-Rezeptor abhängigem LTP und mGluR-Rezeptor abhängigem LTD in hippokampalen Neuronen notwendig ist. Des Weiteren konnte ein kausaler Zusammenhang zwischen fehlregulierten Aktindynamiken, resultierend aus einer Dysregulation der Verfügbarkeit als auch der lokalen Translation von ABP mRNAs, und synaptischen Phänotypen sowie Lerndefiziten im Mausmodell des FXS aufgezeigt werden.

3 Introduction

Over the last millions of years, high intelligence and complex brains have evolved multiple times independently within the animal kingdom. Yet, the human ability to learn from experience and to utilize the past in order to plan the future in nearly constant motion exceeds that of all other animals and is the most advantageous attribute in our survival and development as a species.

To store memories, the human brain is permanently converting external stimuli into constructs that can be consolidated and recalled. Simplified, a memory is a group of encoded neuronal connections (an engram; Semon, 1904) which can be reconstructed by the synchronous firing of neurons which were involved in the original experience. Thus, memories must be actively reconstructed from former neuronal traces. In turn, the integration of new information into already existing engrams, by definition, is learning. However, while it is known that these processes involve the interplay of various brain regions and neuronal circuits, the exact localization of memories in the human brain still remains elusive.

3.1 Contribution of the hippocampal formation to memory

Ever since the famous case study from Henry Molaison starting in 1957 who lost the capability to memorize new declarative events after surgical removal of large parts of the hippocampus (Scoville and Milner, 1957), the hippocampus has been at the forefront of basic research focusing on the principles of memory formation. This study not only suggested that a certain type of experiences has to be processed by the hippocampus before getting stored as long-term memory, additionally, it offered first evidence showing that multiple types of memory exist. Since then, studies analyzing cognitive deficits in patients with hippocampal damage (Milner, 1972; Samuels, 1972) or focusing on pharmacological intervention of hippocampal function (Morris et al., 1986) strongly propose that precisely, the hippocampus mediates the transition of short- into long-term memories.

Being localized in the medial temporal lobe of both hemispheres, the hippocampus is formed by three neuronal layers *stratum oriens*, *stratum pyramidale* and *stratum radiatum* with the *stratum pyramidale* containing the principle neurons in the *cornu ammonis* (CA) (pyramidal neurons; Lorente de Nó, 1934) and the dentate gyrus (granule cells). They form a unique anatomical connectivity, the ‘trisynaptic loop’ which is thought to serve as a spatiotemporal framework within which various sensory and emotional elements of an experience are processed and finally, connected (Andersen et al., 1996) (Figure 1).

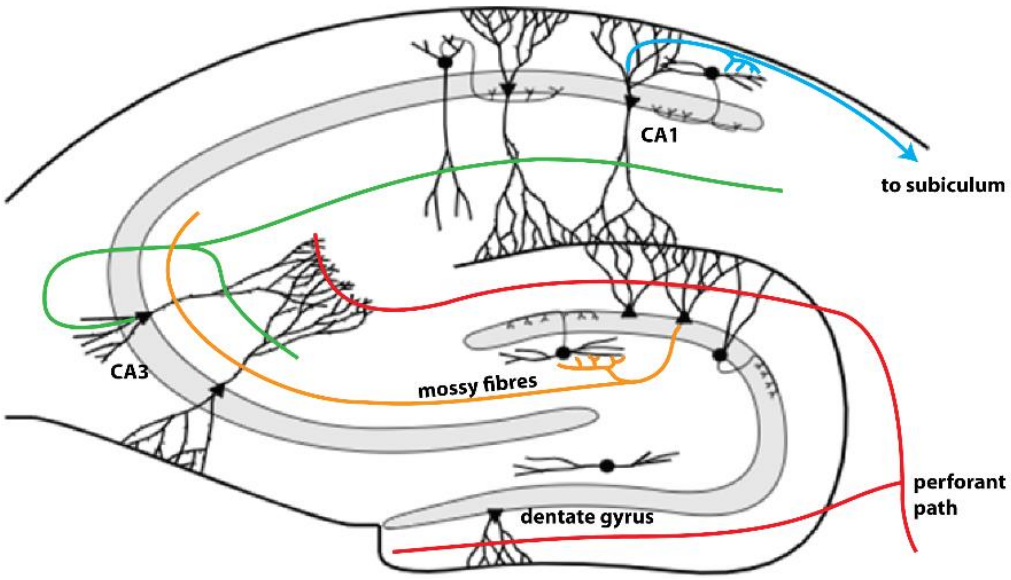

Figure 1 – The trisynaptic loop of the mammalian hippocampus. The hippocampus receives input at granule cells of the dentate gyrus as well as CA3 neurons via the perforant path (red) from axons originating in the enthorinal cortex. In turn, the dentate gyrus projects to CA3 neurons via the mossy fibres (yellow) from where neuronal signals are spread to CA3 neurons of the contralateral hippocampus (associational commisural pathway) as well as to pyramidal neurons in the CA1 region via the Schaffer collateral pathway (green). Finally, CA1 neurons project their axons to the subiculum (blue) and ultimately, output is sent back to the entorhinal cortex. (Adapted from Schultz and Rolls, 1999)

During an experience, cortical regions are simultaneously activated and project to the hippocampus. Thereby, synaptic connections between the interacting neurons are strengthened and correspondingly, the experience is encoded in an engram of synapses of the hippocampus associated with cortical neurons which were active during the original experience (Knierim, 2006; Manns and Eichenbaum, 2006; reviewed in Teyler and DiScenna, 1986). Hence, the memory of an event initially depends on the hippocampus. However, as time passes, memories are either lost or reorganized and transferred to distributed regions of the neocortex, a mechanism that is commonly referred to as ‘systems consolidation’. By increasing the distribution, complexity and connectivity between various neocortical areas, a more permanent memory develops and the importance of the hippocampus for retrieval gradually decreases (for a review see Frankland and Bontempi, 2005; Zola-Morgan and Squire, 1990). Nevertheless, the exact mechanisms how initially hippocampus-dependent memories are transformed into more permanent and sometimes even lifelong memories are still not understood.

3.2 The synaptic plasticity and memory hypothesis

For the longest time it was believed that memories as stable constructs also require stability of the brain. However, this idea crucially reversed (for a review see Gordon, 1969) as it could be shown that the central nervous system (CNS) shows a very high degree of structural plasticity throughout the entire life span of an individual. In fact, by now we know that the acquisition of new, the retention of old and in addition the loss of past information are competing processes as they require flexibility, stability or even fading of neural connections respectively. Therefore, paradoxically, a stable memory crucially depends on the flexible nature of neurons to adapt (von der Malsburg, 1987).

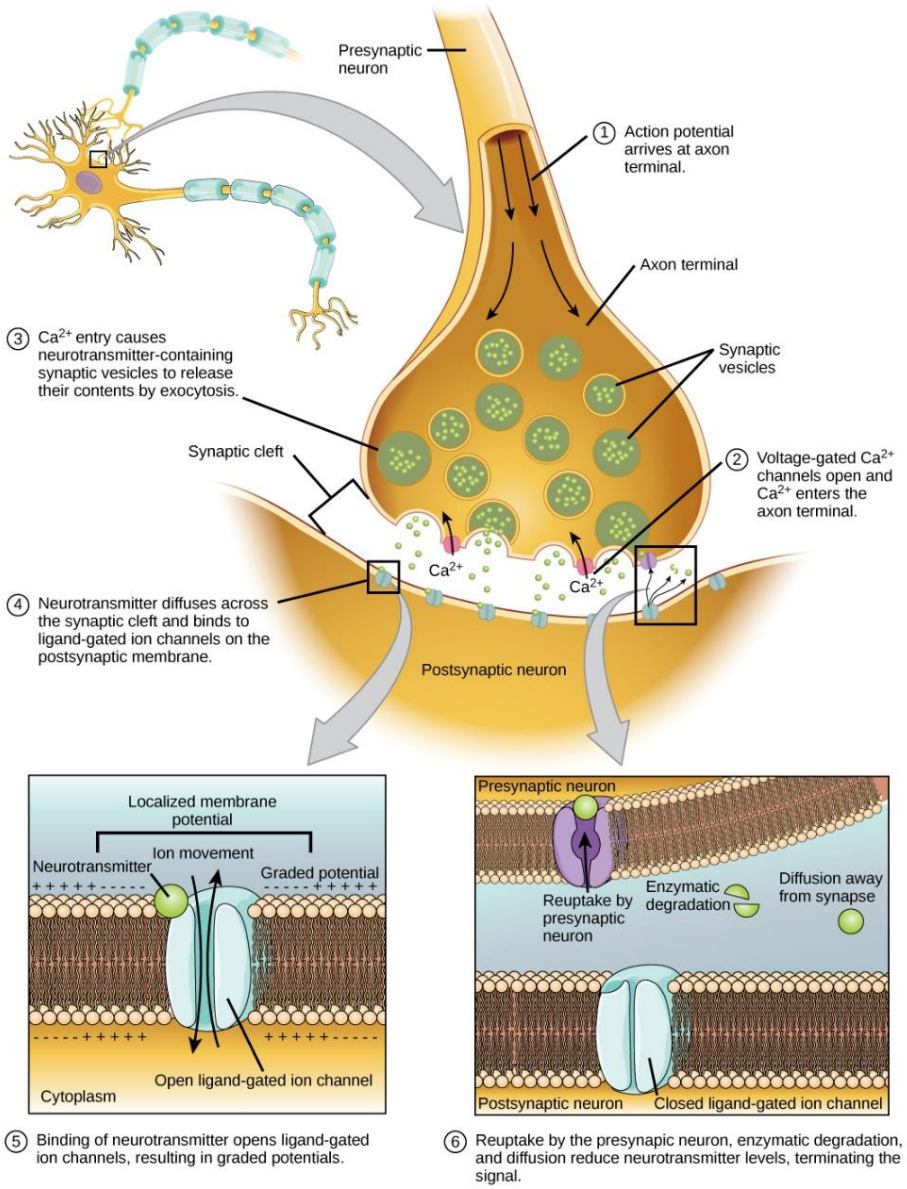

Figure 2 – Neurotransmitter-dependent communication at chemical synapses. Scheme of neurotransmission at a chemical synapse by which an incoming action potential at the axon terminal of the presynapse is spread into the postsynaptic neuron. From: Charles Molnar & Jane Gair, 2015: Concepts of Biology, 1st Canadian Edition, page 664, Fig.16.15. (licensed under a Creative Commons license: https://creativecommons.org/licenses/by/4.0/)

The most popular candidate site for memory storage in the brain is the site of contact between two neurons, the synapse, which has been shown to be especially plastic (Figure 2). Already in 1894, Ramòn y Cajal proposed that structural changes of neuronal connections might be mechanistically involved in the process of memory formation (y Cajal, 1894). While his observations were primarily based on anatomical studies, his theory was importantly expanded by groundbreaking work from Donald Hebb in 1949 showing that synaptic connections between neurons indeed get strengthened when both cells are simultaneously activated (Hebb, 1949). Subsequent studies could prove that synaptic strength indeed is modulated in an activity-dependent manner and that synapses in response to activity changes can not only strengthen (Bliss and Lomo, 1973) but also weaken over time (Maass and Zador, 1999). These observations of long-term plasticity, also known as long-term potentiation (LTP) and long-term depression (LTD) are until today believed to form the cellular basis of memories in the brain as they elegantly propose a model how a memory trace can be rendered stable (and thus be preserved) or unstable (and thus be forgotten) (for a review see McGaugh, 2000).

While the exact molecular pathways are still not completely unraveled, both, LTP and LTD, have been shown to be dependent on the stimulus frequency of presynaptic neurons, with high frequency activity leading to LTP and low frequency activity inducing LTD (Bienenstock et al., 1982). In addition, there is considerable evidence that both phenomena are comprised of an early phase (E-LTP, E-LTD) which is initially based on a regulation of the amount of neurotransmitters released at the presynapse (the axon) and the quantity of neurotransmitter receptors present at the postsynapse (the dendritic spine) (Gaiarsa et al., 2002) and a late-phase that requires *de novo* protein synthesis for long-term maintenance (Lynch, 2004). In this regard, the best studied forms of synaptic plasticity in the hippocampus are the N-methyl-D-aspartate receptor (NMDAR) dependent LTP (Bliss and Collingridge, 1993; Bliss and Lomo, 1973) and the metabotropic receptor (mGluR) dependent LTD (Oliet et al., 1997) at glutamatergic synapses.

In the early-phase of NMDAR-dependent LTP (for a review see Derkach et al., 2007), high-frequency activity of the presynaptic partner leads to repetitive release of the neurotransmitter glutamate which binds to alpha-amino-3-hydroxy-5-methyl-4-isoxazolepropionic acid receptors (AMPARs) at the postsynaptic density (PSD), thereby inducing a Na^+ influx and finally, a depolymerization of the postsynapse. In turn, NMDA receptors are activated by a charge repulsion of Mg^{2+} ions which can block NMDAR function in a voltage-dependent manner, causing a strong Ca^{2+} influx into the postsynapse. Finally, protein kinases are activated which on the one hand are phosphorylating AMPA receptors and thereby increase their ionic conductance and on the other hand induce the insertion of new AMPA receptors into the postsynaptic density.

Contrarily, mGluR-dependent LTD (for a review see Luscher and Huber, 2010) is triggered by group 1 metabotropic receptors (Gp1 mGluRs: mGluR1 & mGluR5) which are expressed postsynaptically, located outside of the postsynaptic density and activated when glutamate is pouring out of the synaptic cleft after constant, low frequency activity of the presynapse. Binding of glutamate to Gp1 mGluRs induces the release of Ca^{2+} from internal stores via the inositol triphosphate 3 (IP3) pathway and in addition activates phospholipase C (PLC) and protein kinase C, which phosphorylates the GluA2 subunit of AMPA receptors and thereby triggers the endocytosis of AMPARs from the postsynaptic density. Various other proteins like extracellular signal-regulated kinases (ERKs), Arc, protein tyrosine phosphatases (PTPs) or p38 mitogen-activated protein kinase (p38 MAPK) have also been shown to be involved in the mediation of Gp1 mGluR-dependent LTD, however, the underlying pathways are still not understood.

While the aforementioned changes of synaptic efficacy can last for up to two hours after stimulation, they are not sufficient to guarantee a permanent change in synaptic transmission that lasts over days, weeks or even months (Frey et al., 1993; Fukazawa et al., 2003). Therefore, the question how changes at individual synapses are maintained over time has been the focus of intensive research over the last decades. As both, late-LTP (l-LTP) and late-LTD (l-LTD), have been shown to be sensitive to inhibitors of protein synthesis (Flexner et al., 1963; Krug et al., 1984; Linden, 1996; Montarolo et al., 1986; Stanton and Sarvey, 1984) and in addition, the presence of polyribosomes near synapses was discovered (Bodian, 1965), it is hypothesized that the maintenance of long-lasting changes in synaptic transmission is mediated by proteins which are synthesized locally (directly at the synapse) in an activity-dependent manner.

3.3 Necessity of local proteome control for the persistence of synaptic plasticity

Notably, already in 1963 it was discovered that memory formation can be blocked via injection of a protein synthesis inhibitor into the brain 1 to 3 days after learning (Flexner et al., 1963), thereby suggesting that the formation of memories is crucially dependent on newly synthesized proteins. Following research could reveal that, specifically l-LTP and l-LTD require the translation of pre-existing mRNAs and the application of protein synthesis inhibitors abolishes long-term changes in synaptic transmission (Linden, 1996; Stanton and Sarvey, 1984), thereby preventing long-term memory formation. However, as neurons are a prime example of cellular asymmetry where each dendritic segment and each synaptic connection serves as a single physiological compartment with an individual computational function (for a review see

Shepherd, 1996), one of the most fundamental questions of neuroscience is how neurons are able to provide synapses with essential proteins in the time-frames needed for the induction of long-term synaptic plasticity.

An elegant model offering a possible answer is based on studies from David Bodian, Oswald Steward and William B. Levy who observed the presence of ribosomes in dendrites directly beneath dendritic spines, thereby indicating their competence for *de novo* protein synthesis (Bodian, 1965; Steward and Levy, 1982). Their observations led to the hypothesis that neurons are able to synthesize proteins directly at the synapse and thus, are able to shape the synaptic proteome locally on a rapid timescale (Figure 3).

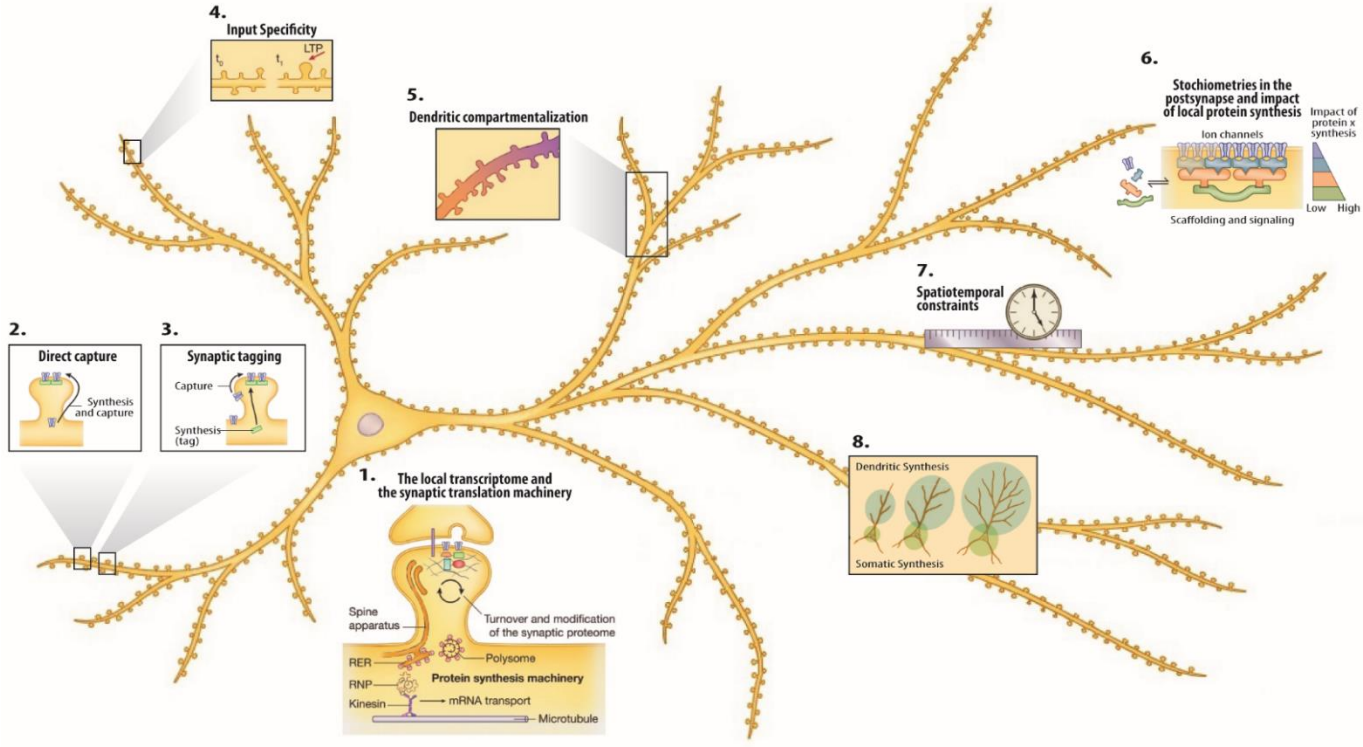

Figure 3 – Description and function of local translation in neurons. Dendrites contain **1.)** the complete cellular machinery required for *de novo,* activity-dependent protein synthesis. Potentially, dendritically synthesized proteins can **2.)** directly be captured by the synapse or **3.)** serve as a ‚synaptic tag' which might be crucial for the generation of **4.)** input specificity at individual dendritic spines as well as **5.)** dendritic compartmentalization. Due to **6.)** the layered organization of the synapse, the stochiometrical impact of local protein synthesis is especially high for proteins with multiple binding slots and binding partners e.g. scaffolding proteins and hence, already the local translation of few important regulatory proteins can have a profound impact on synaptic properties. Overall, regulated dendritic protein translation provides an efficient mean to overcome **7.)** spatiotemporal constraints of protein transport and **8.)** limits of cellular metabolism as above a certain degree of complexity, the soma might not be able to generate sufficient quantities of proteins for the entire cell. (Adapted from Tom Dieck et al., 2014)

By now, it has been experimentally proven that indeed dendrites (Kang and Schuman, 1996), dendritic spines (Scheetz et al., 2000) but also axons (Feig and Lipton, 1993; Torre and

Steward, 1992) are able to synthesize proteins locally in an activity-dependent manner. In addition, thousands of different mRNAs coding for various different classes of molecules have been found in dendrites and axons (Cajigas et al., 2012) suggesting that the capacity of neurons for local proteome control is immense. Although this minimizes the need for the delivery of proteins from the soma, it implies that RNAs need to be actively transported and selectively localized to synaptic sites (Wang et al., 2010). While it has been confirmed that RNAs indeed are actively trafficked (Czaplinski and Singer, 2006; Hirokawa, 2006), the mechanisms of RNA transport in neurons are still only very poorly understood. Dendritic localization signals predominantly seem to be encoded in the untranslated regions (UTRs) of mRNAs (for a review see Andreassi and Riccio, 2009; Mayford et al., 1996), however, the identification of distinct motifs for dendritic mRNA localization is still very challenging as the recognition sites for RNA-binding proteins (RBPs) are often formed by complex secondary and tertiary structures (Gonzalez et al., 1999; Serano and Cohen, 1995). Simplified, the current research state suggests that RBP-RNA complexes assemble into transport granules where RNAs are preserved from degeneration and kept in a translationally silent state while they are transported along microtubules (Kiebler and Bassell, 2006; Thomas et al., 2011). Nevertheless, how transport granules are packed and when, where and how the cargo is released is yet unknown.

Additionally, one of the most intriguing open questions regarding local proteome control in neurons is how specific LTP or LTD proteins are synthesized. On the one hand, distinct patterns of activity might stimulate different signaling cascades or RBPs which target specific mRNAs for translation. This hypothesis is supported by recent studies confirming the specific involvement of the RBPs cytoplasmic polyadenylation element binding-protein (CPEB) (Alarcon et al., 2004) and Fragile X mental retardation protein (FMRP) (Weiler et al., 2004) in NMDAR-dependent LTP and mGluR-dependent LTD in the hippocampus, respectively. While CPEB has been shown to specifically regulate proteins required for LTP (Alarcon et al., 2004), RNA targets of FMRP have been found to be predominantly involved in the mediation of mGluR-dependent LTD (Huber et al., 2002). In addition, it was found that polyribosomes at dendritic spines are not composed equally (Kondrashov et al., 2011) and in turn, ribosomes could theoretically be tuned to preferentially translate specific subsets of RNAs.

On the other hand, LTP and LTD proteins might be synthesized simultaneously and the presynaptic activity pattern may determine which proteins are used. Notably, evidence for this hypothesis comes from the ‘synaptic tagging and capture hypothesis’ originally described by Richard Morris in 1997 (Frey and Morris, 1997). Morris could show that proteins which were locally translated in response to an l-LTP induction at a specific subset of synapses could be captured from a second set of nearby synapses where surprisingly E-LTP was converted into

l-LTP although high-frequency stimulation was missing. Following work could show that similarly, E-LTD can be converted into l-LTD when priorly, nearby synapses underwent l-LTD induction (Sajikumar and Frey, 2004) thereby suggesting that E-LTP and E-LTD might generate a synaptic 'tag' which then mediates the capture of newly synthesized proteins. However, interestingly, E-LTP can also be converted into l-LTP by proteins which were locally translated in response to l-LTD induction and vice versa thereby suggesting that 'cross-tagging' between l-LTP and l-LTD does exist (Sajikumar and Frey, 2004). Hence, one may speculate that similar proteins are translated in response to l-LTP and l-LTD but the synaptic 'tag' determines which long-term change in synaptic transmission is finally initiated.

Current evidence indicates that locally synthesized proteins maintain l-LTP and l-LTD through the regulation of AMPA receptor trafficking at the PSD (Nosyreva and Huber, 2005; Smith et al., 2005), however, most of the studies related to local proteome control focused on protein synthesis and less work has been done on the role of targeted protein degradation. Nevertheless, there is accumulating evidence that a large number of synaptic proteins is degraded in an ubiquitin proteasome system (UPS) dependent manner indicating that similar to local protein synthesis also local protein degradation may be substantially involved in the consolidation of l-LTP and l-LTD (for a review see Cohen and Ziv, 2017).

Importantly, in addition to modulations of pure synaptic strength (functional plasticity) LTP and LTD are accompanied by rapid and substantial structural changes at the synapse (structural plasticity), especially at the postsynapse (Matsuzaki et al., 2004; Zhou et al., 2004). Various studies could demonstrate that the size, shape and density of dendritic spines can change rapidly through activity-dependent mechanisms (Harreveld and Fifkova, 1975; Kwon and Sabatini, 2011; Matsuzaki et al., 2004) suggesting that these parameters are also directly correlated to changes in transmission efficacy. Indeed, the volume of the spine head has been shown to be proportional to the size of the PSD which in turn correlates with the amount of PSD-receptors (Nusser et al., 1998) and thus, synaptic efficacy. Additionally, the morphology of the spine neck is suggested to be crucially involved in the electrical isolation of synaptic inputs (Araya et al., 2006) as its resistance might serve as a filter when excitatory synaptic potentials spread into the dendrite. Hence, activity-dependent changes in the morphology of dendritic spines might have a direct influence on the computation of synaptic transmission at individual synapses. Notably, also the long-term stabilization of activity-dependent morphological adjustments has been shown to be dependent on *de novo* protein synthesis (Briz et al., 2015; Tanaka et al., 2008), indicating that newly synthesized proteins not only stabilize and preserve the receptor density at the synapse but in addition help to maintain structural changes.

3.4 Structural plasticity mediated by synaptic actin

Surprisingly, even on the same dendritic segment, dendritic spines can be found in various morphologically different sizes and shapes, thereby corroborating their high degree of functional diversity (for a review see Nimchinsky et al., 2002). Based on their overall appearance in imaging studies over the last decades, they are typically classified into the three subgroups ‘thin’ (long and thin neck with a small head), ‘stubby’ (small head and no neck) and ‘mushroom’ (large head) (Peters and Kaiserman-Abramof, 1970). Commonly, due to the small size of the spine head diameter, ‘thin’ and ‘stubby’ spines are thought to represent an immature state while ‘mushroom’ spines with a larger head diameter and a larger PSD are often referred to as mature dendritic spines (for a review see Ebrahimi and Okabe, 2014). However, modern super-resolution imaging techniques indicate that the optical resolution that was assessable in past studies was insufficient to properly assign the exact morphology of dendritic spines (Adrian et al., 2017; Nagerl et al., 2008), thereby suggesting that sticking to a strict morphological classification might even be contraproductive in order to understand the exact correlation between structural, biochemical and electrical properties of the dendritic spine.

Nevertheless, numerous studies could confirm that structural modifications of dendritic spines are linked to changes in synaptic transmission. In response to neuronal stimulation, spines immediately undergo a volume change whose physiological function is still unknown, however, in the following hour the dendritic spine volume stabilizes either at a higher (after LTP) (Matsuzaki et al., 2004) or a lower (after LTD) (Zhou et al., 2004) level than before. Even the complete loss or formation of new dendritic spines has been observed in response to LTD or LTP respectively (Nagerl et al., 2004), thus proposing a functional relevance of structural plasticity for learning and memory formation. Indeed, pharmacological blocking of structural changes at the spine prevents l-LTP and l-LTD (Fukazawa et al., 2003; Szabo et al., 2016) and in addition, hippocampus-dependent learning tasks show a positive correlation between behavioral learning and the structural modification of existent as well as the gain of new or the loss of old spines (Leuner et al., 2003; Moser et al., 1994). Nonetheless, although the association between structural plasticity and memory formation led to intensive research regarding the underlying molecular pathways, the exact mechanisms which finally couple protein synthesis dependent structural and functional changes are yet not completely understood.

In general, neuronal shape is defined through the cytoskeleton which is comprised of microtubules, neurofilaments and microfilaments (for a review see Kapitein and Hoogenraad, 2011). Dendrites as well as axons are primarily stabilized by a complex and dense network of microtubules which in addition serve as tracks for the transport of cargo (e.g. of RNA-granules) and an anchor for organelles (for a review see Goldstein and Yang, 2000). In pre- and postsynaptic sites, however, stable microtubules are absent and structural stability is almost purely dependent on actin microfilaments (Kaech et al., 1997) (Figure 4). Formed via polymerization of free actin monomers (globular 'G-actin'), individual actin microfilaments ('F-actin') are comprised of two intertwisted actin polymer helices (Hanson and Lowy, 1964). The assembly of a new filament is driven by actin-nucleating factors and is initiated by the association of G-actin with adenosine triphosphate (ATP) as well as Ca^{2+}. Subsequently, G-actin monomers dimerize under ATP hydrolysis and a new filament can form by the addition of new actin monomers (for a review see Firat-Karalar and Welch, 2011). However, actin filaments are not permanently stable but reside in a dynamic equilibrium where new G-actin monomers are added onto the 'barbed end' of the microfilament while other actin monomers dissociate from the 'pointed end'. This process of constant G-actin turnover in the filament is described as 'treadmilling' (Wegner, 1976). Therefore, if polymerization and depolymerization at both ends of the filament are outbalanced, the overall filament length remains unchanged and stable.

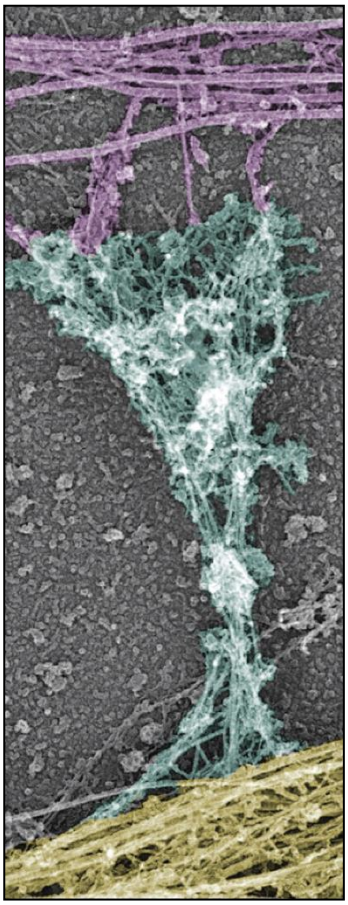

Figure 4 – Cytoskeletal organization of a dendritic spine. Actin and micro-tubular organization in the dendritic spine (cyan), the axon (purple) and the dendrite (yellow) visualized by platinum replica electron microscopy. (From Hotulainen and Hoogenraad, 2010)

Notably, actin has been found to exist in locally restricted populations within the dendritic spine (Honkura et al., 2008; Star et al., 2002). At the centre and base (the 'core'), F-actin has been shown to extend from the spine neck towards the PSD with slow filament turnover times (~17 min) which provides a stable core region that is proposedly needed for proper functionality of the spine. However, the spine tip as well as the periphery are composed of highly dynamic actin microfilaments with turnover times of seconds (~40 s) thereby providing a dynamic platform that allows for rapid morphological modifications (Honkura et al., 2008; Star et al., 2002). These F-actin characteristics suggest that the morphology of a dendritic spine is mediated by a tight and probably local regulation of polymerization and depolymerization of F-actin in the dendritic spine. Indeed, multiple studies could confirm that not only spontaneous

but also activity-mediated morphology changes are initiated by shifts in the equilibrium of G- and F-actin (Okamoto et al., 2004). During an enlargement of spine volume, which is commonly observed after high-frequency stimulation (LTP), the ratio shifts towards F-actin, leading to an increased stability of actin filaments and thus, growth of the spine. In turn, low-frequency stimulation (LTD) was found to shift the equilibrium towards G-actin which destabilizes actin filaments and finally leads to shrinkage or even the complete loss of the dendritic spine (Okamoto et al., 2004). In line with this and confirming a direct link between structural and functional plasticity, pharmacological modification (either an increase or decrease) of F-actin polymerization was found to be sufficient to abolish l-LTP or l-LTD, respectively (Fukazawa et al., 2003; Szabo et al., 2016) and in addition, optical shrinkage of spines which were potentiated during motor learning was shown to disrupt the previously acquired motor task (Hayashi-Takagi et al., 2015). From these observations it was speculated that increasing the polymerization of F-actin might be sufficient to induce LTP alone. Although this assumption was proven to be wrong (Okamoto et al., 2004), additional studies could confirm that an increase in actin polymerization indeed is sufficient to convert early LTP into l-LTP (Huang et al., 2013). Hence, the transformation of short-term into long-term memories and finally, the consolidation of memories is dependent on the precise modulation of F-actin polymerization in dendritic spines.

3.4.1 Synaptic signaling pathways involved in actin remodeling in dendritic spines

For the proper understanding of memory formation, knowledge of the molecular pathways mediating LTP and LTD is crucial. Yet, surprisingly little is known about the signaling cascades that regulate actin remodeling during these forms of synaptic plasticity. By now, a large number of extracellular molecules has been shown to shape the molecular structure of the actin cytoskeleton via signaling through various cell surface receptors like neurotrophin receptors, integrins, cadherins and immunoglobulin superfamily receptors (for a review see Hotulainen and Hoogenraad, 2010). These receptors regulate the activity of downstream signaling molecules which finally converge on various actin-binding proteins (ABPs) and importantly, small GTPases of the Rho-family which are one of the most studied and molecularly best understood classes of actin regulators. The most prominent members of this protein family are RhoA, Rac1 and Cdc42 whose activation has been shown to be required for activity-mediated changes in dendritic spine structure (Rex et al., 2009). They control Rho effector proteins (N-WASP, ROCK, PAK, WAVE1) which ultimately mediate the activity of a large number of ABPs including Arp2/3, cofilin, profilin, cortactin, drebrin and MyosinIIb (for a review see Sit and Manser, 2011). Hence, given the pleiotropic functions of all those ABPs, the Rho GTPase

pathway is crucially involved in the regulation of polymerization, branching and stabilization of F-actin.

Although several ABPs have been shown to be necessary for actin remodeling during synaptic plasticity and the principle regulatory mechanisms mediating their activity are known, it is still elusive how the precise timing and the spatial localization of ABP activity is restricted. Therefore, the localization of ABPs at the dendritic spine and especially the timing of events after LTP or LTD induction were intensively studied.

Following an NMDAR-dependent LTP inducing stimulus, the F-/G-actin ratio is shifted towards F-actin within about 40s (Okamoto et al., 2004), thereby inducing a rapid enlargement of the spine head in the first 1 to 7 minutes after stimulation (Honkura et al., 2008). This first phase of LTP induction is characterized by a rapid initial period of F-actin disassembly and multiple studies offer evidence that various actin-binding proteins (ABPs) are translocating into or out of the dendritic spine. While actin-severing, depolymerizing and capping proteins like cofilin 1 and Aip1 have been shown to enter the dendritic spine (Bosch et al., 2014), actin-stabilizers like N-cadherin (Bozdagi et al., 2000), αN-catenin (Abe et al., 2004), ß-catenin (Murase et al., 2002), cortactin (Hering and Sheng, 2003) and profilin (Bosch et al., 2014) are driven out of the spine. Especially the F-actin severing protein cofilin 1 (Cof1) has been shown to be highly enriched during this phase of early F-actin remodeling thereby suggesting a potential major role (Bosch et al., 2014). In the prevailing view, immediate Cof1 activity after stimulation is needed for a fast breakdown of synaptic F-actin which in turn allows a faster remodeling than pointed end depolymerization. In line with this, two-photon imaging studies revealed that the total F-actin concentration remains unaltered but the amount of actin filaments with medium length increases indicating that F-actin is actively severed into shorter filaments (Chen et al., 2015). Accompanying the active severing of F-actin, calcium/calmodulin-dependent protein kinase II beta (CamKIIß), an actin filament bundling protein gets phosphorylated and dissociates from filaments, thereby destabilizing F-actin (Kim et al., 2015). In the second phase, which lasts for around 1 hour, it is suggested that actin stabilizing and crosslinking proteins like CamKIIß, alpha-Actinin, drebrin A and MyosinIIb return to the spine and increase the bundling and cross-linking status of newly formed structures (Koskinen et al., 2014). In addition, the complexity of new filaments is increased by the branching protein Arp2/3 which has been shown to translocate to potentiated spines (Bosch et al., 2004). Finally, neuronal profilin isoforms (Profilin 1 (Pfn1) (Neuhoff et al., 2005); Profilin 2a (Pfn2a) (Ackermann and Matus, 2003)), which function at ADP/ATP exchanger at G-actin are driven into the spine (Ackermann and Matus, 2003), inducing an additional increase in actin polymerization and a further shift of the F-/G-actin ratio towards F-actin resulting in longer, more stable filaments. Interestingly, an increase in profilin isoform concentrations can also be observed in the nucleus

(Birbach et al., 2006) suggesting that they might act as a 'synaptic tag' that links synaptic activity and *de novo* gene transcription. In the third and last phase, not earlier than 1 hour after induction of LTP, the post-synaptic density is remodeled in a protein-synthesis dependent manner and PSD scaffolds are recruited and stabilize newly inserted postsynaptic AMPA receptors.

In comparison to LTP, the signaling pathways, the involved molecules and especially the spatial timing of actin modulations underlying mGluR-dependent LTD are less well understood. Ca^{2+} release is thought to trigger the activation of the Ca^{2+}-dependent phosphatase calcineurin which in turn dephosphorylates mGluR5 and thus can prolong its activity after glutamate release (Halpain et al., 1998). Additionally, calcineurin activates the phosphatase slingshot which dephosphorylates and activates Cof1 (Hayama et al., 2013), thereby leading to an increased severing of F-actin. Hence, spine shrinkage following LTD-induction is dependent on Cof1. Additionally, profilin is targeted to dendritic spines undergoing LTD (Ackermann and Matus, 2003) indicating that similar to what has been shown during LTP, actin dynamics after the initial breakdown of F-actin by Cof1 are stabilized through profilin recruitment.

Interestingly, actin remodeling pathways during LTP and LTD might employ partially overlapping mechanisms as in both processes actin structures are remodeled first and afterwards, changes in actin architecture are maintained through branching, bundling and stabilization. Thus, it might be that the initial breakdown of F-actin at the spine tip is needed to allow for a better insertion or retraction of AMPA receptors. In turn, these changes have to be re-stabilized as otherwise changes in receptor composition and density and ultimately, l-LTP or l-LTD might not be maintained over time. Notably, cofilin and profilin are activated in both, LTP and LTD and although the spatial and temporal regulation of these proteins during both processes is different, they both seem to be essential for the maintenance and consolidation of l-LTP as well as l-LTD.

3.4.2 Actin dynamics regulated by neuronal profilins and cofilin

In principle, profilin and cofilin are primarily thought to have counteracting functions on actin polymerization, with Pfn activity leading to a net increase (Gurel et al., 2015) and Cof1 activity inducing a net decrease in actin filament length (Pavlov et al., 2007). Thus, in theory, the combined action of both proteins is perfectly suited to mediate the spatial and temporal balance between F-actin breakdown (strong Cof1 and weak Pfn activity) and F-actin stabilization (strong Pfn activity and weak Cof1 activity) during LTP and LTD.

Pfn has been shown to form complexes with Mg^{2+}, G-actin and ATP, thereby catalyzing the exchange of ADP to ATP at actin monomers (Goldschmidt-Clermont et al., 1992; Jockusch et al., 2007). In addition, it enhances the polymerization of ATP-actin onto F-actin resulting in a net elongation of actin filaments. In mammals, Pfn is expressed in four different isoforms (Pfn1 to Pfn4) (Birbach, 2008) and while the sequence homology between the isoforms is fairly low, the three dimensional structure of Pfn isoforms is highly conserved (Polet et al., 2007). The isoforms Pfn3 and Pfn4 have been shown to be specific to testis (Braun et al., 2002; Hu et al., 2001), however, the major isoform Pfn1 is ubiquitously expressed at high levels in nearly all tissues with exception from heart, skeletal muscles and the brain where expression is low (Witke et al., 1998). Pfn2, on the other hand, is expressed in brain, skeletal muscle and kidney tissue (Honore et al., 1993; Witke et al., 1998) and is alternatively spliced into Pfn2a and Pfn2b (Di Nardo et al., 2000; Lambrechts et al., 2000). Interestingly, neuronal tissue is the only tissue where Pfn1 is not the most abundant isoform as with ~75% Pfn2a is the predominantly expressed isoform (Witke et al., 1998). Yet, Pfn1 and Pfn2a share redundancy in their subcellular localization in neurons as none of the isoforms is expressed alone and both isoforms are present in the nucleus (Birbach et al., 2006) as well as at pre- and postsynaptic sites (Neuhoff et al., 2005).

In general, Pfn isoforms have three distinct binding domains and are able to bind to G-actin and actin-related proteins, phosphatidylinositol lipids and poly-(L)-proline rich regions (for a review see Jockusch et al., 2007). Consequently, profilins are interacting with a variety of proteins which have been found to be either directly or indirectly involved in the regulation of the actin cytoskeleton (ARP2 and ARP3, Ena/VASP, formins, WAVE/WASP) (Chang et al., 1996; Miki et al., 1998; Reinhard et al., 1995) or suited to regulate synaptic transmission (gephyrin, phosphatidylinositol-4,5-biphosphate (PIP2)) (Lassing and Lindberg, 1985; Mammoto et al., 1998). Notably, regulated by the Rho GTPase pathway, Ena/VASP, WAVE/WASP and formins are not only binding to Pfn but to actin-Pfn complexes and as their poly-(L)-proline stretches are repetitive, they are able to accommodate several actin-Pfn complexes simultaneously (Lambrechts et al., 1997). Hence, these proteins might be able to provide and deliver Pfn-actin and ATP-G-actin with a high temporal but also spatial resolution to sites of need during phases of structural plasticity after LTP or LTD induction. Contrarily, the functions of Pfn isoforms in the nucleus are less well understood. However, nuclear actin and ABPs have been shown to be involved in chromatin remodeling, nuclear stability but also transcription regulation (for a review see Hofmann and de Lanerolle, 2006) indicating that profilins might be able to serve as a direct link between synaptic activity and *de novo* gene expression.

Highlighting the importance of Pfn isoforms for proper neuronal function and cell viability in general, the conventional knockout of Pfn1 leads to early embryonic death in mice (Witke et al., 2001). However, mice with a conditional knockout of Pfn1 in neurons show no changes in hippocampal basal synaptic transmission, synaptic plasticity or synaptic morphology (Gorlich et al., 2012). In addition, an acute knockdown of Pfn1 does not alter the neuronal ability to undergo activity-dependent structural plasticity at synapses (Gorlich et al., 2012). On the other hand, conventional knockout mice deficient of Pfn2a are vital and have normal brain development but show alterations in vesicle release and synaptic transmission (Pilo Boyl et al., 2007). Moreover, shRNA mediated acute knockdown of Pfn2a results in a reduced neuronal complexity, a reduction in dendritic spine numbers in hippocampal neurons and most importantly, an almost complete lack of structural plasticity (Michaelsen-Preusse et al., 2016; Michaelsen et al., 2010). Surprisingly, overexpression of Pfn1 can rescue spine loss induced by knockdown of Pfn2a, but has no effect on alterations in dendritic complexity and cannot rescue the structural plasticity defect (Michaelsen-Preusse et al., 2016). Overall, these experiments led to the following conclusions: (1) Since Pfn2a is not able to compensate for the loss of Pfn1 in the conventional Pfn1 KO, Pfn1 seems to have an important role during development that is essential for cell survival. This is in line with the fact that Pfn1 is the evolutionarily older isoform that is ubiquitously expressed in the organism. (2) Pfn2a, the evolutionary younger and brain-specific isoform seems to be essentially involved in the regulation of synaptic plasticity processes, a function that Pfn1 is not able to fully compensate for. Earlier studies suggest that these Pfn2a-specific functions might derive from the interaction with isoform-specific binding partners as only Pfn2a was shown to interact with synaptic proteins like mDia2 (Michaelsen et al., 2010), synapsin I and synapsin II (Witke et al., 1998) as well as dynamin (Witke et al., 1998). In addition, the co-localization between gephyrin and Pfn2a is more pronounced than with Pfn1 which suggests that gephyrin has a higher affinity to bind Pfn2a (Murk et al., 2012). Hence, the decreased synaptic transmission observable in Pfn2a deficient neurons might be attributable to an alteration of AMPAR content (mediated by gephyrin) in the PSD, a Pfn2a-specific function that Pfn1 might not be able to compensate. (3) As still, Pfn1 overexpression can rescue certain phenotypes in Pfn2a-deficient neurons both isoforms seem to share functional redundancy and are at least partially able to compensate the loss of one another.

In contrast to neuronal Pfn isoforms, Cof1 activity is mainly associated with a destabilization of F-actin and thus rapid turnover of actin filaments (Bamburg and Bernstein, 2010). It belongs to the ADF/cofilin family which includes the three small ABPs cofilin 1 (Cof1, non-muscle Cof1), cofilin 2 (muscle Cof) and the actin depolymerizing factor (ADF, ‘destrin’). In the adult brain, Cof1 is broadly expressed and localized to presynaptic as well as postsynaptic terminals (Racz and Weinberg, 2006) where it was shown to serve as a key mediator of F-actin assembly and

disassembly in a concentration-dependent manner (Andrianantoandro and Pollard, 2006). At low Cof1 to actin ratios, Cof1 exerts the typically described F-actin severing function and increases the G-actin dissociation rate from F-actin. However, surprisingly, depending on the local G-actin concentration and the activity status of actin-polymerizing proteins this can lead to either assembly or disassembly of F-actin. At high concentrations, Cof1 nucleates and stabilizes F-actin, thereby promoting F-actin assembly. In general, actin binding of Cof1 is regulated by phosphorylation (deactivation) (Gungabissoon and Bamburg, 2003) and dephosphorylation (activation) of a serine residue at position 3 (Ser3) which has been shown to be mediated by LIM kinases (LIMK) (Yang et al., 1998) and slingshot phosphatases (SSH1) (Niwa et al., 2002). Both, LIMK and SSH1 are downstream effectors of RhoGTPases and especially the pathways RhoA-ROCK-LIMK-Cof1, Rac1 & Cdc42-PAK-LIMK-Cof1 and Rac1-SSH1-Cof1 were shown to be involved in the regulation of Cof1 activity at synapses (for a review see Woolfrey and Srivastava, 2016). Overall, the concentration-dependent dual-function of Cof1 for F-actin assembly is consistent with the fact that Cof1 activity has been shown to be crucial for the maintenance and consolidation of both, l-LTP and l-LTD (Chen et al., 2007; Zhou et al., 2004). In line with this, *in vitro* work could show that Cof1 activation is required for the recruitment of AMPA receptors to the PSD (Gu et al., 2010). On the one hand, this suggests that actin filament breakdown is necessary for changes in PSD receptor composition and on the other hand that Cof1 might have receptor-specific effects. Further reinforcing this hypothesis, the analysis of conditional Cof1 knockout mice revealed that the diffusion of extrasynaptic AMPA receptors is compromised in the absence of Cof1 (Rust et al., 2010). Thus, it is believed that Cof1 mediates AMPAR mobility and ultimately, synaptic strength in an actin-dependent mechanism which might be independent of its function during structural plasticity. Therefore, Cof1 might serve as a switch that decouples structural and functional plasticity during LTP and LTD, respectively. Importantly, proper Cof1 function is not only critical for l-LTP and l-LTD but for long-term learning and memory formation in general as conventional Cof1 knockout mice show deficits in long-term spatial memory and associative learning (Rust et al., 2010). However, surprisingly, short-term spatial memory seems to be unaffected in these mice (Rust et al., 2010) which implies that (1) in synaptic plasticity processes, Cof1 function is needed for the manifestation and consolidation of long-term adjustments at the synapse and (2) short-term and long-term memory processes indeed are distinct.

In summary, neuronal Pfn isoforms as well as Cof1 have been found to be crucially involved in learning and memory processes as they are critical for spine morphology and structural and functional aspects of LTP and LTD. Acute or chronic depletion of these proteins is either lethal or heavily impairs learning processes, thereby demonstrating their importance for proper neuronal function and in the end, complex mammalian behavior.

3.5 Dysfunctional actin regulation in neurons contributes to mental retardation

The physiological relevance of actin is emphasized by the contribution of dysregulated actin dynamics to several neurological disorders including mental retardation. Mental retardation is a developmental disability which is characterized by a general deficiency in cognitive abilities and per definition is defined by an intelligence quotient below 70 (reviewed in Chiurazzi and Oostra, 2000). In most cases, low intelligence is the only detectable disability, however, phenotypes can range from neurological and psychiatric symptoms to body or brain malformations, neuroendocrine phenotypes or metabolic defects. Occurring in about 2 to 3 % of the human population, mental retardation phenotypes are strongly heterogenous in severity in regard to the cognitive abilities that are affected (for a review see Chiurazzi and Oostra, 2000).

Notably, neurons of patients suffering from mental retardation show impairments in dendritic arborization, spine density as well as spine structure (for a review see Kaufmann and Moser, 2000). As spine morphology and synaptic efficacy are intimately linked, it is therefore believed that the pathogenesis of mental retardation is related to changes in neuronal connectivity caused by abnormal dendritic spine morphology. Strikingly, these defects are similar to phenotypes which arise from malfunctions of actin regulatory pathways (Ackermann and Matus, 2003; Fukazawa et al., 2003; Hering and Sheng, 2003; Luo et al., 1996; Nakayama et al., 2000) thereby indicating that neurological phenotypes in mental retardation patients might indeed be based on dysregulations of synaptic actin. Importantly, multiple genes which were shown to carry the heritable forms of mental retardation (typically the more severe forms) encode for direct or indirect regulators of actin dynamics, including *pak3* (PAK3) (Allen et al., 1998), *ophn1* (Oligophrenin) (Billuart et al., 1998), *limk-1* (LIMK) (Tassabehji et al., 1996) and *fmr1* (FMRP) (Bongmba et al., 2011; Pyronneau et al., 2017) which all have been linked to Rho GTPase signaling pathways.

3.6 The most frequent single gene cause of mental retardation: the Fragile X Syndrome

Among the heritable forms of mental retardation, the most common monogenetic cause is the Fragile X Syndrome (FXS) (or Martin Bell Syndrome) (Martin and Bell, 1943) affecting approximately 1 in 5000 females and 1 in 2500 males. Patients typically suffer from mild to severe cognitive deficits in working and short-term memory, show behavioral characteristics like hyperactivity, stereotypic motion and disturbed social interaction (autism like behavior) as well as physical phenotypes like facial dysmorphism and macroorchidism (for reviews see

Bardoni et al., 2000; Lightbody and Reiss, 2009). FXS is caused by silencing of the X chromosomal *fmr1* gene which results in loss of its gene product the Fragile X mental retardation protein 1 (FMRP). Normally, 5-50 CGG repeats are harbored in the promotor region of the 5'UTR of exon 1 of *fmr1* which are stably inherited, however, in rare cases these repeats become unstable and get extended to numbers >200 (Verkerk et al., 1991). This leads to a hypermethylation of the promotor region and finally, silencing of *fmr1* and a total loss of the RNA-binding protein FMRP (for a review see Bagni and Oostra, 2013). In healthy individuals, FMRP is ubiquitously expressed with predominant expression in the brain, especially in neurons (Gholizadeh et al., 2015). There, it is considered to be involved in dendritic and axonal RNA transport (Dictenberg et al., 2008) as well as the modulation of activity-dependent local protein synthesis (Feng et al., 1997) as it has been shown to shuttle between the nucleus and dendrites (Eberhart et al., 1996; Feng et al., 1997), thereby translocating ribonucleoprotein complexes which are crucial for translational control. FMRP is able to bind to ~4% of all mRNAs in the brain (Ascano et al., 2012; Brown et al., 2001; Darnell et al., 2011) and structural analysis revealed multiple RNA-binding motifs including two hnRNP-K-homology (KH) domains as well as an arginine-glycine-glycine (RGG) box which allow for high affinity binding of stem-g-quartet loops, WGGA-, ACUK- or GAC-motifs as well as U-rich RNA (Ashley et al., 1993a; Siomi et al., 1993). Interestingly, FMRP has not only been shown to interact with translatable mRNAs but also with untranslatable mRNAs and in addition with its own mRNA *in vitro* (Ashley et al., 1993b).

In contrast to RNA-binding and RNA-transporting functions of FMRP, however, the mechanisms how FMRP interferes with local protein synthesis are less well understood. FMRP was initially found to actively repress translation at polyribosomes (Darnell et al., 2011; Laggerbauer et al., 2001) and thus was thought to excess a pure repressive action. Yet, over the last years it became clear that FMRP is able to modulate mRNA translation bidirectionally. While the phosphorylated form of FMRP was shown to associate with heavy polyribosomes, thereby initiating the translation of transported mRNA in an unknown mechanism (Narayanan et al., 2007; Narayanan et al., 2008), dephosphorylated FMRP was observed to run-off from heavy polyribosomes (Ceman et al., 2003). As FMRP is commonly present in dendrites and directly at dendritic spines (Feng et al., 1997), it is thus perfectly suited to mediate the transport as well as the local synthesis of proteins encoded by FMRP-target mRNAs. Since it was additionally shown to actively migrate into dendrites upon neuronal activity (Dictenberg et al., 2008), it is believed that FMRP is essential for the supply as well as the modulation of activity-dependent translation of mRNAs encoding vital proteins for synaptic plasticity processes. Therefore, the current model suggests that cognitive impairments in FXS result from synaptic dysfunctions caused by alterations in local synaptic protein synthesis and long-term synaptic plasticity.

3.6.1 Molecular phenotypes of the Fragile X Syndrome: impaired hippocampal plasticity

Surprisingly, although FXS patients are suffering from severe live restricting impairments, the neuropathological phenotype is unexpectedly mild. In autopsy and gross imaging studies, brains of FXS individuals appear to be normal and the only prominent neuroanatomical phenotype that was described so far is solely seen microscopically: alterations in dendritic spine morphology (Hinton et al., 1991; Irwin et al., 2000; Irwin et al., 2001). As abundance, size and shape of dendritic spines are important parameters of neuronal connectivity (and function) various studies aimed at analyzing the FXS spine phenotype throughout different regions of the brain either directly in post mortem brain tissue of FXS patients (Hinton et al., 1991; Rudelli et al., 1985) or in the FXS mouse model ('*fmr1* knock-out (KO) mice' with a deletion of *fmr1*) which shows similar phenotypes compared to humans (Dutch-Belgian Fragile X Consortium, 1994). Based on the cognitive symptoms of the disease, the main focus has been laid on the cerebral cortex, the hippocampus and the amygdala. However, the results obtained and the detailed changes in spine morphology and especially spine density are discussed controversial. In regard to spine morphology, a large proportion of studies showed an increase of long and thin 'immature' spines in the cortex (Liu et al., 2011; Meredith et al., 2007; Pan et al., 2010; Su et al., 2011), the hippocampus (Antar et al., 2006; Bilousova et al., 2009; Grossman et al., 2006; Levenga et al., 2011) as well as the amygdala (Qin et al., 2011) in *fmr1* KO mice. As the same observation was made in multiple studies analyzing cortical tissue of FXS patients (Hinton et al., 1991; Irwin et al., 2001; Rudelli et al., 1985), this phenotype is described as the 'classical FXS phenotype', characterized by a hyperabundance of immature spines. Nevertheless, a number of contrasting studies exists that failed to reproduce these data (Braun and Segal, 2000; Cruz-Martin et al., 2010; Hayashi et al., 2007). Similarly, results gained from spine density analyses show controversies. While several studies detected increases in spine density in the cortex of FXS patients (Irwin et al., 2001) as well as in the cortex (Comery et al., 1997; Dolen et al., 2007; Nimchinsky et al., 2001) and the hippocampus of *fmr1* KO mice (Antar et al., 2006; Grossman et al., 2010; Levenga et al., 2011), multiple studies failed to reproduce these observations in *fmr1* KO mice (Braun and Segal, 2000; Segal et al., 2003). However, given the wealth of data, it is getting clear that the synaptic phenotypes in FXS seem to be rather transient than stable and seem to depend on the brain region, the developmental stage and even the cell population analyzed.

As FMRP is highly expressed in the hippocampus (Zorio et al., 2017) and FXS patients show deficits in learning and memory formation, thereby indicating hippocampal dysfunction, special emphasis has been put on analyzing the effects of FMRP loss on hippocampal synaptic plasticity. As FMRP expression was found to be accelerated upon LTD induction triggered by Gp1 mGluR activation in the hippocampus (Weiler et al., 1997), it is suggested that mGluR activation stimulates new protein synthesis and FMRP expression. FMRP might then crucially inhibit further protein synthesis, therefore acting as a brake for mGluR-dependent LTD (Figure 5). This 'mGluR theory' is strongly supported by the observation that *fmr1* KO mice show an enhanced hippocampal mGluR-dependent LTD (Bear et al., 2004; Huber et al., 2002).

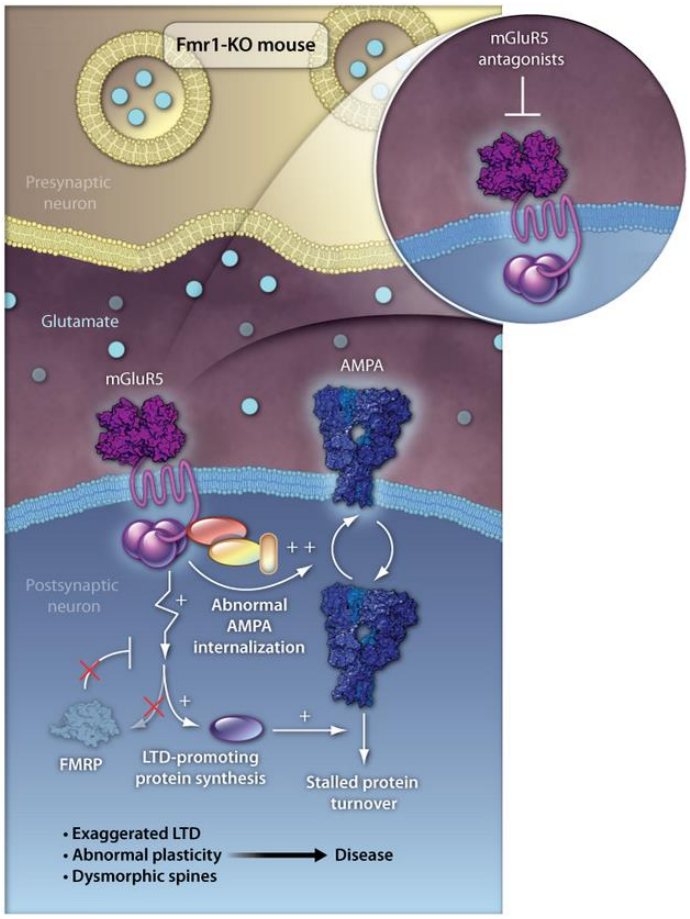

Figure 5 – The ‚mGluR theory' of FXS. In FXS, the mGluR-dependent LTD is exaggerated as an inhibition of local, LTD-promoting protein synthesis by FMRP is missing. As a result, mGluR5 antagonists were extensively studied as potential treatments against FXS. (Adapted from Gomez-Mancilla, 2012)

Notably, this hypothesis gained a lot of attention as pharmacological inhibition and genetically reduced expression of mGluR were shown to rescue behavioral impairments as well as spine phenotypes in *fmr1* KO mice (Dolen et al., 2007). Based on these results, multiple clinical trials testing negative modulators of Gp1 mGluRs were started in humans, however, all of them were closed as they were either unsuccessful (AFQ056, Novartis; STX107, Seaside Therapeutics; Fenobam, Neuropharm Ltd) or had to be shut down due to safety reasons (RG7090, Roche). Contrarily, the effect of FMRP loss on hippocampal LTP is less well understood. While LTP defects could be observed in the somatosensory cortex, the anterior cingulate cortex as well as the lateral amygdala of *fmr1* KO mice (Li et al., 2002; Wilson and Cox, 2007; Zhao et al., 2005), several studies failed to reproduce this phenotype in the hippocampus. Interestingly, strong stimulation protocols led to normal hippocampal LTP (Godfraind et al., 1996; Larson et al., 2005; Paradee et al., 1999), however, when using a more subtle approach e.g. by using 5 instead of 10 thetabursts or chemical induction of NMDAR-dependent LTP via glycine

application, hippocampal LTP was found to be reduced as well (Lauterborn et al., 2007; Shang et al., 2009).

Collectively, both LTP and LTD were found to be dysregulated in the hippocampus of *fmr1* KO mice indicating that indeed, cognitive impairments in FXS could be based on synaptic dysfunction and synaptic plasticity defects. This assumption is strengthened by the fact that in addition, FXS patients as well as *fmr1* KO mice show morphological alterations of dendritic spines as the main neuropathological phenotype. However, since synaptic structure and function are intimately linked, these observations offer room for two different speculations: either 1) dendritic spine morphology is altered because of LTP and LTD deficits or 2) synaptic plasticity processes are defect because of morphological changes in synapse structure. Thus, in order to understand if alterations in dendritic spine structure (which is defined by actin) are the cause or the consequence of synaptic phenotypes in FXS, it will be necessary to understand how the loss of FMRP affects the regulation of synaptic actin.

3.6.2 Imbalance of synaptic actin in the Fragile X Syndrome

Given the overall relevance for the understanding of FXS neuropathology, surprisingly little is known about the direct involvement of actin or ABPs in this disease. Up until now, multiple studies done in *fmr1* KO mice suggest that actin regulation via the Rho GTPase signaling pathway is altered (Boda et al., 2014; Bongmba et al., 2011; Dolan et al., 2013; Pyronneau et al., 2017). It could be shown *in vivo* that these animals have an unnaturally high dendritic spine turnover in the cortex when FMRP expression is at its peak (Cruz-Martin et al., 2010; Harlow et al., 2010), thereby indicating alterations in spine actin dynamics. In addition, activity-dependent spine stabilization was found to be lost in *fmr1* KO neurons but could be rescued by enhancing PI3K signaling which controls both positive and negative regulators of Rho GTPases (Boda et al., 2014). Furthermore, evidence exists that the Rho GTPase Rac1 is overactive which might lead to an over-activation of PAK (Pyronneau et al., 2017) and finally, deficits in activity-dependent actin modulations during synaptic plasticity. In line with this, pharmacological manipulation of Rac1 activity could rescue long-term synaptic plasticity deficits (Bongmba et al., 2011) and inhibition of PAKs rescued spine abnormalities as well as behavioral phenotypes in *fmr1* KO mice (Dolan et al., 2013). Overall, these data suggest a functional link between impaired cognition, plasticity defects, spine morphology and finally, actin regulation in FXS.

Nevertheless, although large scale studies could identify hundreds of FMRP-target mRNAs in neurons so far (Ascano et al., 2012; Darnell et al., 2011), unexpectedly, only very few mRNAs of actin regulators were confirmed as valid FMRP-binding partners. Primarily, ABP mRNAs

with either U-rich or G-rich sequences, which are suggested to fold in to G-quadruplexes were found to be directly interacting with FMRP, including mRNAs encoding for MAP1B (Darnell et al., 2011) as well as Pfn1 (Michaelsen-Preusse et al., 2016). Interestingly, the *Drosophila melanogaster* dFMRP was shown to bind the homologs for Rac1 (Lee et al., 2003), MAP1B (futsch) (Zhang et al., 2001b) and Pfn1 (chickadee) (Reeve et al., 2005) as well, indicating that there might be highly conserved key FMRP-target mRNAs not only in mammals. Remarkably, manipulation of expression of the FMRP-target Pfn1 could even suppress phenotypes of *dfmr1* KO flies (Reeve et al., 2005) as well as rescue the immature spine phenotype in *fmr1* KO mice (Michaelsen-Preusse et al., 2016), thereby highlighting its potential importance for the neuropathology in FXS.

Notably, several other ABP mRNAs encoding for e.g. cortactin, members of the Arp2/3 complex as well as Cof1 are predicted to be bound by FMRP (Ascano et al., 2012) but were not further validated and verified yet. From these, Cof1 might be of special interest as recently, aberrant phosphorylation of Cof1 via the Rac-PAK pathway could be directly linked to impairments in spine morphology as well as synaptic efficacy in FXS (Pyronneau et al., 2017). As in addition, spine immaturity was found to correlate with reduced expression of Cof1 (Hotulainen et al., 2009), this ABP indeed might play an important role in the pathogenesis of FXS. Nevertheless, if FMRP directly interacts with Cof1 mRNA and thus also is able to interfere with global or even local translation of Cof1 is still unknown.

Summed up, from the current knowledge, cognitive impairments in FXS are likely to result from dysregulated protein synthesis at the synapse which leads to synaptic dysfunction and abnormal dendritic spine morphology. As several findings indicate aberrant modulations of synaptic actin, the absence of FMRP might therefore cause changes in the amount of locally available actin regulators. This would affect the general organization of synaptic actin and could provide a potential explanation how dendritic spine pathologies in FXS develop. Thus, to unravel the underlying molecular mechanisms will not only be crucial for understanding the neuropathology of FXS but will be of general relevance to human health, as also in various other forms of mental retardation as well as in autism related disorders (e.g. Rett Syndrome, Down Syndrome, Angelman Syndrome or Tuberous sclerosis) atypical morphologies as well as numbers of dendritic spines can be observed.

3.7 Aim of study

Memory storage is widely believed to involve long-lasting modifications of synaptic efficacy and is associated with either strengthening or weakening of specific synapses. The underlying mechanisms have been shown to be dependent on *de novo* gene transcription but also translation of pre-existing mRNAs. These local translation events allow synapses to autonomously and specifically change their structural and functional properties on a rapid time scale, a phenomenon that crucially depends on a fast remodeling of the actin cytoskeleton mediated by actin-binding proteins. As a large number of ABPs is involved, the question arises how these processes are regulated, if ABPs are locally translated at dendritic spines upon need and if mRNA localization of ABPs is influenced by neuronal activity. As the activity-dependent local translation of actin regulators has not been shown yet, this study aimed to link local ABP translation and actin regulation upon synaptic plasticity in the healthy and diseased central nervous system. As several forms of mental retardation were linked to alterations in actin regulatory mechanisms, this work focused on the most frequent monogenetic form of mental retardation, utilizing the *fmr1* KO mouse model of the Fragile X Syndrome. FXS is characterized by loss of the RNA-binding protein FMRP leading to heavy translational alterations globally as well as locally. In the hippocampus, this leads to impairments in synapse function (NMDAR-dependent LTP as well as mGluR-dependent LTD) and structure pointing towards dysregulated actin dynamics. Thus, to unravel the general as well as the neuropathological relevance of local ABP translation for learning and memory, this study aimed to answer the following core-questions:

1) How are ABP mRNAs distributed in hippocampal *fmr1* wildtype and *fmr1* KO neurons?

2) Are ABP mRNAs found in dendrites or dendritic spines? Are they locally translated? If so, is their local translation activity-dependent? Is local ABP translation dysregulated in FXS?

3) Is ABP mRNA localization in hippocampal neurons changing after the induction of synaptic plasticity (NMDAR-dependent LTP/mGluR-dependent LTD)? Is this mechanism dysregulated in FXS?

This study focused on the analysis of the mRNAs of neuronal Pfn isoforms as well as Cof1 as earlier studies suggested that these mRNAs might be directly interacting with FMRP (Ascano et al., 2012; Reeve et al., 2005) and both proteins were previously confirmed to be involved in mediating NMDAR-dependent LTP as well as mGluR-dependent LTD.

4 Materials and Methods

4.1 Materials

4.1.1 Lab equipment

Equipment	Distributor
24-well plate	Sarstedt
96-well microtest plate	Sarstedt
Binocular	Zeiss
Bunsen burner	Sigma-Aldrich Chemie GmbH
Centrifuge ‘Sigma 4K 15’	Sigma-Aldrich Chemie GmbH
- rotor number 12167	
- rotor number 12256	
- rotor number 12166-H	
CO_2 incubator	Binder
Cover slips (Ø 13 mm)	VWR International
Cryotome ‘CM3050 S’	Leica Biosystems
CURIX cassette MR 200	AGFA Healthcare GmbH
Eppendorf Thermomixer 5436	Eppendorf-Netheler-Hinz GmbH
Falcon tubes 10 ml, 15 ml, 50 ml	Sarstedt
Fluoromount	Electron Microscopy Sciences
Gel casting chamber	Sigma-Aldrich Chemie GmbH
Gel chamber	Sigma-Aldrich Chemie GmbH
Gel documentation system ‘Herolab E.A.S.Y. RH’	Herolab GmbH
Gloves ‚Style Grape L‘	Med Comfort
Heating block ‘Dri Block DB.2A	Techne
Incubator ‘kelvitron® t’	Heraeus Instruments
Laser scanning microscope ‘BX61WI’	Olympus Europa SE & Co. KG
- 40x oil objective ‘UPLFLN’	
- 60x water objective ‘LUMPLFLN’	
LucentBlue X-ray films	advansta
Magnetic stirrer ‚Ikamat Ret‘	Janke & Kunkel GmbH & Co. KG
Micropipettes 10 µl, 20 µl, 100 µl, 200 µl, 1000 µl	Gilson
Microscope slides	VWR International
MIDI-PREP Kit	Qiagen
MilliQ H_2O producer ‘MilliQ Biocel A10’	Millipore Corporation
MINI-PREP Kit	Qiagen

Equipment	Distributor
MRX microplate reader	Dynatech Medical Products
Neubauer counting chamber	Carl Roth GmbH & Co. KG
Pasteur pipettes	Sigma-Aldrich
Petri dishes	TPP
Precision scale ‘BP 221S - OCE’	Sartorius AG Göttingen
Power supply ‘BluePower 500’	Serva
Razor blades	MARTOR KG
Reaction tubes 1,5 ml	Eppendorf AG
Roti-Fluoro PVDF membrane 0,2 µm	Carl Roth GmbH & Co. KG
Safe lock reaction tubes 1,5 ml	Sarstedt
Safe lock reaction tubes 1,5 ml Rnase-free	Sarstedt
Semidry blotter	Fröbel Labortechnik
Shaker ‘Type RS-PL 28-10’	Heto Lab Equipment
Sterile filter (Ø 0.2 µm)	Schleicher & Schuell
Table centrifuge ‘Perfect Spin’	Peqlab
Thermocycler for DNA ligations	Landgraf Laborsysteme
Thermocycler for PCR ‘PTC 200’	MJ Research
UV table	Biometra
Vortex Genie 2	Bender & Hobein AG
Water bath type 3047	Köttermann GmbH & Co.KG
Water maze (d = 160 cm, h = 60 cm)	TSE Systems
- platform (d = 10 cm)	custom made
- camera ‘VK-1316S / 12V’	eneo
Whatman paper	Carl Roth GmbH & Co. KG

4.1.2 Reagents

4.1.2.1 Reagents used for genotyping

Compound	Distributor
Agarose	Sigma-Aldrich Chemie GmbH
EDTA	Applichem
EDTA *Na_2*2 H_2O	Applichem
Ethanol	VWR International
HCl	Sigma-Aldrich Chemie GmbH
Isopropanol	VWR International
NaCl	Grüssing GmbH
Proteinase K	Thermo Scientific

Compound	Distributor
SDS	Carl Roth GmbH & Co. KG
TRIS	Applichem

4.1.2.2 Reagents used for the preparation of cultures

Compound	Distributor
B27	Gibco
Boric acid	Merck KGaA
$CaCl_2$	Applichem
$CaCl_2 * 2 H_2O$	Applichem
D-Glucose	Applichem
DMEM	Gibco
FCS	PAA Laboratories
KCl	Applichem
KH_2PO_4	Applichem
L-Glutamin	Gibco
$MgCl_2 * 6 H_2O$	Applichem
$MgSO_4 * 7 H_2O$	Applichem
N2	selfmade
NaCl	Grüssing GmbH
Na_2HPO_4	Applichem
$NaHCO_3$	Applichem
NaH_2PO_4	Applichem
NaOH 10M	Applichem
Neurobasal- medium	Gibco
Paraformaldehyde	Sigma-Aldrich Chemie GmbH
Poly-L-lysin	Sigma-Aldrich Chemie GmbH
Sodium tetraborate decahydrate	Sigma-Aldrich Chemie GmbH
Sucrose	Carl Roth GmbH & Co. KG
Trypsin EDTA solution	Sigma-Aldrich Chemie GmbH

4.1.2.3 Reagents used for transfections

Compound	Distributor
B27	Gibco
L-Glutamin	Gibco
Lipofectamine® 2000	Invitrogen
N2	selfmade

Compound	Distributor
Neurobasal$^-$ medium	Gibco

4.1.2.4 Reagents used for the chemical induction of long-term plasticity

Compound	Distributor
B27	Gibco
$CaCl_2$ * 2 H_2O	Applichem
DHPG	Roche
Glucose	Applichem
Glycine	Applichem
HBSS 10x	Sigma-Aldrich Chemie GmbH
KCl	Applichem
L-Glutamine	Gibco
Mg^{2+}-free Ca^{2+}-free HBSS 10x	Sigma-Aldrich Chemie GmbH
$MgCl_2$ * 6 H_2O	Applichem
N2	selfmade
NaCl	Grüssing GmbH
$NaHCO_3$	Applichem
NaH_2PO_4	Applichem
Neurobasal$^-$ medium	Gibco
Paraformaldehyde	Sigma-Aldrich Chemie GmbH
Strychnine	Sigma-Aldrich Chemie GmbH

4.1.2.5 Reagents used for Fluorescence *in situ* hybridizations

Compound	Distributor
Acetic anhydride	Fluka Biochemie
Agarose	Sigma-Aldrich Chemie GmbH
Blocking reagent	Roche
BSA 10x	Sigma-Aldrich Chemie GmbH
Chloroform	Carl Roth GmbH & Co. KG
Cut smart buffer	New England Biolabs
DAPI	Applichem
DIG-RNA labeling mix	Roche
Dithiotreitol	Promega Corporation
EcoRI High Fidelity	New England Biolabs
Formamide 99.5%	Sigma-Aldrich Chemie GmbH
Ethanol 96%	VWR International

Compound	Distributor
H_2O_2 30%	Applichem
KCl	Applichem
KH_2PO_4	Applichem
Lithium chloride	Sigma-Aldrich Chemie GmbH
Maleic acid	Sigma-Aldrich Chemie GmbH
Na_2HPO_4	Applichem
NaAc	Applichem
NaCl	Grüssing GmbH
NotI	New England Biolabs
Paraformaldehyde	Sigma-Aldrich Chemie GmbH
Phenol-chloroform	Carl Roth GmbH & Co. KG
RNase-free H_2O	Deltamedica
Rnasin	Promega Corporation
RQ1 Rnase-free Dnase	Promega Corporation
T3 RNA polymerase	Promega Corporation
T7 RNA polymerase	Promega Corporation
Transcription buffer 5x	Promega Corporation
Triethanolamine	Fluka Biochemie
Tri-Sodium citrate dihydrate	Applichem
Triton-X 100	Carl Roth GmbH & Co. KG
TSA Cyanine 3 System	Perkin Elmer
- blocking reagent	
- TSA Cy3	
- TSA Cy3 Fluorophore Working solution	
Tween-20	Carl Roth GmbH & Co. KG
Urea	Applichem
XhoI	New England Biolabs

4.1.2.6 Reagents used for local translation experiments

Compound	Distributor
Anisomycin	Sigma-Aldrich Chemie GmbH
Ampicillin	Carl Roth GmbH & Co. KG
Agarose	Sigma-Aldrich Chemie GmbH
ATP 10 mM	New England Biolabs
$CaCl_2$ * 2 H_2O	Applichem
Cut smart buffer	New England Biolabs
DNA elution Kit	Qiagen

Compound	Distributor
DNA sample buffer 6x	Thermo Scientific
Glucose	Applichem
Glycine	Applichem
HBSS 10x	Sigma-Aldrich Chemie GmbH
10x Mg^{2+}-free Ca^{2+}-free HBSS	Sigma-Aldrich Chemie GmbH
MIDI Prep Kit	Qiagen
MINI Prep Kit	Qiagen
NaCl	Grüssing GmbH
$NaHCO_3$	Applichem
NheI	New England Biolabs
Ligation buffer 10x	Thermo Scientific
Strychnine	Sigma-Aldrich Chemie GmbH
T4 DNA ligase	Thermo Scientific
Trypton	Applichem
XhoI	New England Biolabs
Yeast extract	DIFCO

4.1.2.7 Reagents used for Western blotting

Compound	Distributor
APS	Applichem
ß-Mercaptoethanol	Applichem
Bromphenol Blue	Applichem
BSA	Sigma-Aldrich Chemie GmbH
Chaps	Serva
Coomassie Brilliant Blue G250	Applichem
Complete protease inhibitor	Roche
Ethanol	VWR International
Glycerol 87%	Applichem
Glycine	Applichem
KCl	Applichem
Luminata™ Crescendo	Millipore Corporation
Methanol	Fischer Scientific UK
$MgCl_2$	Applichem
Milk powder	Sucofin
NaCl	Grüssing GmbH
PageRuler Plus Prestained Protein Ladder	Thermo Scientific
Phosphoric acid	Applichem

Compound	Distributor
PhosSTOP phatase inhibitor	Roche
Polyacrylamide 37.5%	Carl Roth GmbH & Co. KG
Roentogen Developer	TETENAL Europe GmbH
Roentogen Superfix	TETENAL Europe GmbH
Saccharose	Applichem
SDS	Carl Roth GmbH & Co. KG
TEMED	Sigma-Aldrich Chemie GmbH
TRIS	Applichem
Triton-X 100	Carl Roth GmbH & Co. KG
Tween 20	Carl Roth GmbH & Co. KG

4.1.2.8 Reagents used for the manipulation of actin dynamics

Compound	Distributor
$CaCl_2$ * 2 H_2O	Applichem
CytochalasinD	Sigma-Aldrich Chemie GmbH
Glucose	Applichem
Glycine	Applichem
HIV-TAT pcof1 peptide	Thermo Scientific
Jasplakinolide	Sigma-Aldrich Chemie GmbH
10x Mg^{2+}-free Ca^{2+}-free HBSS	Sigma-Aldrich Chemie GmbH
$NaHCO_3$	Applichem
Paraformaldehyde	Sigma-Aldrich Chemie GmbH
Strychnine	Sigma-Aldrich Chemie GmbH

4.1.2.9 Reagents used for the analysis of mRNA transport

Compound	Distributor
Agarose	Sigma-Aldrich Chemie GmbH
Ampicillin	Carl Roth GmbH & Co. KG
ATP 10mM	New England Biolabs
Cut Smart buffer	New England Biolabs
DNA Sample buffer 6x	Thermo Scientific
EcoRI	New England Biolabs
T4 DNA Ligase	Thermo Scientific
XhoI	New England Biolabs

4.1.3 Buffers and solutions

4.1.3.1 Buffers and solutions used for genotyping

Solution	Composition	
Lysis buffer	Tris-HCl pH 8.0	100 mM
	EDTA	5 mM
	NaCl	200 mM
	SDS	0.2 %
	Proteinase K	100 µg/mL
	diluted in dH_2O	
TAE buffer 10x	Tris-HCL pH 7.5	48.46 g
	Eisessig	12.01 g
	EDTA *Na_2*2 H_2O	3.72 g
	in MQ-H_2O	1 L
TAE buffer 1x	TAE buffer 10x	100 mL
	in MQ-H_2O	900 mL
TRIS-HCL	TRIS diluted (in H_2O)	10 mM or 100 mM
	adjust pH with HCl to 7.5 or 8.0	

4.1.3.2 Buffers and solutions used for culture preparation

Solution	Composition	
30% sucrose	sucrose	30%
	in MQ-H_2O	
4% Paraformaldehyde	paraformaldehyde	4%
	in 1x PBS	
aCSF	$CaCl_2$ * 2 H_2O	2 mM
	KCl	2.5 mM
	NaH_2PO_4	1.25 mM
	NaCl	125 mM
	$MgCl_2$ * 6 H_2O	1 mM
	$NaHCO_3$	26 mM
	D-Glucose	26 mM

Solution	Composition	
Borate buffer	Boric acid	0.31 g
	Sodium tetraborate decahydrate	0.475 g
	in H_2O	100 mL
	adjust pH to 8.5	
complete medium	Neurobasal$^-$ medium	45 mL
	N2	5 mL
	B27	1 mL
	L-Glutamin 200 mM	125 µL
GBSS	NaCl	8 g
	D-Glucose	1 g
	KCl	0.37 g
	KH_2PO_4	0.03 g
	$MgCl_2$ * 6 H_2O	0.21 g
	$MgSO_4$ * 7 H_2O	0.07 g
	$NaHCO_3$	0.227 g
	Na_2HPO_4	0.12 g
	$CaCl_2$	0.22 g
	in H_2O	1 L
Serum medium	DMEM	10 mL
	FCS	200 µL

4.1.3.3 Buffers and solutions used for transfections

Solution	Composition	
Neurobasal$^+$ medium	Neurobasal$^-$ medium	45 mL
	N2	5 mL
	B27	1 mL
	L-Glutamin 200 mM	125 µL

4.1.3.4 Buffers and solutions used for the chemical induction of long-term plasticity

Solution	Composition	
1x HBSS	10x HBSS	50 mL
	$NaHCO_3$	0.175 g
	$CaCl_2$ * 2 H_2O	0.147 g
	Glucose	1.351 g
	in MQ-H_2O	500 mL
1x Mg^{2+}-free HBSS	10x Mg^{2+}-free Ca^{2+}-free HBSS	5 mL
	$CaCl_2$ * 2 H_2O	4 mM
	in MQ-H_2O	45 mL
Paraformaldehyde 4%	paraformaldehyde	4%
	in 1x PBS	
Glycine-aCSF	Glycine	10 mM
	$CaCl_2$ * 2 H_2O	2 mM
	KCl	2.5 mM
	NaH_2PO_4	1.25 mM
	NaCl	125 mM
	$MgCl_2$ * 6 H_2O	1 mM
	$NaHCO_3$	26 mM
	Glucose	26 mM
Neurobasal$^+$ medium	Neurobasal$^-$ medium	45 mL
	N2	5 mL
	B27	1 mL
	L-Glutamin 200 mM	125 µL

4.1.3.5 Buffers and solutions used for Fluorescence *in situ* hybridizations

Solution	Composition	
10x PBS	NaCl	80 g
	KCl	2 g
	$Na2HPO_4$ x 2 H_2O	14.4 g
	KH_2PO_4	2.4 g
	in RNase-free H2O	1 L
	adjust pH to 7.4	

Solution	Composition	
1x PBS	10x PBS	50 mL
	in RNase-free H_2O	450 mL
20x SSC	NaCl	175.3 g
	Tri-Sodium citrate dihydrate	88.25 g
	in RNase-free H_2O	
	adjust pH to 7.0	
5x SSC	20x SSC	12.5 mL
	in RNase-free H_2O	37.5 mL
2x SSC	20x SSC	5 mL
	in RNase-free H_2O	45 mL
0.2x SSC	20x SSC	0.5 mL
	in RNase-free H_2O	49.5 mL
Blocking reagent 10%	Blocking reagent	10 g
	Maleic acid buffer	100 mL
	autoclave solution	
Ethanol 80%	Ethanol 96 %	80 mL
	in MQ-H_2O	20 mL
Ethanol 70%	Ethanol 96 %	70 mL
	in MQ-H_2O	30 mL
Hybridization mix	20x SSC	3.75 mL
	Formamide or Urea 8M	7.5 mL
	Blocking reagent 10%	3 mL
	in RNase-free H_2O	0.75 mL
H_2O_2 3%	H_2O_2 30%	1 mL
	in RNase-free H_2O	9 mL
Lithium chloride 8M	Lithium chloride	8 M
	in RNase-free H_2O	

Solution	Composition	
Maleic acid buffer	Maleic acid	11.6 g
	NaCl	8.75 g
	in RNase-free H_2O	1 L
	adjust pH to 7.5	
	autoclave solution	
NaAc 3 M	NaAc	3 M
	in RNase-free H_2O	
Paraformaldehyde 4%	paraformaldehyde	4%
	in 1x PBS	
TNB buffer	Tris-HCl pH 7.5 1 M	10%
	NaCl	0.15 M
	Tween-20	0.05%
TNT buffer	Tris-HCl pH 7.5 1 M	10%
	NaCl	0.15 M
	Blocking reagent from TSA Cy3	0.5%
	add slowly while heating to 55°C	
Tris-HCl buffer	TRIS	0.01 M or 1 M
	in MQ-H_2O	
	adjust pH to 7.5	
Triton-X 0.5% 1x PBS	1x PBS	50 mL
	Triton-X 100	250 µL
TSA working solution	TSA Cyanine 3	
	in RNase-free H_2O	300 µL
Urea 8M	Urea	8 M
	in RNase-free H_2O	

4.1.3.6 Buffers and solutions used for local translation experiments

Solution	Composition	
1x HBSS	10x HBSS	50 mL
	$NaHCO_3$	0.175 g
	$CaCl_2$ * 2 H_2O	0.147 g
	Glucose	1.351 g
	in MQ-H_2O	500 mL
1x Mg^{2+}-free HBSS	10x Mg^{2+}-free Ca^{2+}-free HBSS	5 mL
	$CaCl_2$ * 2 H_2O	4 mM
	in MQ-H_2O	45 mL
Lysogeny broth medium	Trypton	10 g/L
	NaCl	10 g/L
	Yeast extract	5 g/L

4.1.3.7 Buffers and solutions used for Western blotting

Solution	Composition	
10x MeOH blot buffer	TRIS	0.25 M
	Glycine	1.5 M
	in MQ-H_2O	2 L
	adjust pH to 8.6	
1x MeOH blot buffer	Methanol	100 mL
	10x MeOH blot buffer	100 mL
	in MQ-H_2O	800 mL
10x TBS-T	TRIS	0.2 M
	NaCl	1.37 M
	Tween 20	0.1%
	in MQ-H_2O	
	adjust pH to 7.6	
1x TBS-T	10x TBS-T	200 mL
	in MQ-H_2O	1.8 L

Solution	Composition	
10x TBS-X	TRIS	0.2 M
	NaCl	1.37 M
	Triton-X 100	0.1%
	in MQ-H_2O	
	adjust pH to 7.6	
1x TBS-X	10x TBS-X	200 mL
	in MQ-H_2O	1.8 L
Bradford reagent 5x	Phosphoric acid	100 mL
	Ethanol	50 mL
	Coomassie Brilliant Blue G250	100 mg
	in MQ-H_2O	100 mL
Developing solution	Roentogen Developer	
	in H_2O	
Fixing solution	Roentogen Superfix	
	in H_2O	
Lysis buffer	Tris-HCl pH 7.5	30 mM
	NaCl	150 mM
	Chaps	1%
	in MQ-H_2O	
milk 5% in TBS-T	Milk powder	5%
	in 1x TBS-T	
SDS buffer 4x	Tris-HCL pH 7.5	0.375 M
	SDS	2%
	Glycerol 87%	12%
	Bromphenol blue	0.05%
	ß-Mercaptoethanol	10%
STKM buffer	Saccharose	250 mM
	Tris-HCL pH 7.5	50 mM
	KCl	25 mM
	$MgCl_2$	5 mM
	adjust pH to 7.5 at 4°C	

4.1.3.8 Buffers and solutions used for the manipulation of actin dynamics

Solution	Composition	
1x HBSS	10x HBSS	50 mL
	$NaHCO_3$	0.175 g
	$CaCl_2 * 2 H_2O$	0.147 g
	Glucose	1.351 g
	in MQ-H_2O	500 mL
1x Mg^{2+}-free HBSS	10x Mg^{2+}-free Ca^{2+}-free HBSS	5 mL
	$CaCl_2 * 2 H_2O$	4 mM
	in MQ-H_2O	45 mL
Paraformaldehyde 4%	paraformaldehyde	4%
	in 1x PBS	

4.1.4 Antibodies

Antibody	Antibody type	Host	Final dilution	Distributor	Product No.
anti-cofilin1	primary	rabbit	1:15000	abcam	ab11062
anti-Digoxygenin HRP	primary	sheep	1:2000	Roche	11207733910
anti-GAPDH	primary	rabbit	1:9000	Sigma	G9545
anti-GFP	primary	Hyb. cell	1:500	Clontech	632381
anti-mouse Cy2	secondary	goat	1:1000	Dianova	115-225-146
anti-profilin 1 C-terminal	primary	rabbit	1:5000	Sigma	P7624
anti-profilin 2a as361	primary	rabbit	1:20000	Bioscience	-
anti-rabbit HRP	secondary	goat	1:20000	Sigma	A0545

4.1.5 DNA plasmids

Plasmid	Backbone	Insert	Distributor	Database signature
pBS SK mCof1	pBS SK(-)	cDNA mCof1	-	B142
pBS SK mPfn1	pBS SK(-)	cDNA mPfn1	-	B134
pBS SK mPfn2a	pBS SK(-)	cDNA mPfn2a	-	B135
pcDNA3-LCK-MYR-eGFP	pcDNA3	-	-	E507

Plasmid	Backbone	Insert	Distributor	Database signature
pcDNA3-LCK-MYR-eGFP 3'UTR ß-actin	pcDNA3	3'UTR ß-actin	-	E438
pcDNA3-LCK-MYR-eGFP 3'UTR Cof1	pcDNA3	3'UTR Cof1	-	E441
pcDNA3-LCK-MYR-eGFP 3'UTR Pfn1	pcDNA3	3'UTR Pfn1	-	E440
pcDNA3-LCK-MYR-eGFP 3'UTR Pfn2a	pcDNA3	3'UTR Pfn2a	-	E439
pcDNA3-LCK-MYR-eGFP 3'UTR 5'UTR Pfn2a	pcDNA3	3'+5' UTR Pfn2a	-	E443
pEGFP-F	-	-	-	E190
pmApple-N1	-	-	-	L81
pmA-T-mCof1 3'UTR	pmA-T	mCof1 3'UTR	Invitrogen	B136
pmA-RQ-mCof1 5'UTR	pmA-RQ	mCof1 5'UTR	Invitrogen	B137
pmA-T-mPfn1 3'UTR	pMA-T	mPfn1 3'UTR	Invitrogen	B138
pmA-RQ-mPfn1 5'UTR	pmA-RQ	mPfn1 5'UTR	Invitrogen	B139
pmA-RQ-mPfn2a 3'UTR	pmA-RQ	mPfn2a 3'UTR	Invitrogen	B140
pmA-RQ-mPfn2a 5'UTR	pmA-RQ	mPfn2a 5'UTR	Invitrogen	B141
pSL-MS2-12x	12x-MS2	-	Addgene	E383
pMS2-GFP	MS2-GFP	-	Addgene	E385
pcDNA3	-	-	-	L70
pcDNA3-12x MS2	12x MS2	-	-	B144
pcDNA3-12xMS2-3'UTR Cof	12x MS2	3'UTR Cof1	-	E442

4.1.6 Software

Software	Distributor
Adobe Illustrator	Adobe Systems Software
AnyMaze	Stoelting Europe
EasyWin32	Herolab GmbH
ImageJ	Wayne Rasband, NIH, USA
Microsoft Excel	Microsoft Corporation
Microsoft Word	Microsoft Corporation
Prism Graphpad 5	Graph Pad Software Incorporation
SPSS Statistics Client	IBM

4.2 Methods

4.2.1 Mouse strains

fmr1 KO mice in a FVB129 background were obtained from the Jackson laboratory (Strain 004624) and back-crossed for at least ten generations into C57 BL/6JOlaHsd *fmr1* wildtype mice expressing enhanced green fluorescent protein (eGFP) under the Thy-1 promotor. As the *fmr1* gene is located on the X chromosome, GFP positive *fmr1*$^{y/-}$ males and GFP positive *fmr1*$^{+/-}$ females were bred to obtain offspring carrying the GFP positive *fmr1* wildtype (*fmr1* WT) or the GFP positive *fmr1* knockout (*fmr1* KO) genotype which were used for all experiments done in this study. For genotyping, tissue was collected via tail biopsy.

All animals were kept in standard conditioned cages, exposed to a 12 h dark/light cycle with *ad libitum* access to food and water. Additionally, all mice bred for experiments were used for preplanned experiments and randomized to experimental groups while visibly sick animals were excluded before data collection. Overall, the experimental design and handling of mice were identical across experiments. All experiments performed were authorized by the LAVES (Oldenburg, Germany, Az. §4 (02.05) TSchB TU BS) and the animal welfare representative of the TU Braunschweig.

4.2.2 Genotyping of transgenic animals

For the isolation of DNA, tissue was obtained via tail biopsy. Individual tail tips were digested over-night in 500 µL lysis buffer with freshly added proteinase K at 55 °C, followed by removal of cellular debris by 4 °C centrifugation at 14.000 x g for 10 min. The supernatant was transferred into a new reaction tube containing 500 µL isopropanol and inverted ten times to precipitate the DNA. Subsequently, the solution was centrifuged for 15 min at 4 °C and 14.000 x g and the pellet was washed with 1 mL of ethanol. Afterwards, the solution was centrifuged for 15 min at 14.000 x g and 4 °C and the supernatant was discarded. Finally, the remaining pellet was air-dried, rehydrated for 1h at 37 °C in 50 µL TAE-buffer and stored at 4 °C. The amplification of the respective alleles was done via polymerase chain reaction (PCR) (Table 1, Table 2) using specific primer sequences against *fmr1* and GFP (Table 3). Lastly, the amplified DNA fragments were separated by gel electrophoresis in a 1.5 % agarose gel running for 45 min at 80 V and 150 mA.

Table 1 - Polymerase chain reaction for *fmr1*

Sample preparation		PCR protocol		
Component	**Concentration**	**Step**	**Temperature [°C]**	**Time [s]**
PCR buffer	1x	1	94	500
$MgCl_2$	2 mM	2	94	30
dNTPs	10 nM	3	62	30
Forward primer	100 nM	4	72	60
Reverse primer	100 nM		Steps 2-4 repeated 34 cycles	
GoTaq polymerase	1 unit	5	10	hold
DNA	1 µL			
Filled up with ddH_2O				

Table 2 - Polymerase chain reaction for GFP

Sample preparation		PCR protocol		
Component	**Concentration**	**Step**	**Temperature [°C]**	**Time [s]**
PCR buffer	1x	1	94	120
$MgCl_2$	2 mM	2	94	20
dNTPs	10 nM	3	65	15
Primer IL-2 fwd (G28)	0.5 µM	4	68	10
Primer IL-2 rev (G29)	0.5 µM		Steps 2-4 repeated 10 cycles	
Primer 15731 (G113)	0.5 µM	5	94	15
Primer 16072 (G114)	0.5 µM	6	60	15
GoTaq polymerase	0.5 µM	7	72	10
DNA	0.5 µL		Steps 5-7 repeated 28 cycles	
Filled up with ddH_2O		8	72	120
		9	10	hold

Table 3 - Primers used for genotyping

Primer	Target	Primer type	Sequence
oIMR2060 (G70)	*fmr1* KO	Mutant fwd	5’ TGT GAT AGA ACT AGT GAG ACG TG 3’
oIMR6734 (G71)	*fmr1* WT	Wildtype fwd	5’ TGT GAT AGA ATA TGC AGC ATG TGA 3’
oIMR6735 (G72)	*fmr1* WT	Common	5’ CTT CTG GCA CCT CCA GCT T 3’
Primer IL-2 fwd (G28)	GFP	Thy1 GFP fwd	5’ CTA GGC CAC AGA ATT GAA AGA TCT 3’
Primer IL-2 rev (G29)	GFP	Thy1 GFP rev	5’ GTA GGT GGA AAT TCT AGC ATC ATC C 3’
Primer 15731 (G113)	GFP	Transgene rev	5’ CGG TGG TGC AGA TGA ACT T 3’
Primer 16072 (G114)	GFP	Transgene fwd	5’ ACA GAC ACA CAC CCA GGA CA 3’

4.2.3 Culture systems

4.2.3.1 Preparation of coverslips

Coverslips were incubated in 10 M NaOH for 3 to 5 h at 100 °C and washed 5 times for 20 min with MQ-H_2O. Afterwards, they were dried for 6 h at 225 °C before coating with poly-L-lysine 0.5 $\frac{mg}{ml}$ in borate buffer was performed over-night at 4 °C. Finally, coverslips were washed 5 times with MQ-H_2O, dried at room temperature and placed and stored until use in 24-well plates at 4 °C.

4.2.3.2 Preparation of primary embryonic hippocampal cell cultures

For the preparation of primary embryonic hippocampal cell cultures, hippocampi were harvested at embryonic day E18.5. Therefore, time mated female mice were rapidly killed by cervical dislocation and the peritoneum and uterus were opened by scissors. Subsequently, the embryos were taken out and decapitated. The heads of the embryos were placed in ice cold GBSS and individually dissected as fast as possible. By forceps, the skin and the skull were removed, the brain was taken out and afterwards, the two hemispheres were separated using a spatula. The *pia mater* was pulled off and finally, the hippocampi were removed. Collectively, prepared hippocampi were stored in ice cold GBSS, then transferred into 1 mL of a trypsin EDTA solution and were incubated by 37 °C for 27 min while being inverted multiple times. With a pipette, the trypsin solution was removed and the hippocampi were washed with 1 mL of serum medium 6 times. Afterwards, they were homogenized by carefully syringing them through a narrowed Pasteur pipette and centrifuged for 5 min with 1.500 rpm. Finally, the supernatant was discarded and the cell pellet was resolved in 1 mL of complete medium. The number of isolated cells was determined by counting a 1:10 dilution in a Neubauer counting chamber and the needed number of cells was diluted in the correct amount of complete medium. For 1 well of a 24 well plate (containing 1 poly-L-lysine coated Ø 15 mm coverslip) 70.000 cells in 150 µl complete medium were sowed. Subsequently, cells were incubated at 37 °C for 3 h followed by an addition of 350 µl prewarmed complete medium. Finally, until use after 21 days *in vitro* (DIV) cells were kept in an incubator at 37 °C with 5% CO_2 with weekly medium changes of 10%.

4.2.3.3 Preparation of hippocampal slices

For the preparation of hippocampal slices, mice were killed by cervical dislocation and subsequently decapitated. By forceps, the skin and skull cap were removed and the brain was taken out and placed in ice cold GBSS. The *pia mater* was removed, the two hemispheres were separated using a razor blade and finally, the hippocampi were taken out and post-fixated in 4% PFA for 2 h. Afterwards, they were incubated for 24 h in 30% sucrose solution before they were embedded in Tissue Tek® and stored at -70 °C for later use. Upon need, the frozen hippocampi were cut into 30 µm thick slices using a cryotome.

4.2.3.4 Preparation of acute hippocampal slices

For acute hippocampal slice preparation, mice were anesthetized with isoflurane and decapitated immediately. Via forceps, the skin and the skull cap were removed from the head and the brain was taken out and placed in ice cold, CO_2 saturated artificial cerebrospinal fluid (aCSF) for 3 min. Then, the *pia mater* was removed, the two hemispheres were separated using a razor blade and the hippocampi were taken out. Subsequently, they were glued in front of a small agarose block on a solid metal plate which was then fixed on a vibratome and submerged in ice cold, CO_2 saturated aCSF. Finally, using the vibratome, the hippocampi were cut in 400 µm thick slices which were collected with a brush and placed in a 'pool' containing ice cold, CO_2 saturated aCSF.

4.2.4 Transfection of plasmid DNA

To induce the expression of a specific protein (or multiple proteins) in individual neurons, primary embryonic hippocampal cell cultures were transfected with the respective DNA plasmids using Lipofectamine® 2000. Therefore, plasmid DNA (1 µg per well of a 24 well plate) as well as Lipofectamine® (2 µl per well) were individually incubated (50 µL per well) for 5 min in 37 °C prewarmed Neurobasal$^-$ (NB^-) medium. Afterwards, both solutions were mixed (= a total of 100 µL per well), shortly vortexed and incubated for 20 min at room temperature. In the meantime, Neurobasal$^+$ (NB^+) medium was placed in the incubator at 37 °C and 5% CO_2 (150 µL per well). After 20 min, 350 µL NB^+ medium (per well) were taken off of the primary embryonic hippocampal cell culture, mixed with the preincubated new NB^+ medium and kept in the incubator for later use. Subsequently, 100 µL of the transfection mix containing plasmid DNA and Lipofectamine® were gently added to each well and the plate was incubated for 50 min at 37 °C and 5% CO_2 in the incubator. Finally, the ligation mix was removed completely and 500 µL of the preincubated NB^+ medium were added to each well. Afterwards, the cultures

were kept at 37 °C and 5% CO_2 for either 24 h or 48 h before they were used for experiments. A list of all DNA plasmids that were used for transfections can be found in Table 4.

Table 4 – List of DNA plasmids used for transfections

Plasmid	Expression of	Generated by	Database signature
pEGFP-F	eGFP	A. Wolf	E190
pmApple-N1	mApple	M.W. Davidson	L81
pcDNA3-LCK-MYR-eGFP	MYR-eGFP	J. Feuge	E507
pcDNA3-LCK-MYR-eGFP 3'UTR ß-actin	MYR-eGFP-3'UTR ß-actin	R. Blum	E438
pcDNA3-LCK-MYR-eGFP 3'UTR Pfn1	MYR-eGFP-3'UTR Pfn1	J. Feuge	E440
pcDNA3-LCK-MYR-eGFP 3'UTR Pfn2a	MYR-eGFP-3'UTR Pfn2a	J. Feuge	E439
pcDNA3-LCK-MYR-eGFP 3'UTR Cof1	MYR-eGFP-3'UTR Cof1	J. Feuge	E441
pcDNA3-LCK-MYR-eGFP 3'UTR 5'UTR Pfn2a	MYR-eGFP-3'UTR-5'UTR Pfn2a	J. Feuge	E443

4.2.5 Chemical induction of long-term synaptic plasticity

4.2.5.1 cLTP induction in primary embryonic hippocampal cell cultures

Dissociated hippocampal primary cultures were taken out of the incubator and incubated in 1x Hank's Balanced Salt Solution (HBSS) for 20 min at room temperature. Afterwards, they were stimulated for 10 min using 1x Mg^{2+}-free HBSS containing the NMDAR agonist glycine (200 µM) and the glycine receptor blocker strychnine (3 µM). Subsequently, the Mg^{2+}-free HBSS was replaced with 1x HBSS and the cultures were incubated for a time course of up to 60 minutes. Finally, cultures were fixed using a 4% PFA solution.

4.2.5.2 cLTD induction in primary embryonic hippocampal cell cultures

For the induction of cLTD in dissociated hippocampal primary cultures, the group1 mGluR agonist Dihydroxyphenylglycine (DHPG) was diluted in 37 °C preincubated NB^- medium to a concentration of 100 µM. Subsequently, this solution was used to replace the NB^+ culture medium in all wells that were supposed to be stimulated (500 µL per well). After 10 min of

stimulation (in the incubator), the stimulation solution was removed and replaced by NB^+ medium. Cultures were then incubated for a time course of up to 60 min at 37 °C and 5% CO_2 and finally, for experimental use, cultures were fixed using a 4% PFA solution.

4.2.5.3 cLTP induction in acute hippocampal slices

Chemical long-term potentiation in acute hippocampal slices was induced 90 min after slice preparation. Slices were stimulated by transitionally replacing the aCSF solution with a 10 mM glycine containing aCSF solution for 10 min. Sixty minutes after the induction of cLTP, slices from the same hippocampus were pooled and used for Western blotting.

4.2.6 Analysis of mRNA localization via Fluorescence *in situ* Hybridization

The localization of mRNAs can reliably be analyzed via *in situ* hybridization. In this study, Digoxygenin-labelled antisense RNA against Pfn1, Pfn2a and Cof1 mRNA was produced *in vitro* which binds to its cellular sense mRNA strand. Hence, its localization can be observed by detecting the digoxygenin. Here, a horse reddish peroxidase (HRP) coupled antibody against digoxygenin was used in combination with the TSA Cyanine 3 System™ which utilizes the HRP to catalyze covalent deposition of cyanine 3.

4.2.6.1 *In vitro* synthesis of riboprobes

For the synthesis of sense or antisense RNA strands, plasmids containing the cDNA of either mouse Pfn1, Pfn2a or Cof1 flanked by T7 and T3 RNA polymerase promotors were used (Table 5). To avoid the synthesis of unspecific riboprobes, prior to *in vitro* transcription, plasmids were linearized using restriction enzymes (depending on whether sense or antisense riboprobes should be produced) (Table 5). Linearization was achieved by incubating the following mix for at least 2 h at 37 °C: 5 µg of plasmid DNA, 10 µl 10x BSA, 10 µl Cut Smart buffer, 0.5 µl EcoRI, XhoI or NotI and RNAse free H_2O with a total volume of 100 µl.

Table 5 – Plasmids used for *in vitro* riboprobe synthesis

Plasmid	Generated by	Vector backbone	Restriction enzyme used for..	
			sense probes	antisense probes
pBS SK mPfn1	J. Feuge	pBS SK (Stratagene)	XhoI	EcoRI
pBS SK mPfn2a	J. Feuge	pBS SK (Stratagene)	XhoI	EcoRI
pBS SK mCof1	J.Baumann	pBS SK (Stratagene)	EcoRI	NotI

Afterwards, the linearized plasmid DNA was extracted via phenol chloroform extraction. Therefore, 100 µL of a phenol chloroform 1:1 solution were added, vortexed and centrifuged at 13.000 rpm for 5 min. Subsequently, the upper aqueous layer was transferred into a new reaction tube. 100 µL chloroform were added, vortexed and again centrifuged at 13.000 rpm for 5 min. The upper layer was transferred into a new reaction tube and 250 µL 96% ethanol and 10 µL 3 M sodium acetate were added. Finally, the DNA was precipitated over-night at -20 °C.

The following day, the DNA was centrifuged at 13.000 rpm for 15 min at 4 °C. The supernatant was discarded, the pellet was washed with 80% ethanol and centrifuged for 15 min at 13.000 rpm, 4 °C. Afterwards, the pellet was air-dried and resuspended in 10 mM TRIS buffer (30 µL, pH 7.5). To confirm correct linearization, a 0.8% agarose gel was run.

Once linearization was confirmed, *in vitro* transcription was performed by addition of a digoxygenin-labeled nucleotide mix as well as addition of the respective RNA polymerase (T7 or T3) (the complete *in vitro* transcription mix can be found in Table 6).

Table 6 - *In vitro* transcription mix

Reagent	Volume
linearized DNA	1 µg
5x transcription buffer	4 µL
Dithiotreitol	1 µL
Digoxygenin-RNA labeling Mix	2 µL
RNasin	1 µL
T3 or T7 RNA polymerase	1 µL
H_2O	Fill up to 20 µL
Total Volume	**20 µL**

The *in vitro* transcription mix was incubated at 37 °C for a total of 2 h while after 1 h incubation, 1 additional µL of the respective RNA polymerase was added. After 2 h of incubation, 1 µL of the mix was removed for a control gel and 2 µL of RQ1-RNase free DNase were added for further 20 min of incubation at 37 °C. Lastly, ice cold 96% ethanol (300 µL), 8 M lithium chloride (5 µL) and RNase free H_2O were (100 µL) added and the RNA was precipitated over-night at -20 °C.

On the next day, the RNA was centrifuged at 13.00 rpm, 4 °C for 20 min and the pellet was washed two times with 70% ethanol and centrifugation for 20 min at 13.000 rpm at 4 °C. Next, the pellet was air-dried and the RNA was dissolved in 11 µL RNase free H_2O. 1 µL was removed as a control and a 0.8% agarose control gel with both controls was run (80 V, 150 mA, 150 W, 45 min). Finally, the RNA was stored at -20 °C for later use.

4.2.6.2 Fluorescence *in situ* Hybridization in cultured hippocampal neurons

In vitro Fluorescence *in situ* Hybridization (FISH) against Pfn1, Pfn2a and Cof1 mRNA was performed in eGFP transfected dissociated hippocampal primary cultures derived from *fmr1* WT and *fmr1* KO mice (48 h after transfection). To keep cellular mRNA in place, cells were fixed for 10 min in 500 µL 4% paraformaldehyde in 1x PBS per well and washed 3 times with 500 µL of 1x PBS for 5 min each on a shaker. To quench naturally expressed HRP, 500 µL H_2O_2 (3%) were added and cells were incubated for 10 min. The cultures were then washed 3 times for 5 min with 500 µL 1x PBS while shaking. During the last washing step 25 µL acetic anhydride and 140 µL tri-ethanolamine were added to 10 mL RNase free H_2O and cells were then incubated in the freshly prepared solution for 10 min again followed by 3 times washing with 1x PBS. Next, cells were permeabilized by incubation in 500 µL 0.5% Triton-X 100 in 1x PBS for 10 min with subsequent 3x washing in 1x PBS. Cells were then equilibrated in 5xSSC for 5 min before 3 h incubation in a prehybridization mix containing 250 µL formamide, 100 µL 10% blocking reagent, 125 µL 20x SSC and 25 µL RNase free H_2O per well. In the meantime, the riboprobes were diluted in RNase free H_2O (final amount used: 1 µL RNA per 1 mL of hybridization solution), denatured at 80 °C for 5 min using a thermoshaker and placed on ice. Before use, the riboprobes were added into fresh prehybridization mix, thereby generating the hybridization solution. Cells were then incubated with 500 µL of hybridization solution per well in a humid chamber at 68 °C over-night. Thus, all non-used wells of the 24-well plate were filled with 50% formamide in 5x SSC and the plate was sealed properly using tape.

On the following day, all cultures were washed (shaking) 2 times 15 min with 500 µL 2x SSC, 2 times 30 min with 500 µL 0.2x SSC and 1 time 20 min with 2x SSC at room temperature. Lastly, cells were incubated for 1 h in TNB buffer, followed by over-night incubation shaking at 4 °C in TNB buffer containing the following primary-antibodies: an anti-digoxygenin HRP coupled antibody (diluted 1:2000) and an anti-GFP antibody (diluted 1:500) (a list of all antibodies used in this study can be found in 4.1.4).

Next morning, cells were washed at room temperature 3 times with TNT buffer (shaking) followed up by a 90 min incubation in TNT buffer containing an anti-mouse Cy2 secondary

antibody (diluted 1:1000) (a list of all antibodies used in this study can be found in 4.1.4). All cultures were then washed 3 times with TNT buffer, nuclei were stained for 5 min using DAPI (1:1000 in TNT buffer) and afterwards washed 3 times with TNT buffer. Then, cultures were incubated in 150 µL TSA Cyanine 3 fluorophore working solution for ~8 min (non-shaking). Finally, each well was washed 3 times 5 min with TNT buffer and cover slips were mounted on microscope slides using Fluoromount. *In situ* hybridizations were then imaged using an Olympus BX61WI Laser scanning microscope. Detailed information on the analysis as well as the imaging setup and the general imaging settings that were used can be found under paragraph 4.2.12.2.

4.2.6.3 Fluorescence *in situ* Hybridization in hippocampal tissue

Ex vivo fluorescence *in situ* hybridization against Pfn1, Pfn2a and Cof1 mRNA was performed in hippocampal slices derived from 3 month old *fmr1* WT and *fmr1* KO mice expressing GFP under the Thy1 promotor. The procedure for *ex vivo* FISH was in all steps similar to the *in vitro* FISH protocol with the following exceptions: 1) Hippocampal slices were kept in a net during the procedure and by default were incubated in 1.5 mL instead of 0.5 mL of the respective solutions. 2) The formamide in the hybridization mix was replaced with 8 M urea. 3) The use of an anti-GFP antibody as well as the secondary antibody incubation were omitted. 4) Instead of 150 µL, 500 µL of TSA Cyanine 3 fluorophore working solution were used per well.

4.2.7 Analysis of local translation

To locate dendritic localization signals in ABP mRNAs (Pfn1, Pfn2a, Cof1) and to enable the analysis of local translation, a membrane-anchored eGFP variant (MYR-eGFP) was utilized where eGFP was fused to a five amino acid linker sequence (GGSGG) and the myristoylation/palmitoylation site of the LCK protein tyrosine kinase. This results in membrane-anchoring of the GFP directly after translation and thus minimal lateral diffusion of the construct. As expression of MYR-eGFP is primarily restricted to the cell body, untranslated regions (UTRs) of Pfn1, Pfn2a and Cof1 mRNA were introduced in order to see whether they contain dendritic localization sequences which would lead to MYR-eGFP expression in dendrites. Additionally, Fluorescence Recovery after Photobleaching experiments (FRAP) were performed in distal dendrites to confirm local translation of the respective construct.

4.2.7.1 Generation of plasmids used for the analysis of local ABP translation

An MYR-eGFP construct fused to the 3'UTR of ß-actin was obtained as a gift from a collaboration partner (R. Blum, University of Würzburg). As the 3'UTR of ß-actin was previously shown to be sufficient to include a dendritic localization sequence (Rathod et al., 2012), this plasmid additionally served as a positive control. In order to locate possible dendritic localization sequences in the untranslated regions of Pfn1, Pfn2a as well as Cof1 mRNA, the 3'UTR of ß-actin was replaced with the either the 3' UTRs or the 3' and 5' UTR of the mRNAs mentioned before.

Therefore, a linearized vector backbone that allowed the insertion of the respective ABP UTRs was created by cutting the 3'UTR of ß-actin out of the MYR-eGFP 3'UTR ß-actin construct (Table 7).

Table 7 – Vector linearization and insert generation

Component	Volume
DNA	2 µg
10x Cut Smart buffer	2 µL
NheI	0.5 µL
XhoI	0.5 µL
H_2O	Fill up to 20 µL
Total Volume	**20 µL**
Incubation	**2 h, 37 °C**

In addition, plasmids containing the respective UTRs of Pfn1, Pfn2a or Cof1 mRNA were obtained from Invitrogen (Table 8) and the UTRs were cut out using the same restriction enzymes which were used to cut the vector backbone (Table 7).

Table 8 – Purchased plasmids containing either the 3‘ or 5’UTR of Pfn1, Pfn2a or Cof1 mRNA

Plasmid	Backbone	Insert	Distributor	Database signature
pmA-T-mCof1 3’UTR	pmA-T	mCof1 3’UTR	Invitrogen	B136
pmA-RQ-mCof1 5’UTR	pmA-RQ	mCof1 5’UTR	Invitrogen	B137
pmA-T-mPfn1 3’UTR	pMA-T	mPfn1 3’UTR	Invitrogen	B138
pmA-RQ-mPfn1 5’UTR	pmA-RQ	mPfn1 5’UTR	Invitrogen	B139
pmA-RQ-mPfn2a 3’UTR	pmA-RQ	mPfn2a 3’UTR	Invitrogen	B140
pmA-RQ-mPfn2a 5’UTR	pmA-RQ	mPfn2a 5’UTR	Invitrogen	B141

Afterwards, 4 µL 6x DNA sample buffer were added to each sample and all were loaded on a 0.8% agarose gel which was run for 45 min at 80 V, 150 mA and 150 W. Subsequently, the desired DNA fragments (identified under UV light) were cut out of the gel by using a razor blade and were eluated from the agarose (according to the manufacturer’s instructions of QIAGEN). Finally, the vector was ligated with the respective inserts by incubating a ligation mix at 25 °C for 4 h (Table 9).

Table 9 – DNA Ligation mix

Component	Volume
10x Ligation buffer	1 µL
Vector backbone (linearized)	0.5 µL
Insert	4 µL
H_2O	2.5 µL
10’ incubation at 70 °C	
T4 DNA Ligase (Thermo Fischer)	1 µL
10 mM ATP	1 µL
Total Volume	**10 µL**

After ligation, XL1 blue competent cells (*E.coli*) were transformed with the newly generated DNA plasmids. Therefore, 200 µL competent *E.coli* were slowly thawed on ice and 10 µL of the respective ligation mix were added followed up by 30 min incubation on ice. Next, each sample underwent a heat shock for 90 s at 42 °C, subsequent addition of 500 µL lysogeny broth medium (LB-medium) and 30 min incubation at 37 °C in a thermoshaker (strongly shaking). Finally, 150 µL from each sample were plated out on an agar plate containing

Ampicillin (which specifically restricted unwanted bacteria from growing) and all plates were incubated headfirst at 37 °C over-night.

The following day, individual single colonies were sterilely picked and used for a MINI preparation according to the manufacturer's instructions (QIAGEN). Afterwards, 1 µg of DNA from all MINI preparations was cut using XhoI and NheI (cutting out the insert again and thereby confirming a correct ligation) and separated on a 0.8% agarose gel (80 V, 150 mA, 150 W, 45 min). Once correct ligation was confirmed, all plasmids were sent out to Eurofins for sequencing. A list of all plasmids that were used and all that were newly generated can be found in Table 10.

Table 10 – Plasmids used for the identification of dendritic localization sequences and the analysis of local ABP translation

Plasmid	Insert 1	Insert 2	Cloned by	Database signature
MYR-eGFP	-	-	J. Feuge	
MYR-eGFP 3'UTR ß-actin	3'UTR ß-actin	-	R. Blum	E438
MYR-eGFP 3'UTR Pfn1	3'UTR Pfn1	-	J. Feuge	E440
MYR-eGFP 3'UTR Pfn2a	3'UTR Pfn2a	-	J. Feuge	E439
MYR-eGFP 3'+5'UTR Pfn2a	3'UTR Pfn2a	5'UTR Pfn2a	J. Feuge	E443
MYR-eGFP 3'UTR Cof1	3'UTR Cof1	-	J. Feuge	E441

4.2.7.2 Identification of dendritic localization sequences

To locate dendritic localization sequences in the mRNAs of Pfn1, Pfn2a and Cof1, different Myr-eGFP constructs fused to UTR(s) of the respective ABPs were used. Therefore, all plasmids (a list can be found in Table 10) were individually co-expressed with mApple (via transfection) in primary dissociated hippocampal cultures (21 DIV) from *fmr1* WT and *fmr1* KO mice. 48 h after transfection, live cell imaging was performed using an Olympus BX61WI Laser scanning microscope. Therefore, cells were incubated in a slow but constant flow of 37 °C prewarmed 1x HBSS in an imaging chamber directly below the objective and GFP as well as mApple expression were imaged. Here, mApple allowed the visualization of individual neurons while the pure Myr-eGFP construct (without additionally added UTRs) where GFP expression is primarily restricted to the cell body served as a negative control confirming that GFP expression cannot be seen dendritically. In contrast, the Myr-eGFP 3'UTR ß-actin construct served as a positive control as the 3'UTR of ß-actin is known to be sufficient to induce dendritic targeting and thus induced GFP-expression also in dendrites. Finally, it was analyzed whether the respective UTRs of Pfn1, Pfn2a and Cof1 are also able to induce dendritic GFP expression,

thereby indicating the existence of a dendritic localization motif in the UTR that was tested. Detailed information on the imaging setup and the general imaging settings that were used can be found under paragraph 4.2.12.4.

4.2.7.3 Analysis of local ABP translation via Fluorescence Recovery after Photobleaching

To confirm that Myr-eGFP constructs that showed dendritic GFP expression indeed undergo local translation, FRAP experiments using the GFP signal in dendritic segments of dissociated hippocampal *fmr1* WT neurons which were at least 100 µm far away from the cell body were performed over a time course of 60 min with or without the presence of the translation blocker anisomycin. Overall, the same experimental setup was used as already described under 4.2.7.2. Cells were kept in a slow but constant flow of 37 °C prewarmed 1x HBSS in an imaging chamber directly below the objective and dendritic GFP signals were bleached at individual dendritic segments using the 405 nm laser line at a power of 2.3-3 mW (approx. 30%) for 2 s. Acquisition at 488 nm (GFP) was recorded directly before the bleaching, directly after the bleaching as well as 5, 10, 20, 30, 40, 50 and 60 min after bleaching. In addition, acquisition at 568 nm (mApple) was recorded before as well as 60 min after the bleaching to confirm that the overall dendritic structure was unharmed during the bleaching process. Finally, experiments were repeated 1) in the presence of the translational blocker anisomycin (final conc. 150 µM) and 2) directly after the induction of glycine-induced NMDAR-dependent chemical LTP. Detailed information on the analysis as well as the imaging setup and the general imaging settings that were used can be found under paragraph 4.2.12.5.

4.2.8 Protein expression level analysis via Western blotting

Protein expression levels of Pfn1, Pfn2a and Cof1 in hippocampal protein samples from *fmr1* WT as well as *fmr1* KO animals were determined via sodium dodecyl sulfate polyacrylamide gel electrophoresis (SDS-PAGE) and subsequent Western blotting and immunostaining. For SDS-PAGE, proteins were complexated and denatured by SDS, thereby covering the natural protein charge with the negative charge of the SDS. As this is directly correlated to the molecular weight, a sample separation via electrophoresis allowed for a distinct distribution and analysis of individual protein contents.

4.2.8.1 Generation of protein samples suitable for Western blotting

For the generation of Western blot samples, individual hippocampi (prepared as described in 4.2.3.3 but non-cut) or acute hippocampal slices (prepared as described in 4.2.3.4) were homogenized in either STKM buffer (1 µL per 1 mg of an individual hippocampi sample) or lysis buffer (1 µL per 1 mg weight of acute hippocampal slices) containing a protease as well as a phosphatase inhibitor. Afterwards, all samples were centrifuged at 4 °C, 19.000 x g for 30 min, the supernatant was transferred into a new reaction tube and the amount of buffer was doubled. Finally, the protein amount of each individual sample was determined via the Bradford protein assay. Thus, 1:50, 1:100 and 1:200 dilutions of the supernatant in buffer were prepared in a 96-well plate and used for the measurement. In addition, concentrations of 20 $\frac{\mu g}{mL}$ to 200 $\frac{\mu g}{mL}$ of BSA were used to calibrate the protein content. Lastly, all samples were mixed with 100 µL of Bradford reagent and the absorption at 595 nm (Coomassie Brilliant Blue) was measured with an ELISA reader. Once the protein content of all samples was determined, all brain samples were set to a concentration of 0.2 $\frac{\mu g}{mL}$ in 4x-SDS buffer followed by heating at 92 °C for 10 min with invertings every 3 min.

4.2.8.2 Protein separation via SDS-PAGE and subsequent Western blotting

For protein separation via electrophoresis, 15% polyacrylamide gels were utilized which were prepared using the protocol described in Table 11.

Table 11 – Preparation of 15% polyacrylamide gels

Collecting gel		Separating gel	
MQ H_2O	62 mL	MQ H_2O	30 mL
Collecting gel buffer	25 mL	Separating gel buffer	30 mL
acrylamide 37.5%	13 mL	acrylamide 37.5%	60 mL
TEMED	50 µL	TEMED	40 µL
10% APS	1000 µL	10% APS	800 µL

10 µl of sample (equaling 2 µg of protein) were loaded on each pocket of the gel and as a protein standard 7 µl of the PageRuler Plus Prestained Protein Ladder were used. The gel was run at 225 V, 100 W and 10 mA until the proteins reached the separating gel. Then, the current was increased to 20 mA per gel until the protein separation was manually stopped.

Afterwards, the separated proteins were transferred onto a polyvinylidene fluoride membrane (PVDF membrane) via Western blotting. Therefore, the PVDF membrane was incubated in MeOH for 20 min, followed by incubation in 10% 1x MeOH blotting buffer (at least 10 min). Four pieces of 10% 1x MeOH blotting buffer equilibrated Whatman paper were placed on a blotter and the equilibrated PVDF membrane was placed on top. Subsequently, the separating gel was put on top and overlaying edges of the Whatman paper as well as the membrane were cut off via scissors. Lastly, 4 pieces of Whatman paper were added on top and again, overlapping edges were cut off by scissors. Remaining air bubbles in the stack were removed by gently rolling over the stack with a glass pipette. Placing two gels in one blotter, proteins were transferred onto the PVDF membrane for 1h using 10 W, 100 V and 200 mA (100 mA per gel).

Next, remaining binding capacities of the PVDF membrane were blocked through incubation in 5% milk powder in 1x TBS-T for 1 h at room temperature (shaking). Afterwards, the milk was removed by repeating washing steps with 1x TBS-T. Then, the membrane was cut and individual membrane pieces were incubated at 4 °C over-night (shaking) in 3 mL of 1x TBS-T containing a primary antibody (a list of all antibodies used for Western blotting can be found in Table 12*,* a list of all antibodies used in this study can be found in 4.1.4).

Table 12 – List of antibodies used for Western blotting

Antibody	Antibody type	Host	Final dilution	Distributor	Product No.
anti-profilin 1 C-terminal	primary	rabbit	1:5000	Sigma	P7624
anti-profilin 2a as361	primary	rabbit	1:20000	Bioscience	-
anti-cofilin1	primary	rabbit	1:15000	abcam	ab11062
anti-GAPDH	primary	rabbit	1:9000	Sigma	G9545
anti-rabbit HRP	secondary	goat	1:20000	Sigma	A0545

The next day, each membrane piece was washed repeatedly with 1x TBS-T and then incubated for 90 min in 3 mL 1x TBS-T containing a 1:20000 diluted anti-rabbit HRP coupled antibody. Subsequently, membranes were repeatedly washed with 1x TBS-T, 1x TBS-X and then H_2O. Afterwards, the membranes were dried using Whatman paper and incubated in Luminata™ Crescendo Western HRP (~2 mL) for approximately 2 min. Again, the membrane pieces were dried using Whatman paper and then placed in a CURIX cassette. Finally, X-ray

films were developed in a darkroom. An undeveloped film was placed above the individual membrane pieces and incubated for up to 2 min (timing depended on the respective strength of the antibody signal). Subsequently, the film was developed in developer solution, washed with H_2O and then fixated in fixing solution. All films were photographed using a Herolab E.A.S.Y. RH system and analysis of single spots was performed using the Herolab software.

4.2.9 Assessment of spatial memory formation

As neural mechanisms ultimately determine the behaviour of an animal, a hippocampus-dependent behavioral test was used to study the functional relevance of ABP mRNA regulation for learning and memory (Morris, 1984). Therefore, the Morris Water Maze task was performed which assesses hippocampus-dependent spatial learning and memory formation with great sensitivity and accuracy.

4.2.9.1 The Morris Water Maze task

Animals were trained in the hidden platform version of the Morris Water Maze task and all experiments were carried out by the same experimenter at the same time of the day. All mice were kept in individual cages in the training room during the entire training session, had *ad libitum* access to water and food and were maintained in a 12:12 h light/dark cycle. Experiments were carried out in a 160 cm wide water tank (water temperature 19 - 21°C) with a submerged platform directly below the water surface at a fixed position and signs were put up on the walls around the water maze to serve as an orientation help. Ultimately, over a time period of 8 training days, mice were supposed to learn to use the spatial cues to locate the hidden platform in the pool.

However, first, to accustom all mice to the experimental setup and the experimenter as well as to test whether all mice are physically healthy, a pre-training with a visible platform was performed for a total of 3 days. Here, each mouse had to perform 2 trials per day for up to 60 s with different starting positions and switching platform positions. After the pre-training period, mice were not trained for 2 days before the hidden platform version of the task was performed over 8 consecutive days. Here, all animals had to perform 4 trials each per day starting from 4 fixed starting positions (with switching orders between different training days) where they had to locate the hidden platform at a fixed position in up to 60 s. If an animal failed to find the platform in the given time window, it was placed on top of it and had to remain there for 15 s before being put back into its cage. On training day 6 and after the 8 day period of daily training (on training day 9), a memory reference tests was performed where the hidden

platform was removed from the tank and each mouse had to swim for 45 s. For all parts of the behavior test, trials were recorded using a digital video camera connected to the Any-maze tracking software which was also used to analyze the data. Detailed information on the analysis of the Morris Water Maze data can be found in 4.2.12.7.

4.2.10 Chemical manipulation of actin dynamics

Actin dynamics were manipulated in GFP-expressing dissociated hippocampal primary cultures (transfected DIV21) using the actin-stabilizing agent Jasplakinolide (final concentration 50 nM), the inhibitor of actin polymerization Cytochalasin D (final concentration 100 nM) or a peptide consisting of the first 16 residues of Ser3-phosphorylated cof1 (final concentration 6 µM) which functions as an endogenous inhibitor of cof1. The respective agents were applied either during the induction of cLTP (diluted in 1x Mg^{2+}-free HBSS containing glycine and strychnine) and for 60 min after the induction of cLTP (diluted in 1x HBSS) or only after the stimulation period. Finally, all cells were fixed using 4% PFA, washed 3 times with 1x PBS and cover slips were mounted on microscope slides using Fluoromount.

4.2.11 Analysis of mRNA transport via the MS2-vector system

For the analysis of mRNA transport via live-imaging, the MS2-vector system was utilized. The MS2-vector system is based on the interaction between GFP-tagged MS2-proteins and MS2-binding sites which are repetitively introduced into the mRNA of interest and form tertiary structures that can be recognized by MS2. Hence, in theory, the GFP-tagged MS2 proteins recognize and bind to the MS2-binding sites which were introduced into the mRNA of interest and individual mRNAs become visible as GFP puncta which allows for live-tracking of mRNA transport in living cells.

Therefore, two plasmids were bought from Addgene: 1) a plasmid containing 12x MS2-binding sites (Addgene #27119, pSL-MS2-12x) and 2) a plasmid containing GFP-tagged MS2 (Addgene #27121, pMS2-GFP). First, to allow for a wider variability of restriction sites, the sequence coding for 12x MS2-binding sites was cut out of the Addgene plasmid and inserted into the multiple cloning site of a pcDNA3 vector backbone using the restriction mix shown in Table 13.

Table 13 – Restriction mix used for the cloning of 12x MS2-binding sites

Component	Volume
pSL-MS2-12x or pcDNA3	2 µg
10x Cut Smart buffer	2 µL
EcoRI	0.5 µL
XhoI	0.5 µL
H_2O	Fill up to 20 µL
Total Volume	**20 µL**
Incubation	**2 h, 37 °C**

Afterwards, 4 µL 6x DNA sample buffer were added to each restriction and all were loaded on a 0.8% agarose gel which was run for 45 min at 80 V, 150 mA and 150 W. Subsequently, the desired DNA fragments (identified under UV light) were cut out of the gel by using a razor blade and were eluated from the agarose (according to the manufacturer's instructions of QIAGEN). Finally, the DNA fragment coding for 12x MS2-binding sites was ligated with the pcDNA3 vector by incubating a ligation mix at 25 °C for 4 h (Table 14).

Table 14 – DNA ligation mix used for the generation of pcDNA3-12x MS2

Component	Volume
10x Ligation buffer	1 µL
pcDNA3 (linearized)	0.5 µL
12x MS2-binding site insert	4 µL
H_2O	2.5 µL
10' incubation at 70 °C	
T4 DNA Ligase (Thermo Fischer)	1 µL
10 mM ATP	1 µL
Total Volume	**10 µL**

After ligation, XL1 blue competent cells (*E.coli*) were transformed with the newly generated plasmid. Therefore, 200 µL competent *E.coli* were slowly thawed on ice and 10 µL of the respective ligation mix were added followed up by 30 min incubation on ice. Next, each sample underwent a heat shock for 90 s at 42 °C, subsequent addition of 500 µL lysogeny broth medium (LB-medium) and 30 min incubation at 37 °C in a thermoshaker (strongly shaking). Finally, 150 µL from each sample were plated out on an agar plate containing Ampicillin (which

specifically restricted unwanted bacteria from growing) and all plates were incubated headfirst at 37 °C over-night.

The following day, individual single colonies were sterilely picked and used for a MINI preparation according to the manufacturer's instructions (QIAGEN). Afterwards, 1 µg of DNA from all MINI preparations was cut using XhoI and EcoRI (cutting out the insert again and thereby confirming a correct ligation) and separated on a 0.8% agarose gel (80 V, 150 mA, 150 W, 45 min). Once correct ligation was confirmed, the plasmid was sent out to Eurofins for sequencing.

Afterwards, to allow for a live-tracking of Cof1 mRNA, the 3'UTR of Cof1 was cloned into the newly generated pcDNA3-12x MS2-binding site plasmid using NheI and XhoI and the protocols as described in Table 13 and Table 14. A list of all bought and generated plasmids can be found in Table 15 as well as under paragraph 4.1.5.

Table 15 – List of plasmids used for the analysis of mRNA transport

Plasmid	Insert 1	Insert 2	Cloned by	Database signature
pSL-MS2-12x	12x-MS2	-	Addgene	E383
pMS2-GFP	MS2-GFP	-	Addgene	E385
pcDNA3	-	-	-	L70
pcDNA3-12x MS2	12x MS2	-	J. Feuge	B144
pcDNA3-12x MS2-3'UTR Cof1	12x MS2	3'UTR Cof1	J.Feuge	E442

Finally, DIV21 dissociated hippocampal neurons were co-transfected with pcDNA3-12x MS2-3'UTR Cof1 as well as pMS2-GFP and 48 h after transfection, live-imaging was performed.

4.2.12 Image acquisition, analysis and statistics

In all experiments, imaging was done with an Olympus BX61WI Laser scanning microscope using either a 40x UPLFLN oil objective (NA 1.30) or a 60x LUMPLFLN water objective (NA 1.0) and the Olympus Fluoview Software Ver. 4.0a. The management of data was performed in Microsoft Excel and statistics were done using either PRISM 5 or SPSS. Detailed information on microscopical settings as well as the analysis and statistics for individual experiments can be found in the following paragraphs.

4.2.12.1 Imaging and analysis of dendritic spine properties

For the analysis of dendritic spine properties (e.g. spine head diameter) in primary dissociated hippocampal neurons, individual GFP-expressing neurons were imaged. Therefore, single dendritic segments were imaged as a stack (one per cell) using the 40x oil objective with the following microscopical settings: 5x zoom, image size 800 x 800 pixels with a final pixel size of 99 $\frac{nm}{px}$ and Z-stack steps of 0.35 µm. Images were then opened in ImageJ where spine properties could be measured using the 'freehand lines' and the 'measure tool'. Finally, the results were copy pasted into an excel sheet where the data from all imaged dendrites was collected and analyzed. Finally, the statistic program SPSS was used to perform a two-way ANOVA to compare the effects between genotype (*fmr1* WT/*fmr1* KO) as well as treatment (unstimulated/cLTP or cLTD). Once a two-way ANOVA showed a significant interaction between genotype*treatment, a one-way ANOVA with a post-hoc Tuckey Test was performed to directly compare different treatments.

4.2.12.2 Imaging and analysis of Fluorescence *in situ* Hybridizations in cultured neurons

For the analysis of *in vitro* FISH experiments, individual GFP-expressing neurons were imaged. Therefore, the cell body of a GFP-expressing neuron was orientated in the middle of the picture so that the whole cell body as well as proximal dendrites were imaged as a stack using the 40x oil objective with the following microscopical settings: 5x zoom, image size 800 x 800 px with a final pixel size of 99 $\frac{nm}{px}$ and Z-stack steps of 0.35 µm. For the excitation of fluorophores, the following lasers were used: 405 nm for DAPI, 488 nm for Cy2 (GFP) and 559 nm for Cy3 (RNA). Images were then opened in ImageJ and the analysis of mRNA puncta was done manually. Therefore, the total amount of mRNA puncta per cell (divided into nuclear, cell body and dendritic signals) was manually counted and compared between unstimulated cells as well as 20, 40 and 60 min after induction of chemically-induced NMDAR-dependent LTP or mGluR-dependent LTD in *fmr1* WT as well as *fmr1* KO neurons (Figure 6).

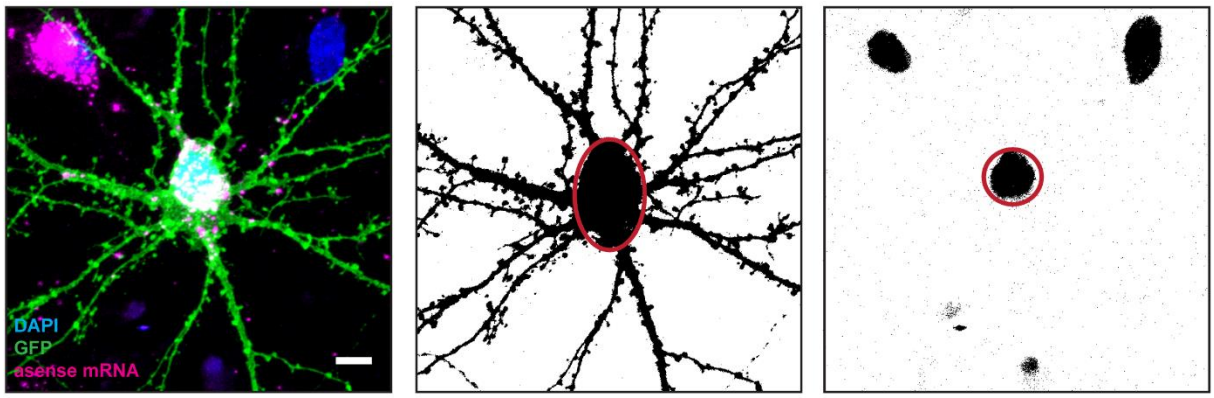

Figure 6 - Analysis of mRNA puncta following Fluorescence *in situ* Hybridization. Visible mRNA puncta in the nucleus (overlap with DAPI), the cell body as well as in dendrites of an individual neuron were manually counted and normalized to compartment size. Therefore, the GFP channel was binarized into an black and white image and the respective compartment sizes were analyzed using the ‚particles' tool in ImageJ (red circles only for demonstration, areas were defined using the 'freelines' tool). Scale bar – 10 µm.

Finally, the results were copy pasted into an excel sheet where the data from all analyzed neurons was collected. For statistics, the statistic program SPSS was used to perform a two-way ANOVA to analyze the interaction between genotype (*fmr1* WT/*fmr1* KO) and treatment (unstimulated/cLTP or cLTD) followed up by a one-way ANOVA with a post-hoc Tuckey Test to directly compare different treatments.

4.2.12.3 Imaging and analysis of Fluorescence *in situ* Hybridizations in tissue

For the analysis of *ex vivo* FISH experiments, hippocampal slices were imaged using the 40x oil objective with the following microscopical settings: 640 x 640 px with a final pixel size of 497 $\frac{nm}{px}$ and Z-stacks of 0.35 µm. For the excitation of fluorophores, the following lasers were used: 405 nm for DAPI, 488 nm for Cy2 (GFP) and 559 nm for Cy3 (RNA). Thus, to analyze whether mRNA puncta can be found dendritically, large field of view images were taken where the *stratum pyramidale* (hippocampal CA1 region) was located horizontally on the top side of the image which allowed a good visualization of the *stratum radiatum*. Images were then opened in ImageJ where unspecific signals in the RNA channel (Cy3) were removed using the 'Gaussian Blur Filter' as well as the 'Remove Outliners' tool which allowed an overall better visualization and detection of mRNA signals.

4.2.12.4 Imaging and identification of dendritic localization sequences in ABP mRNAs

As the pure MYR-eGFP construct that was used as a negative control in these experiments induced GFP expression only in the cell body, dendritic localization sequences could be

located once a construct containing an untranslated region of either Pfn1, Pfn2a or Cof1 mRNA showed dendritic GFP expression. Therefore, individual neurons co-expressing mApple as well as the respective MYR-eGFP construct were imaged using the 40x oil objective with the following microscopical settings: 1024 x 1024 px with a final pixel size of 155 $\frac{nm}{px}$ and Z-stacks of 0.35 µm. For the excitation of fluorophores, the following lasers were used: 488 nm for GFP and 568 nm for mApple.

4.2.12.5 Imaging and analysis of local ABP translation

For the analysis of local ABP translation, individual neurons co-expressing mApple as well as a dendritically localized MYR-eGFP construct were imaged and FRAP experiments on dendritic segments which were at least 100 µm away from the cell body were performed as described in 4.2.7.3. Therefore, stack images of individual dendrites were taken before as well as directly after and 5, 10, 20, 30, 40, 50 and 60 min after the photobleach using the 60x water objective with the following microscopical settings: 1024 x 320 px with a final pixel size of 55 $\frac{nm}{px}$ and Z-stacks of 0.5 µm. For the excitation of fluorophores, the following lasers were used: 488 nm for GFP and 568 nm for mApple. Images were then opened in ImageJ were a region of interest was drawn into the dendritic segment that was imaged. Using the 'Multi Measure Tool', the fluorescence intensity inside the region of interest was analyzed in all images of the stack and the highest intensity value was copy pasted into an excel sheet and used for analysis. In Excel, the fluorescence intensity of GFP before the photobleach was compared to the fluorescence intensities measured at various time points after the photobleach and these ratios were used for the generation of FRAP curves in PRISM 5. Finally, the statistic program SPSS was used to compare FRAP curves between genotypes (*fmr1* WT/ *fmr1* KO) and treatments (anisomycin/no anisomycin) with a Repeated Measures ANOVA and once two FRAP curves were proven to be significally different from each other, unpaired Student's t-tests were used to compare different time points between the curves.

4.2.12.6 Analysis of Western blots

Single spot analysis of Western blot signals was done using the Herolab software which calculated a volume of each individual spot. For at least 3 gels with the same samples, the volume values of all signals (loading control as well as protein of interest) were calculated 3 times and copy pasted into an Excel sheet. Per gel, the average volume from the 3 measurements was calculated for each sample and the values from the protein of interest were normalized to the highest average loading control volume that was detected on the gel.

From each of the gels done, normalized values from the same sample were averaged and lastly, different samples from the same treatment were averaged. Finally, different treatments were compared to each other by calculating a ratio of the average signal volume to the average signal volume of the control condition. For statistics, the statistic program SPSS was used to perform a two-way ANOVA to analyze the interaction between genotype (*fmr1* WT/*fmr1* KO) and treatment (unstimulated/cLTP or untrained/trained) followed up by a One-way ANOVA with a post-hoc Tuckey test to directly compare data sets.

4.2.12.7 Analysis of Morris Water Maze data

Morris Water Maze data was analyzed using the Any-maze software which was also utilized to document all training trials during training. To allow for a more detailed analysis of swimming behavior, in Any-maze, the water tank was divided into distinct zones (as shown in Figure 7) which could be analyzed individually.

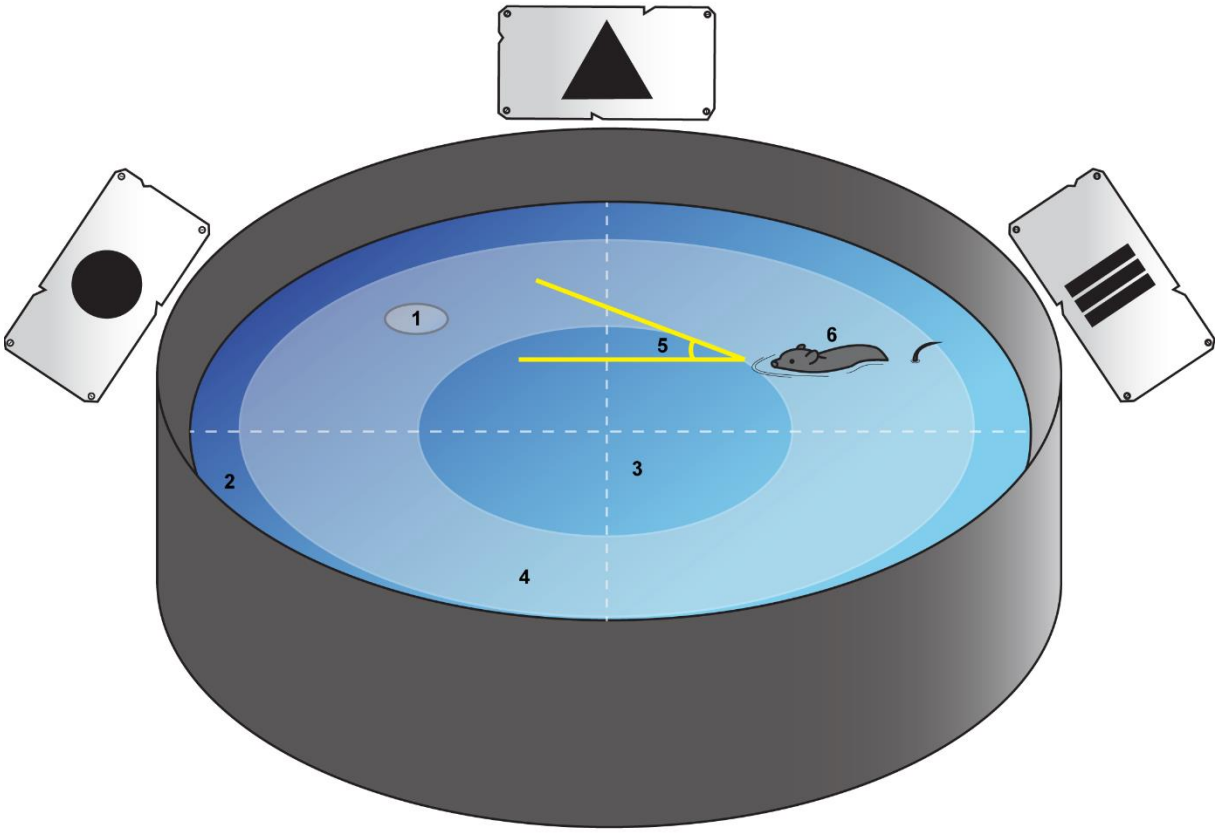

Figure 7 - Analysis of swimming patterns in the Morris Water Maze. For analysis, the tank was divided into 4 equally sized quadrants with 1 of them containing (**1**) the hidden platform zone ('target quadrant'). In addition, (**2**) the outer region of the water maze, (**3**) the inner region, (**4**) an annulus zone as well as (**5**) a goal corridor ranging from (**6**) the starting position of the mouse pointing towards the hidden platform were defined.

For the analysis of regular training trials, parameters like escape latency or total distance travelled were analyzed, averaged per training day and statistically compared between the two genotypes (*fmr1* WT, *fmr1* KO). In addition, for the analysis of the reference memory test, behavioral strategies for finding the platform were identified by analyzing the amount of time spent in the respective areas. Afterwards, specific swim patterns were associated with and classified into the 6 following distinct hippocampus-dependent or -independent search strategies (as shown in Figure 8): 1) 'Thigmotaxis' - Looping in the border region or floating. 2) 'Random Search' - Lack of preference for any region of the tank. 3) 'Chaining' - Circular swimming in the annulus region. 4) 'Scanning' - Searching in the centre region. 5) 'Direct Search' - Swimming towards the platform but with exploratorive loops. 6) 'Direct Swimming' - Swimming directly towards the platform. From these, Direct Swimming and Direct Search represent allocentric, hippocampus-dependent search strategies while Thigmotaxis, Random Search, Chaining and Scanning represent egocentric, hippocampus-independent search strategies.

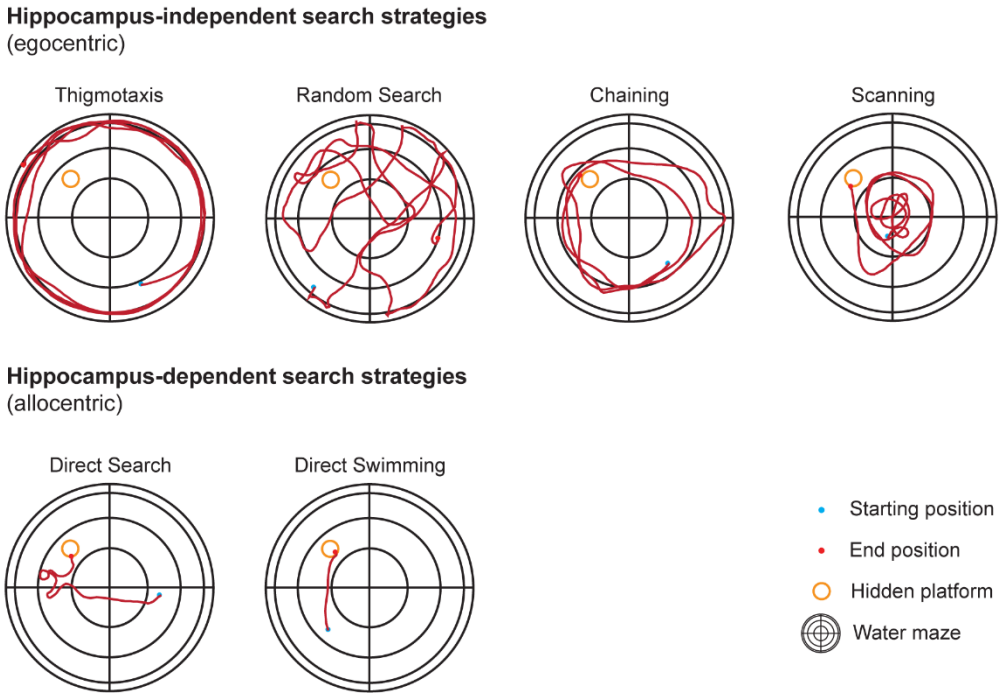

Figure 8 – Analysis of swimming patterns. Overview of the different hippocampus-independent (Thigmotaxis, Random Search, Chaining, Scanning) and hippocampus-dependent (Direct Search, Direct Swimming) search strategies used by mice in the Morris Water Maze training.

In general, over the training course of 8 days, mice are expected to learn to locate the hidden platform using spatial cues, thereby increasing the amount of hippocampus-dependent search strategies over time while decreasing their escape latency.

4.2.12.8 Data presentation

All graphs were generated using PRISM 5 and show means ± standard error of the mean (SEM) if not described otherwise. Significances are indicated by *p value < 0.05, **p value < 0.01 and ***p value < 0.001.

5 Results

5.1 Neuronal profilin and cofilin 1 mRNAs as potential targets of FMRP

Morphological alterations of dendritic spines and abnormal actin dynamics imply a crucial involvement of actin and a potential role of actin-binding proteins in the neuropathology of FXS. However, surprisingly, although hundreds of FMRP-target RNAs were discovered so far (Ascano et al., 2012; Darnell et al., 2011), only very few mRNAs of actin-binding proteins were confirmed as valid FMRP-targets. Thus, as the mRNAs of the ABPs Pfn1 and Cof1 were suggested previously to be direct targets of FMRP (Ascano et al., 2012; Reeve et al., 2005), an *in silico* analysis was performed to confirm the presence of FMRP-binding sites in the predicted binding-partners (Table 16). Indeed, a search for the most prominent and well described FMRP-binding sequences (WGGA motifs, G-rich sequences) revealed that the mRNAs of Pfn1 and Cof1 both contain FMRP-binding sites. Notably, the mRNA of Pfn1 was found to contain clustered guanine bases forming a G-rich region followed by two WGGA motifs. In addition, in line with the prediction from RNA-immunoprecipitation experiments against FMRP (Michaelsen-Preusse et al., 2016), no binding motifs could be detected in the mRNA of Pfn2a. Interestingly, while no clustered WGGA motifs were found in the mRNA of Cof1, a G-rich region containing multiple guanine clusters could be found. Importantly, all sequences that were found in the analysis were similar to those present in already validated FMRP-target mRNAs like PSD-95 mRNA (Zalfa et al., 2007) or FMRP mRNA (Ashley et al., 1993b).

Table 16 – Identification of potential FMRP binding sites in neuronal profilins and Cof1. Search for WGGA motifs (magenta) and G-rich sequences (green) in already validated FMRP-targets (PSD-95 & FMRP mRNA) as well as potential FMRP-binding partners (Pfn1, Pfn2a & Cof1 mRNA).

Gene/Protein	Species	Transcript Sequence
fmr1 FMRP	*Homo sapiens*	**5' GGCGTGGAGGGGGAGGAAGAGGACAAGGAGGAAGAGGA 3'**
	Mus musculus	**5' GGCGTGGAGGAGGAGGAAGAGGACAAGGAGGAAGAGGA 3'**
dlg4 PSD-95	*Homo sapiens*	**5' AACGGGACCGAGGGGGAGATGGAATACGAGGAAATCACA 3'**
	Mus musculus	**5' AACGGAACAGAGGGGGAGATGGAGTATGAGGAGATCACA 3'**
pfn1 Pfn1	*Homo sapiens*	**5' CCACATGGGCTGGGGGCCAGGGCTGGATGGACAGACACC 3'**
	Mus musculus	**5' CCACATGGGCTGGGGGCTGGGGCTGGATGGACAGACACC 3'**
pfn2a Pfn2a	*Homo sapiens*	-
	Mus musculus	-
cof1 Cof1	*Homo sapiens*	**5' ACCGGAGGGGCTGGGGGGATCCCAGCAGGGGGAGGGCA 3'**
	Mus musculus	**5' ACCGGAGGGGCTGGGGGGATCCCAGCAGGGGGAGGGCT 3'**

Summed up, *in silico* analysis of potential FMRP-binding sites in the mRNAs of Pfn1, Pfn2a and Cof1 suggests the mRNAs of Pfn1 and Cof1 as direct targets for FMRP. Intriguingly, these findings could be strengthened by RNA Co-Immunoprecipitation experiments that confirmed a direct interaction between FMRP and the mRNAs of Pfn1 and Cof1 but not Pfn2a (data not shown as experiments were performed by a different PhD student, data is published in Feuge et al., 2019; Michaelsen-Preusse et al., 2016).

5.2 Age-dependent expression of profilins and cofilin 1 in *fmr1* KO mice

As suggested by Fluorescence Recovery after Photobleaching (FRAP) experiments utilizing eGFP-actin, actin dynamics are altered in hippocampal neurons from *fmr1* KO mice already under basal conditions (Feuge et al., 2019) thereby indicating potential alterations in the activity of ABPs. Thus, to unravel whether neuronal profilins or cofilin 1 are differentially expressed in FXS, hippocampal protein expression of these proteins was analyzed via Western blotting. As Pfn1 was shown to be predominantly expressed during development (Michaelsen-Preusse et al., 2016) hippocampal expression of both Pfn isoforms was first analyzed at postnatal days 0 and 14 (P0, P14) in *fmr1* WT as well as *fmr1* KO mice (Figure 9A). Interestingly, expression of Pfn1 was significantly reduced in *fmr1* KO mice at P0 but not P14 while Pfn2a expression was unaltered at both analyzed time points. However, in mature mice at postnatal day 120 (Figure 9B), hippocampal expression of both isoforms was equal between *fmr1* WT and *fmr1* KO mice. On the contrary, hippocampal Cof1 expression at P120 was significantly decreased in *fmr1* KO mice in comparison to the wild-type.

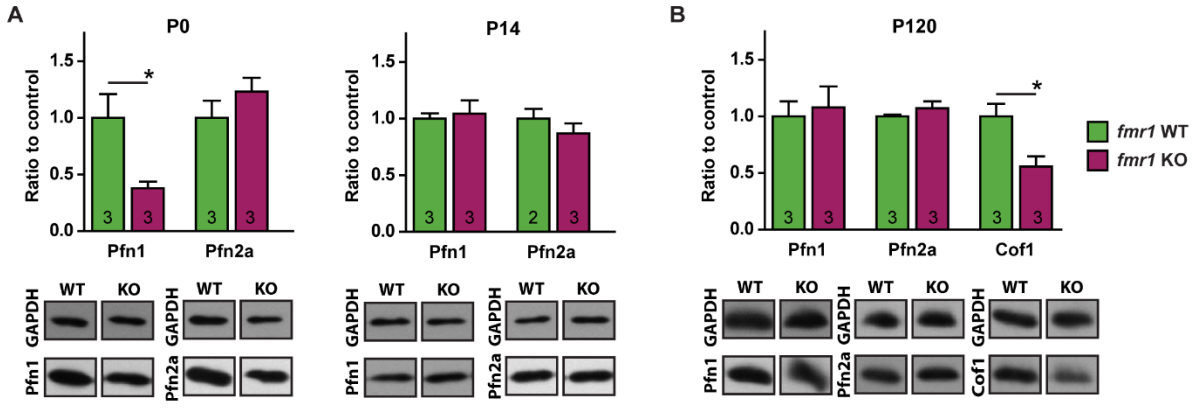

Figure 9 – Age-dependent hippocampal expression of neuronal profilins and cofilin 1 in *fmr1* KO mice. A) Western blot analysis of hippocampal Pfn1 and Pfn2a expression at postnatal day 0 and 14 in *fmr1* WT and *fmr1* KO mice. **B)** Western blot analysis of hippocampal Pfn1, Pfn2a and Cof1 expression at postnatal day 120 in *fmr1* WT and *fmr1* KO mice. All data is presented as mean ± SEM. Significances are indicated by *p value < 0.05, **p value < 0.01 and ***p value < 0.001. A list of all values and statistics can be seen in paragraph 9.1.

Altogether, supporting the previously discussed data that suggested the mRNAs of Pfn1 and Cof1 as direct targets for FMRP (Feuge et al., 2019; Michaelsen-Preusse et al., 2016), hippocampal expression of both of these proteins was found to be significantly altered in *fmr1* KO mice thereby indicating a regulatory function of FMRP for the translation of those mRNAs. In line with this, hippocampal expression of Pfn2a, whose mRNA was not predicted as an FMRP-target, was unaltered in all developmental stages analyzed.

5.3 Dendritic and synaptic localization of ABP mRNAs in the hippocampus

The first set of experiments hinted towards the fact that ABP expression in the hippocampus might be influenced by FMRP. As FMRP was found to specifically modulate local translation in dendrites (Feng et al., 1997) but neither the local translation nor the presence of Pfn1, Pfn2a or Cof1 mRNAs in dendrites had been shown before, Fluorescence *in situ* Hybridization experiments were performed *in vitro* as well as *ex vivo* in order to analyze the overall mRNA distribution of these proteins in hippocampal neurons (Figure 10).

5.3.1 Dendritic and synaptic ABP mRNA localization *in vitro*

To analyze the mRNA distribution of neuronal Pfn isoforms and Cof1 *in vitro*, FISH experiments were performed in DIV21 primary embryonic hippocampal cultures. Fluorescent labeling of antisense riboprobes against the mRNAs of Pfn1, Pfn2a as well as Cof1 allowed for visualization of the mRNA signals as puncta in individual GFP-transfected hippocampal neurons (Figure 10A). To confirm the specificity of all antisense riboprobes, FISH was repeated with the respective sense riboprobes which showed only marginal staining in the cell body, thereby confirming specificity of the generated riboprobes (Figure 10B). Importantly, analysis of the overall distribution pattern of mRNAs detected by antisense riboprobes showed that mRNAs of Pfn1, Pfn2a and Cof1 are present not only in the cell body and the nucleus but also in dendrites as well as directly in dendritic spines (Figure 10A, C) suggesting that indeed ABP mRNAs are actively transported into dendrites.

All in all, FISH experiments confirmed the presence of the mRNAs of Pfn1, Pfn2a as well as Cof1 in dendrites and dendritic spines of hippocampal neurons *in vitro* thereby indicating dendritic mRNA targeting and local translation of these proteins.

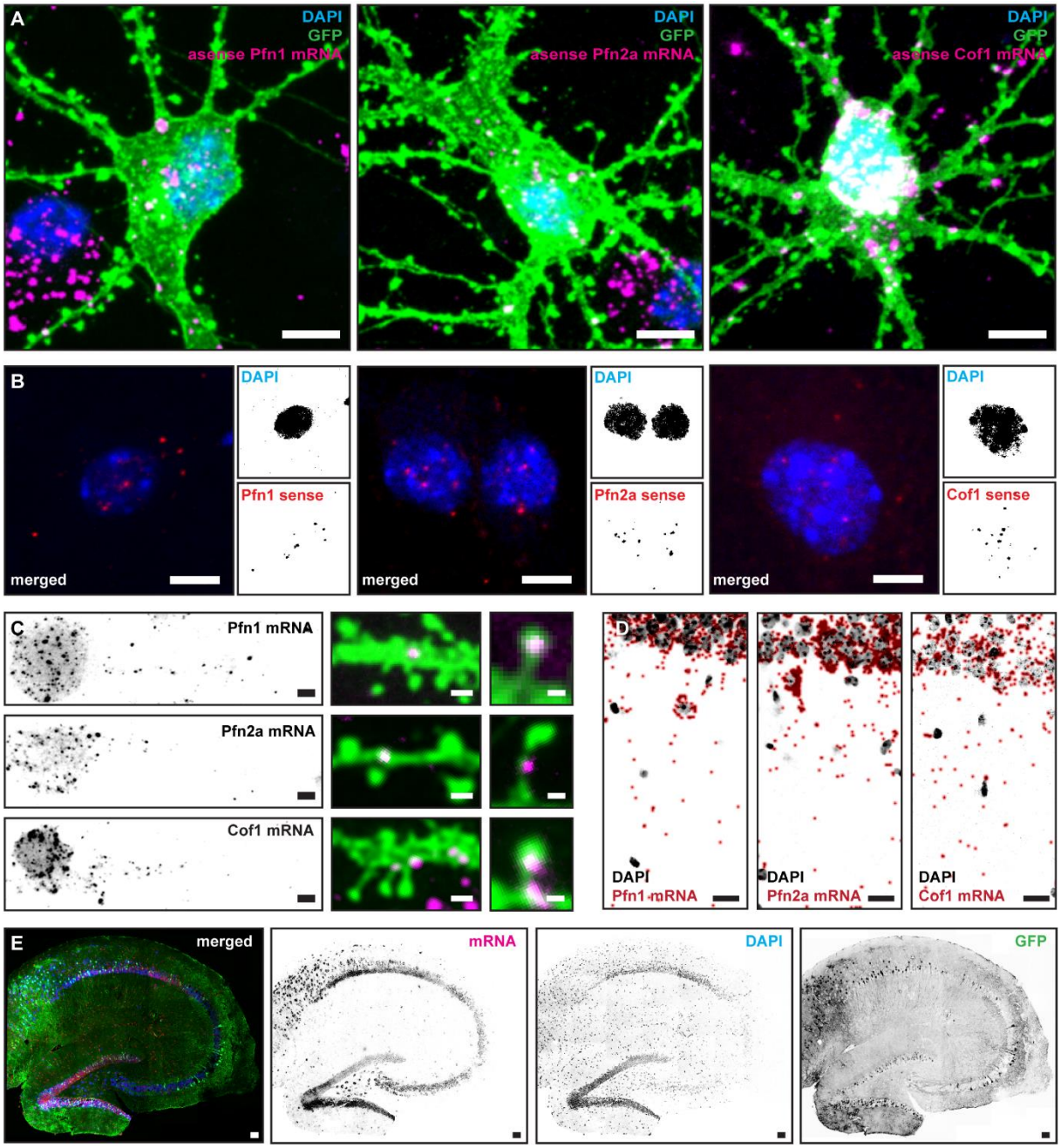

Figure 10 – Analysis of ABP mRNA distribution via Fluorescence *in situ* Hybridization. FISH experiments utilizing **A)** antisense (magenta) or **B)** sense riboprobes (red) against the mRNAs of Pfn1, Pfn2a or Cof1 in individual GFP-transfected (green) and DAPI stained (blue) hippocampal neurons of *fmr1* WT mice. Scale bars – 5 µm **C)** Detection of Pfn1, Pfn2a and Cof1 mRNA in dendrites as well as directly in dendritic spines *in vitro*. Scale bars – 5 µm, 1 µm, 0,5 µm (left to right) **D)** Detection of Pfn1, Pfn2a and Cof1 mRNA (red puncta) in the dendritic layer (nuclear DAPI staining in black) of the CA1 region in hippocampal slices (*ex vivo)*. Scale bars – 10 µm **E)** Example of a hippocampal slice where mRNA was detected via FISH (RNA – magenta, GFP expression under the Thy1 promotor – green, DAPI – blue). Scale bars – 100 µm

5.3.2 Dendritic ABP mRNA localization *ex vivo*

To confirm that the dendritic localization of Pfn1, Pfn2a and Cof1 mRNAs can not only be observed *in vitro* but potentially also *in vivo*, FISH experiments were repeated in hippocampal

slices derived from *fmr1* WT mice where the architecture of the hippocampus is preserved (Figure 10D, E). Notably, the mRNAs of all three proteins were detectable not only in nuclei and cell bodies but also in the *stratum oriens* and the *stratum radiatum* of the hippocampus thereby suggesting that ABPs are locally synthesized in dendrites also *in vivo*.

5.4 Local translation of ABPs in the hippocampus

The presence of ABP mRNAs in dendrites and even directly at dendritic spines opened the possibility that ABPs are locally translated. Thus, to unravel whether neuronal Pfn isoforms and Cof1 indeed are synthesized locally, we utilized a membrane-targeted eGFP construct with minimal lateral diffusion. As earlier studies could show that dendritic targeting and local translation of the construct can be induced by the addition of a dendritic localization sequence (primarily encoded in untranslated regions e.g. the 3' untranslated region (UTR) of ß-actin) (Rathod et al., 2012; Zhang et al., 2001a) (schematically shown in Figure 11A), different UTRs of the proteins of interest (Pfn1, Pfn2a, Cof1) were fused to MYR-eGFP in order to identify dendritic localization signals (Figure 11B).

5.4.1 Dendritic localization motifs in the mRNAs of profilin 1, profilin 2a and cofilin 1

To confirm that the addition of a dendritic localization sequence indeed induces dendritic targeting as well as local translation of the construct, the 3'UTR of ß-actin was fused to the membrane-targeted eGFP. Notably, expression of the eGFP construct alone in DIV21 hippocampal neurons led to visible GFP expression solely in the cell body, confirming that the GFP is not targeted to or diffusing into dendrites (Figure 11B). After addition of the 3'UTR of ß-actin, however, GFP expression was detectable all over the dendritic tree indicating that as was confirmed by previous studies (Rathod et al., 2012; Zhang et al., 2001a), the ß-actin 3'UTR is sufficient to induce dendritic targeting of the construct (as shown by an overlap of GFP and mApple expression in Figure 11B). Hence, as functionality of the construct could be confirmed, it was utilized to identify the presence of dendritic localization sequences in the mRNAs of neuronal profilins as well as Cof1 (Figure 11B).

Notably, dendritic localization and local translation could be induced by addition of the 3'UTR of Pfn1 as suggested by albeit low but visible GFP-expression in dendrites of hippocampal *fmr1* WT neurons. On the contrary, the 3'UTR of Pfn2a was not sufficient to induce dendritic targeting of the construct as no dendritic GFP expression was visible. However, after addition of the 5'UTR of Pfn2a, GFP dendritic expression could be detected thereby suggesting that in

case of Pfn2a, a dendritic localization sequence might be encoded in the 5'UTR and not in the 3'UTR. Similar to the MYR-eGFP-3'UTR Pfn1 construct, however, dendritic expression of MYR-eGFP-3'UTR-5'UTR Pfn2a was low. Notably, expression of MYR-eGFP fused to the 3'UTR of Cof1, though, led to very strong GFP-expression all over the dendritic tree which was clearly detectable even in dendritic spines.

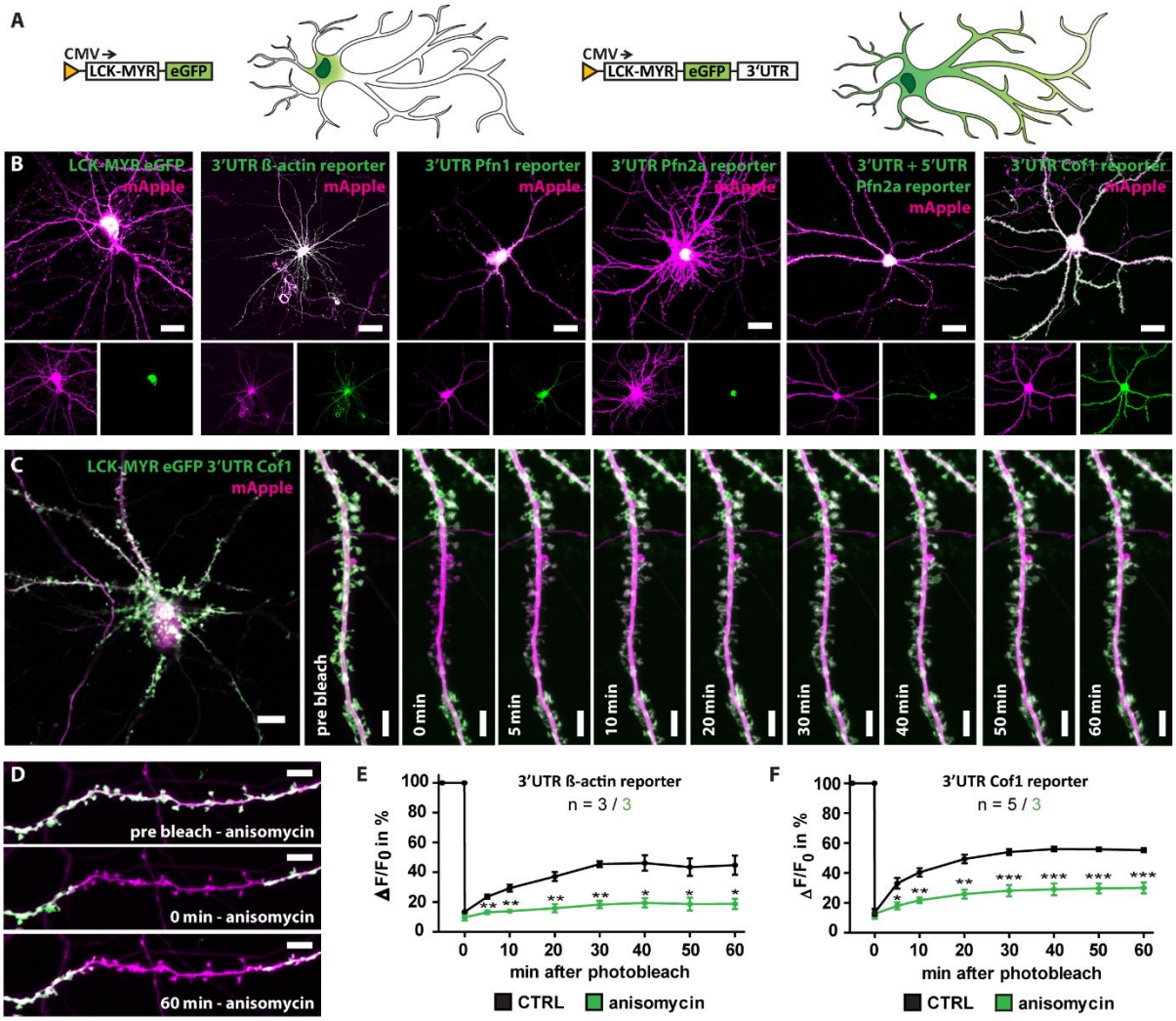

Figure 11 – Dendritic localization and local translation of ABP mRNAs. A) Scheme of the MYR-eGFP construct used for the analysis of local ABP translation. While eGFP expression is restricted to the cell body when expressing the pure construct, addition of a dendritic localization sequence induces dendritic targeting and local translation. **B)** Example images of cellular co-expression of mApple (magenta) and the following MYR-eGFP constructs in hippocampal neurons (green): MYR-eGFP fused to the 3'UTRs of ß-actin, Pfn1, Pfn2a, Cof1 or fused to the 3' and 5'UTR of Pfn2a. Note that the 3'UTRs of ß-actin, Pfn1 and Cof1 as well as the 5'UTR of Pfn2a are sufficient to induce dendritic GFP expression. Scale bars - 5 µm. **C)** Example images of a FRAP experiment performed in a distal dendrite of an mApple (magenta) and MYR-eGFP 3'UTR Cof1 (green) expressing hippocampal neuron. Note that GFP expression visibly recovers in a time course of up to 60 min after the photobleach. Scale bars - 10 µm (left), 5 µm. **D)** Example images of a FRAP experiment in the presence of the translational blocker anisomycin. Note that GFP fluorescence (green) recovery is abolished. Scale bars - 5 µm. **E)** FRAP of dendritic MYR-eGFP 3'UTR ß-actin signals with or without the presence of anisomycin. Fluorescence recovery was analyzed 0, 5, 10, 20, 30, 40, 50 and 60 min following the photobleach. **F)** FRAP of dendritic MYR-eGFP 3'UTR Cof1 signals with or without the presence of anisomycin. Fluorescence recovery was analyzed 0, 5, 10, 20, 30, 40, 50 and 60 min following the photobleach. Scale bars - 5 µm. All data is presented as mean ± SEM. Significances are indicated by *p value < 0.05, **p value < 0.01 and ***p value < 0.001. A list of all values and statistics can be seen in paragraph 9.1.

Summing up, dendritic localization motifs could be identified in the untranslated regions of both, neuronal profilins as well as Cof1 thereby suggesting that in line with the FISH data described above, the mRNAs of neuronal Pfn isoforms as well as Cof1 are transported into dendrites where they are locally translated upon need.

5.4.2 Local translation of cofilin 1

Although dendritic GFP expression of the different MYR-eGFP variants already indirectly confirmed local translation of the constructs, Fluorescence Recovery after Photobleaching experiments were performed to prove that dendritic GFP signals indeed derive from local protein synthesis. Therefore, individual dendritic branches which were at least 100 µm away from the cell body (to rule out possible diffusion effects) were bleached and fluorescence recovery was analyzed over a time course of up to 60 min either with or without the presence of the translational blocker anisomycin (Figure 11C,D). As local translation of ß-actin had already been shown previously (Surrey et al., 2018; Welshhans and Bassell, 2011), the MYR-eGFP 3'UTR ß-actin vector was used as a control. Interestingly, after bleaching of dendritic MYR-eGFP 3'UTR ß-actin signals, ~45% of GFP fluorescence recovered in the following 60 min (Figure 11E). However, when performing the same experiment in the presence of anisomycin, fluorescence recovery was almost abolished thereby confirming that indeed, dendritic GFP expression derives from local synthesis of the respective MYR-eGFP variant. As dendritic fluorescence from the MYR-eGFP 3'UTR Pfn1 as well as MYR-eGFP 3'UTR-5'UTR Pfn2a vectors was too low for FRAP experiments, focus was put on Cof1. FRAP experiments on distal dendrites expressing MYR-eGFP 3'UTR Cof1 showed a GFP fluorescence recovery of ~50% in the following 60 min which again was almost completely abolished in the presence of the translational blocker anisomycin (Figure 11F).

Altogether, these results confirm that dendritic MYR-eGFP expression derives from local protein synthesis. In addition, they suggest that the UTRs of neuronal profilins as well as Cof1 are sufficient to induce dendritic localization of the respective mRNAs. Finally, the local synthesis of Cof1 in dendrites could be confirmed.

5.5 Analysis of ABP mRNA distribution in *fmr1* WT and *fmr1* KO mice

The experiments and results discussed above hinted towards the fact that ABPs are locally translated in neurons. As especially l-LTP and l-LTD were shown to be dependent on *de novo* synthesis of proteins (Flexner et al., 1963; Krug et al., 1984; Linden, 1996; Montarolo et al., 1986; Stanton and Sarvey, 1984), this opened the possibility that the local synthesis of specific

ABPs might be crucially involved in mediating activity-dependent structural as well as functional changes at dendritic spines. As in theory, local translation could be mediated either by regulation of translation itself or by regulation of overall mRNA availability, the general mRNA distribution of neuronal Pfn as well as Cof1 mRNA was analyzed in DIV21 primary embryonic hippocampal *fmr1* WT and *fmr1* KO neurons using FISH. Therefore, the amount of detectable mRNA puncta in the nucleus, the cell body as well as proximal dendrites was manually counted in individual GFP-expressing neurons and normalized to cell compartment size (Figure 12).

In *fmr1* WT neurons, Pfn1 mRNA was primarily detectable in the cell body as well as in the nucleus, however, at similar levels (Figure 12A). On the contrary, the amount of Pfn1 mRNA puncta in proximal dendrites was approximately 10 times less in comparison to the other two compartments analyzed. Surprisingly, the same distribution could be shown for Pfn2a mRNA as the overall number of detectable Pfn2a mRNA puncta was nearly identical in comparison to those of Pfn1 mRNA in all compartments analyzed suggesting an equal distribution of Pfn1 and Pfn2a mRNA throughout hippocampal neurons (Figure 12A). Interestingly, also Cof1 mRNA could primarily be detected at comparable levels in the nucleus as well as the cell body but lower levels in proximal dendrites (Figure 12A). In comparison to neuronal Pfn isoforms, however, Cof1 mRNA puncta were detected at significantly higher numbers in the nucleus as well as the cell body. Contrarily, dendritic mRNA puncta of Cof1 were slightly increased in comparison to dendritic Pfn1 mRNAs but significantly higher in comparison to Pfn2a mRNAs.

In summary, probably as a result of nuclear transcription, ABP mRNAs were primarily found in the nucleus as well as the cell body of hippocampal *fmr1* WT neurons. Here, on average, mRNAs coding for Pfn1 or Pfn2a were present at similar numbers while Cof1 mRNA numbers were significantly higher. Yet, for all ABP mRNAs analyzed, a proportion of mRNAs could be found dendritically and notably, dendritic mRNA levels were fairly similar between all three mRNAs analyzed.

In *fmr1* KO neurons, FISH against the mRNA of Pfn1, Pfn2a and Cof1 revealed that the overall distribution of these mRNAs is similar in comparison towards the WT. The largest amount of mRNA for all three ABPs was present in the nucleus as well as the cell body and dendritic mRNA puncta were found less frequently (Figure 12B). In addition, Pfn1 and Pfn2a mRNAs were detectable at similar levels in all cellular compartments that were analyzed and the amount of detectable Cof1 mRNA puncta was always significantly higher in comparison to those of the two Pfn isoforms (Figure 12B), thereby mirroring the distribution that was found in the *fmr1* WT. Interestingly, the amount of detectable mRNA puncta in the cell body was completely unchanged for all three ABP mRNAs analyzed. However, *fmr1* KO neurons had

significantly less Pfn1 as well as Pfn2a puncta in the nucleus as well as in proximal dendrites in comparison to *fmr1* WT neurons (Figure 12C).

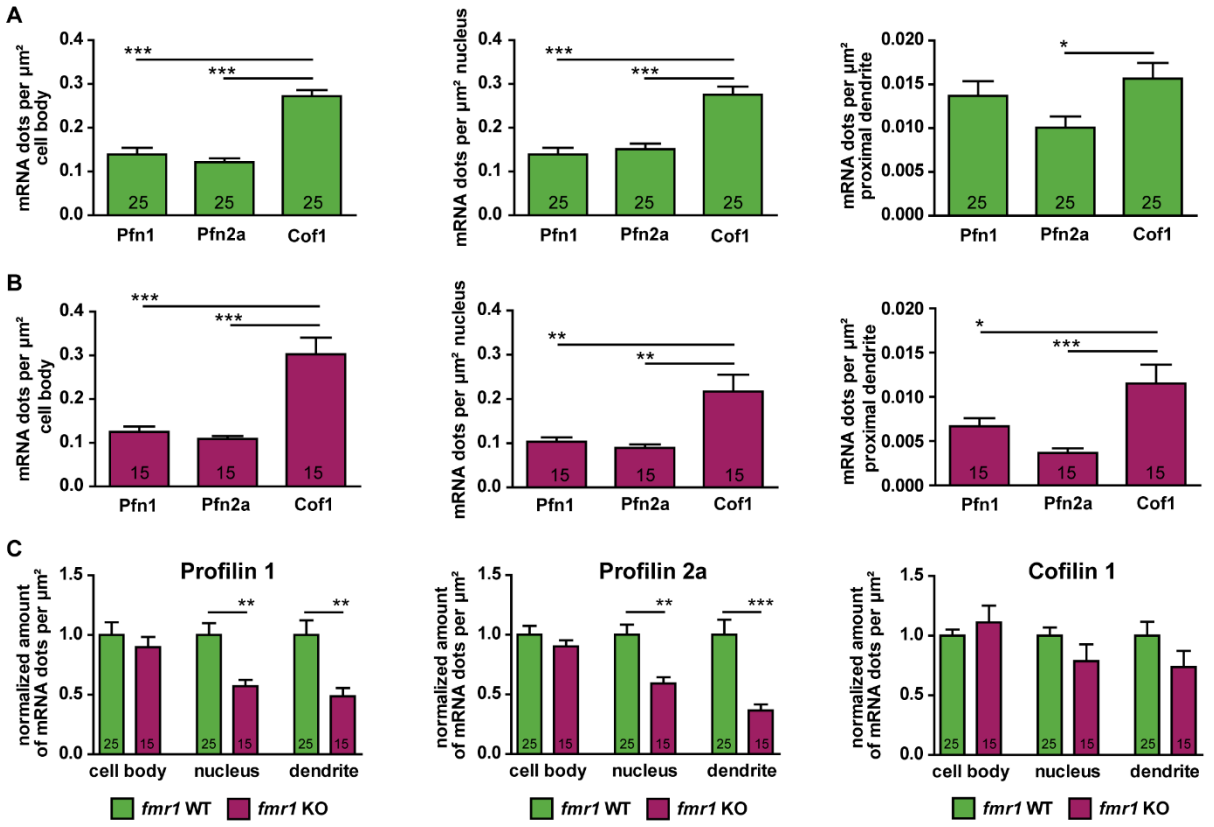

Figure 12 – ABP mRNA distribution in hippocampal *fmr1* WT and *fmr1* KO neurons. Distribution of Pfn1, Pfn2a as well as Cof1 mRNAs in the nucleus, the cell body as well as proximal dendrites of **A)** hippocampal *fmr1* WT and **B)** *fmr1* KO neurons. **C)** Comparison of Pfn1, Pfn2a and Cof1 mRNA distribution in hippocampal neurons derived from *fmr1* WT and *fmr1* KO neurons. All data is presented as mean ± SEM. Significances are indicated by *p value < 0.05, **p value < 0.01 and ***p value < 0.001. A list of all values and statistics can be seen in paragraph 9.1.

To sum up, in line with the fact that synaptic phenotypes in the FXS mouse model are proposed to derive from translational dysregulations rather than from transcriptional changes, the overall mRNA distribution of Pfn1, Pfn2a and Cof1 mRNA was unaltered in *fmr1* KO neurons. In addition, although the dendritic availability of Pfn1 and Pfn2a mRNAs was found to be decreased in the *fmr1* KO, mRNAs of all three ABPs were present in dendrites indicating their competence for *de novo* protein translation of ABPs. Hence, *fmr1* KO neurons do not seem to lack dendritically localized ABP mRNAs which suggests that alterations in the expression of Pfn1 and Cof1 in *fmr1* KO mice are caused either by direct translational alterations or by mRNA localization/availability changes that take place in an activity-dependent manner.

5.6 Analysis of ABP mRNA localization and local translation after NMDAR-dependent LTP

Previous studies suggested that on the protein level, neuronal profilins as well as Cof1 are mediated in an activity-dependent manner (Ackermann and Matus, 2003; Bosch et al., 2014). The fact that mRNAs of these proteins were found to be dendritically localized in the *fmr1* WT as well as the *fmr1* KO opened the possibility that mRNA localization and local ABP translation of these ABPs are mediated in an activity-dependent manner as well. Thus, to be able to analyze the activity-dependency of these mechanisms *in vitro*, a chemical protocol was established that reliably induced NMDAR-dependent LTP in dissociated hippocampal neurons via application of glycine and potential activity-dependent mRNA modulations were analyzed in dissociated hippocampal *fmr1* WT and *fmr1* KO neurons in response to the stimulus.

5.6.1 Activity-dependent modulations of ABP mRNA localization

As a readout, to confirm that long-term synaptic plasticity was induced, the average spine head diameter of stimulated hippocampal neurons was analyzed 20, 40 and 60 minutes after stimulation (Figure 13H). In *fmr1* WT neurons, as expected, a significant increase in the average spine head diameter could be observed over time. While the increase was not yet significant 20 min after stimulation, a significant growth was detectable 40 and 60 min after NMDAR-dependent LTP induction. Importantly, however, in *fmr1* KO neurons no significant changes in the average spine head diameter were detectable, thereby indicating that structural plasticity cannot be properly induced in these neurons.

To unravel whether the overall availability of ABP mRNAs in dendrites or at dendritic spines is mediated in an activity-dependent manner and whether the structural plasticity defect in *fmr1* KO neurons can be attributed to a missing mRNA modulation, the localization of Pfn1, Pfn2a and Cof1 mRNAs was analyzed in the same neurons and at the same time-points at which the spine head diameter analysis was performed.

In *fmr1* WT neurons, the induction of NMDAR-dependent LTP led only to marginal changes in the distribution of Pfn1 mRNAs. In comparison to the distribution in unstimulated neurons, none of the analyzed time-points (20, 40, 60 minutes post stimulation) showed significant changes indicating that on average, the level of detectable mRNA puncta remained stable in the nucleus, the cell body as well as proximal dendrites of all analyzed hippocampal neurons (Figure 13A). Notably, 60 minutes after stimulation a trend towards decreased Pfn1 mRNAs levels in all three cellular compartments could be observed. However, these reductions were

significant only in the cell body and the nucleus and only in comparison with the time-point 20 min after stimulation.

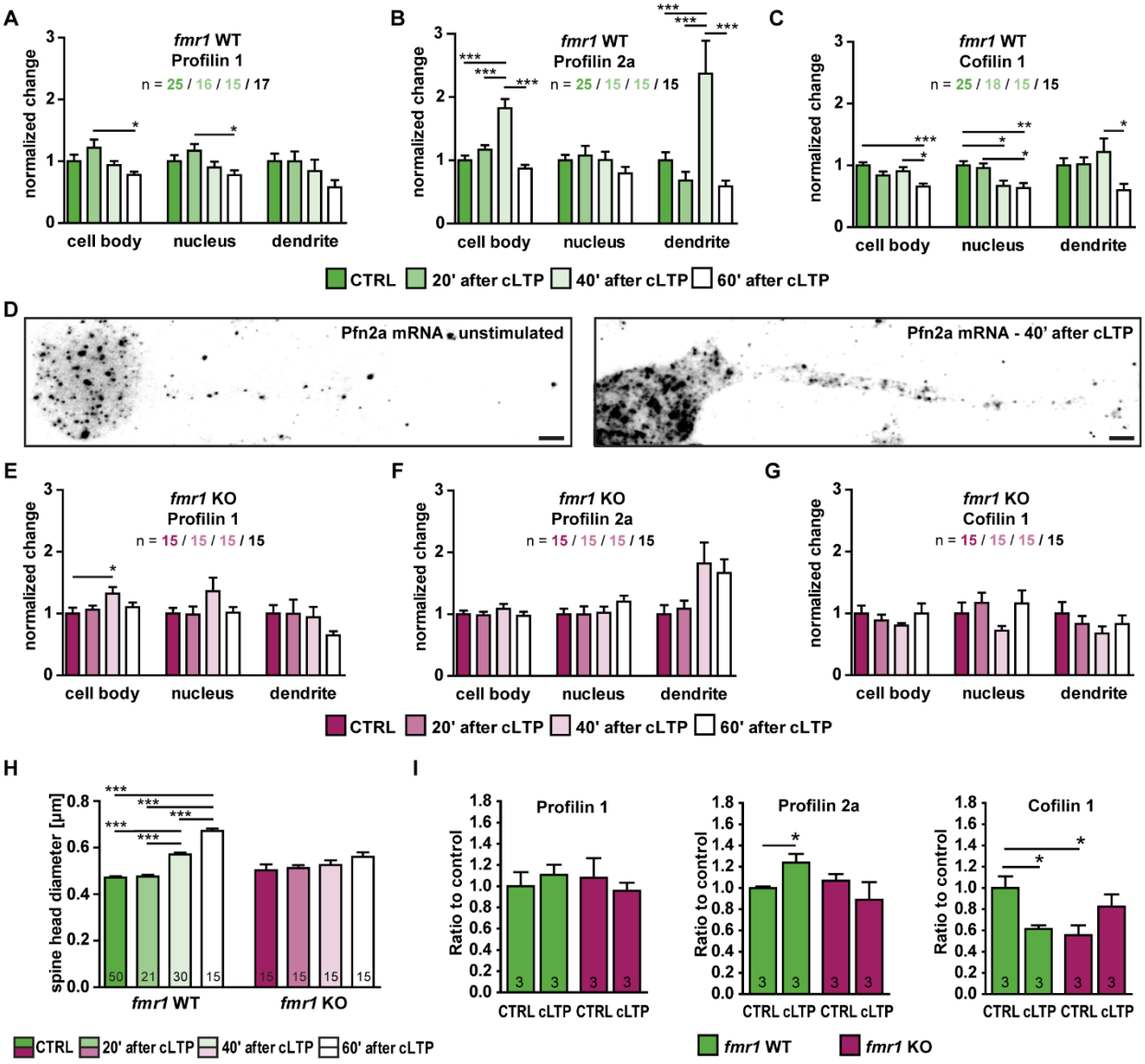

Figure 13 – Regulation of Pfn1, Pfn2a and Cof1 mRNA availability as well as protein expression after chemically-induced NMDAR-dependent LTP. A,B,C) Analysis of Pfn1, Pfn2a and Cof1 mRNA distribution in hippocampal *fmr1* WT neurons before and 20, 40 and 60 minutes after chemical induction of NMDAR-dependent LTP. **D)** Example images showing a FISH against Pfn2a mRNA in unstimulated hippocampal neurons as well as in stimulated neurons 40 minutes after the induction of cLTP. Scale bars – 5 µm. **E,F,G)** Pfn1, Pfn2a and Cof1 mRNA distribution in hippocampal *fmr1* KO neurons before and 20, 40 and 60 minutes after chemical induction of NMDAR-dependent LTP. **H)** Average spine head diameter in unstimulated hippocampal *fmr1* WT and *fmr1* KO neurons as well as 20, 40 and 60 minutes after cLTP. **I)** Hippocampal expression of Pfn1, Pfn2a and Cof1 prior and 60 minutes after the chemical induction of NMDAR-dependent LTP. All data is presented as mean ± SEM. Significances are indicated by *p value < 0.05, **p value < 0.01 and ***p value < 0.001. A list of all values and statistics can be seen in paragraph 9.1.

In case of Pfn2a mRNA, however, a clear activity-dependent modulation could be observed. While nuclear levels of Pfn2a mRNA remained stable and unchanged at all time-points analyzed (Figure 13B), in the cell body and interestingly, especially prominent in proximal

dendrites, the amount of Pfn2a mRNA significantly increased 40 minutes after induction of cLTP (Figure 13B, D). Surprisingly, this effect seemed to be very tightly regulated in time as these effects were not visible 20 minutes after stimulation and in addition, were gone 60 minutes after stimulation. In contrast to this, the availability of Cof1 mRNAs was found to be downregulated after cLTP induction (Figure 13C). In comparison to the average Cof1 mRNA amount in unstimulated hippocampal neurons, cLTP induction led to a significant reduction of Cof1 mRNA levels beginning at 40 minutes after stimulation. Here, a significant reduction in nuclear Cof1 mRNA could be observed which then 60 minutes after cLTP, was detectable also in the cell body as well as proximal dendrites indicating a clear activity-dependent regulation of Cof1 mRNA availability.

Taken together, these data suggest an activity-dependent regulation of Pfn2a as well as Cof1 mRNA availability in dendrites of hippocampal neurons after NMDAR-dependent LTP induction. While the level of Pfn2a mRNA in dendrites was shown to be specifically upregulated 40 minutes after cLTP, the available amount of dendritically localized Cof1 mRNAs was found to be downregulated 60 minutes after cLTP. Hence, the availability of ABP mRNAs and thus, potentially also the local translation of ABPs which might be needed for structural plasticity in dendritic spines is mediated by synaptic activity in hippocampal *fmr1* WT neurons.

While the results presented above clearly indicated an activity-dependent modulation of Pfn2a and Cof1 mRNA availability in dendrites, analysis of mRNA distribution in hippocampal *fmr1* KO neurons revealed that these modulations are completely absent in *fmr1* KO mice (Figure 13E, F, G). Here, the induction of cLTP had no effect on the overall distribution of Pfn2a as well as Cof1 mRNA as compared to unstimulated neurons, no significant changes in the overall mRNA level were detectable at 20, 40 or 60 minutes after stimulation in any of the cellular compartments analyzed (Figure 13F, G). Notably, also in case of Pfn1 mRNA no significant changes in the nuclear as well as dendritic levels of Pfn1 mRNA were found 20, 40 or 60 minutes after cLTP induction in *fmr1* KO neurons (Figure 13E). The only significant modulation that was observable was an increase of Pfn1 mRNA in the cell body 40 minutes after cLTP induction. However, in comparison to unstimulated controls, no changes were detectable 20 or 60 minutes after the induction of NMDAR-dependent LTP.

To sum up, these results suggest that an activity-dependent modulation of ABP mRNA localization and ultimately, availability at dendritic spines is missing in hippocampal *fmr1* KO neurons. Importantly, modulations of dendritically localized Pfn2a and Cof1 mRNAs that were shown to take place in *fmr1* WT neurons were completely lacking over a time course of up to 60 minutes after induction of NMDAR-dependent LTP in *fmr1* KO cells. In addition, potentially as a direct result from these dysregulations, structural plasticity was completely absent in *fmr1* KO neurons.

5.6.2 Activity-dependent regulation of hippocampal ABP expression *in vitro*

The fact that the localization of ABP mRNAs was found to be altered upon NMDAR-dependent LTP opened the possibility that also ABP expression might be modulated following synaptic activity. To test for this, acute hippocampal slices were prepared from *fmr1* WT and *fmr1* KO mice and either kept unstimulated or were stimulated via application of glycine and strychnine. Afterwards, hippocampal slices that underwent the same treatment and originated from the same animal were pooled, homogenized and hippocampal expression of Pfn1, Pfn2a and Cof1 was analyzed via Western blotting (Figure 13I).

Interestingly, the results completely mirrored the data that was gained from the mRNA distribution analysis. In *fmr1* WT mice, similar to what was observable on the mRNA level, expression of Pfn1 was unaltered 60 min after the induction of NMDAR-dependent LTP while hippocampal expression of Pfn2a significantly increased (Figure 13I). Importantly, also in line with the mRNA data, Cof1 expression significantly decreased 60 minutes after cLTP induction.

As already described above, in *fmr1* KO mice, none of the neuronal profilins was differently expressed under basal conditions, however, hippocampal Cof1 expression was significantly decreased already under basal conditions (Figure 9B, Figure 13I). Nevertheless, the expression of these ABPs was not significantly altered in the hippocampus 60 minutes after cLTP. Notably, while the hippocampal expression of neuronal Pfn isoforms was fairly equal in unstimulated and stimulated hippocampal slices, Cof1 expression was found to be rather increased upon cLTP, however, the increase was not statistically significant (Figure 13I).

Altogether, these results indicate that not only the localization and availability of ABP mRNAs is mediated in an activity-dependent manner but also hippocampal ABP expression. In line with the results gained from the mRNA analysis, the analysis of hippocampal Pfn1, Pfn2a and Cof1 expression after NMDAR-dependent LTP revealed that Pfn2a as well as Cof1 levels are altered upon stimulation in *fmr1* WT mice. In *fmr1* KO neurons, however, supporting the observation that ABP mRNA modulations upon cLTP were absent, also activity-dependent modulations of hippocampal ABP expression where missing.

5.6.3 Activity-dependent local translation of cofilin 1

Based on various previous studies, the predominant theory of FXS neuropathology is based on the assumption that phenotypes in FXS derive from a dysregulation of local protein synthesis in dendrites (Feng et al., 1997). Since earlier experiments indicated that mRNA availability as well as protein expression of Pfn2a as well as Cof1 are mediated in an activity-dependent manner and dysregulated in the mouse model of FXS, the question arose whether

local translation of these proteins is dysregulated in these animals as well. However, as it could already be shown that only the mRNA of Cof1 but not Pfn2a is a direct target of FMRP, focus was put especially on the analysis of local Cof1 synthesis utilizing the same MYR eGFP construct and the same FRAP approach that was used in paragraph 5.4. Therefore, first, to identify whether also the local synthesis of Cof1 is dependent on synaptic activity, local Cof1 translation was analyzed for a time window of up to 60 min after induction of NMDAR-dependent LTP in DIV21 dissociated hippocampal *fmr1* WT neurons (Figure 14A). Importantly, fluorescence recovery was significantly decreased 10 to 40 min after the LTP stimulus thereby providing evidence that local Cof1 translation is negatively modulated in an activity-dependent manner.

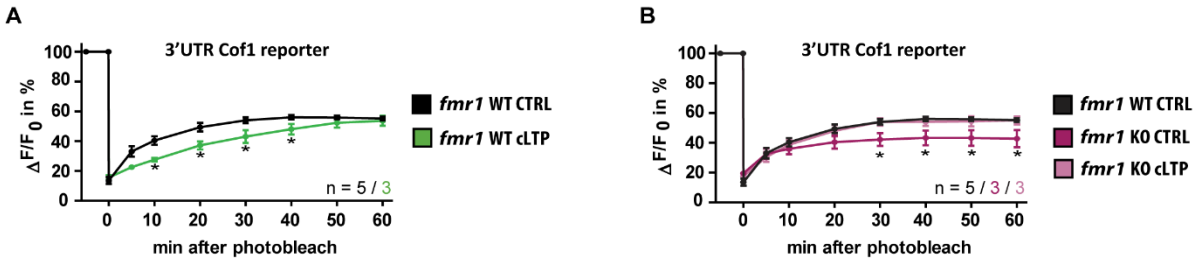

Figure 14 – Local cofilin 1 synthesis in hippocampal *fmr1* WT and *fmr1* KO neurons after NMDAR-dependent LTP. Fluorescence recovery curves after FRAP of dendritic MYR-eGFP 3'UTR Cof1 signals in **A)** hippocampal *fmr1* WT or **B)** *fmr1* KO neurons. Fluorescence recovery was analyzed 0, 5, 10, 20, 30, 40, 50 and 60 min following the photobleach which was applied either on unstimulated distal dendrites or immediately after chemical induction of NMDAR-dependent LTP. All data is presented as mean ± SEM. Significances are indicated by *p value < 0.05, **p value < 0.01 and ***p value < 0.001. A list of all values and statistics can be seen in paragraph 9.1.

Intriguingly, repeating these experiments in *fmr1* KO neurons revealed that local translation of the LCK-MYR-eGFP-3'UTR Cof1 construct was significantly reduced already under baseline conditions as indicated by significantly reduced fluorescence recovery (Figure 14B). Moreover, in contrast to the results in *fmr1* WT neurons, LTP induction led to an increase in LCK-MYR-eGFP-3'UTR cof1 translation 20 to 60 min post-stimulation.

Collectively, these data clearly indicate that the amount of dendritically synthesized Cof1 is modulated in a specific time window after induction of synaptic plasticity. In addition, these experiments provide evidence that this modulation is impaired in the FXS mouse model.

5.7 Spatial memory formation in *fmr1* KO mice

As the *in vitro* data suggested a crucial role of neuronal profilins as well as Cof1 for hippocampal synaptic plasticity, the question arose whether hippocampal ABP levels are modulated in a similar fashion *in vivo* during spatial memory formation. Therefore, *fmr1* WT and *fmr1* KO mice were trained for 8 days in the hippocampus-dependent Morris Water Maze task and hippocampal Pfn1, Pfn2a and Cof1 levels were analyzed directly after a spatial memory reference test on training day 9 (Figure 15).

5.7.1 Morris Water Maze performance of *fmr1* WT and *fmr1* KO mice

Mice of both genotypes performed equally well in the 3 days pre-training period (Figure 15A) and showed a significant reduction of the escape latency over the total training period indicating spatial memory formation (Figure 15B). Nevertheless, while escape latencies on the last day of training were not significantly different between the two genotypes, the escape latency of *fmr1* KO mice on training day 1 was found to be significantly elevated (Figure 15C). In line with the fact that spatial memory was formed, analysis of the searching strategies revealed that similar to *fmr1* WT mice, *fmr1* KO mice increased the use of hippocampus-dependent, allocentric search strategies over time (Figure 15D). Yet, interestingly, *fmr1* KO mice were found to be less accurate in localizing the correct hidden platform position during the reference memory test. Although both, *fmr1* WT and *fmr1* KO mice, performed similarly well in probe trials on training day 6 (Figure 15E) and training day 9 (Figure 15F) and showed a significant preference for the target quadrant, heatmaps of the groups center point (Figure 15G) as well as analysis of the number of platform crossings on probe trial day 9 (Figure 15H) revealed that *fmr1* KO mice were less precise in localizing the former platform position in comparison to *fmr1* WT animals.

In sum, compared to *fmr1* WT mice, *fmr1* KO animals show impairments in precise memory recall in the Morris Water Maze as indicated by less accurate performances in the probe trials.

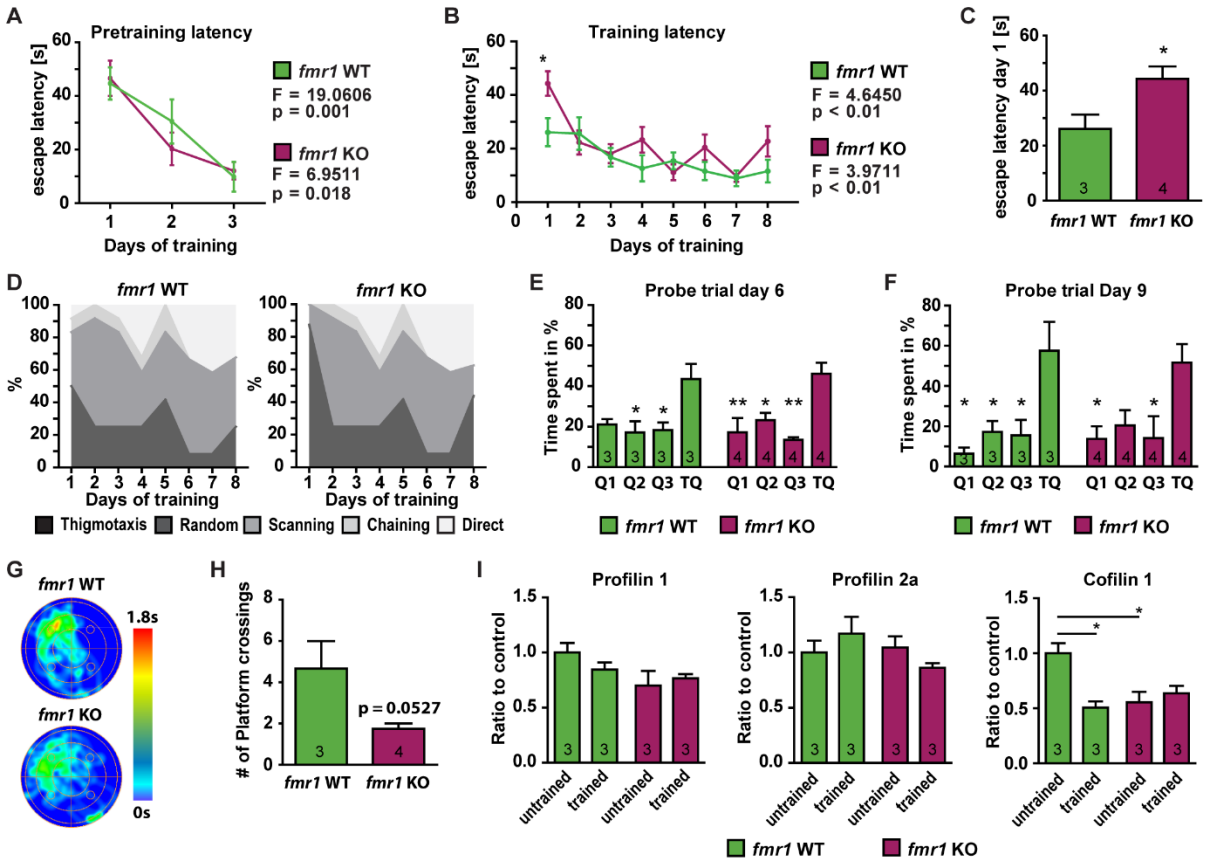

Figure 15 – *Fmr1* KO mice show deficits in spatial memory formation and dysregulations in hippocampal ABP expression. A) Latency of *fmr1* WT (n = 3) and *fmr1* KO (n = 4) mice trained with a visible platform in a pre-training period of 3 days. **B)** Escape latency of *fmr1* WT and *fmr1* KO mice trained for 8 days in the hidden platform version of the Morris Water Maze. **C)** Escape latency on training day 1. **D)** Analysis of the different searching strategies used throughout the training session including Thigmotaxis as well as hippocampus-dependent (Direct) and hippocampus-independent strategies (Random, Scanning, Chaining). **E)** Analysis of the average time spent in the target quadrant (TQ) as well as the other quadrants of the Water maze (Q1, Q2, Q3) on the reference memory test on training day 6. **F)** Analysis of the average time spent in the target quadrant (TQ) as well as the other quadrants of the Water maze (Q1, Q2, Q3) on the reference memory test on training day 9. **G)** Heatmap of the center point of both test groups during the probe trial. **H)** Number of platform crossings during the reference memory test on training day 9. **I)** Hippocampal Pfn1, Pfn2a and Cof1 expression in untrained and Water maze trained *fmr1* WT and *fmr1* KO mice. All data is presented as mean ± SEM. Significances are indicated by *p value < 0.05, **p value < 0.01 and ***p value < 0.001. A list of all values and statistics can be seen in paragraph 9.1.

5.7.2 Activity-dependent regulation of hippocampal ABP expression *in vivo*

Directly after the probe trial on training day 9, all mice were sacrificed and hippocampal protein samples were prepared that allowed for the analysis of hippocampal Pfn1, Pfn2a and Cof1 expression via Western blotting (Figure 15I).

Intriguingly, in *fmr1* WT mice, neither hippocampal Pfn1 nor Pfn2a expression was significantly altered after 9 days of training in the Morris Water Maze while Cof1 expression was found to be significantly decreased. In *fmr1* KO mice, hippocampal expression of Pfn1 and Pfn2a was

unchanged in untrained animals when compared to *fmr1* WT mice and in addition, expression of both Pfn isoforms was not significantly altered after training in the Morris Water Maze. However, Cof1 expression was significantly reduced already in naive *fmr1* KO mice compared to WT animals and in addition, a negative regulation of hippocampal Cof1 expression as could be shown for *fmr1* WT mice was absent.

Summing up, while previous *in vitro* results suggested an activity-dependent modulation of hippocampal Pfn2a as well as Cof1 expression in *fmr1* WT neurons, only Cof1 levels were found to be significantly changed after training in the Morris Water Maze in *fmr1* WT mice. Moreover, in line with the *in vitro* data that indicated a negative modulation of Cof1 mRNA availability as well as local Cof1 synthesis, Cof1 expression was decreased after spatial memory formation. Most notably, experience-dependent alterations in ABP expression could not be detected in the hippocampus of *fmr1* KO animals after the training period indicating that also *in vivo*, an activity-dependent modulation of ABP expression, as could be shown here for Cof1, is missing.

5.8 Manipulation of actin dynamics in *fmr1* KO neurons *in vitro*

So far, all results suggested that the induction of NMDAR-dependent LTP leads to a negative modulation of Cof1 activity as indicated by a decrease in Cof1 mRNA availability, local Cof1 synthesis and overall Cof1 expression levels in a specific time window after LTP in *fmr1* WT mice. As this modulation was absent in *fmr1* KO mice, in a next step it was analyzed whether a similar modulation of either actin dynamics in general or Cof1 activity specifically would be able to rescue the structural plasticity defect in hippocampal *fmr1* KO neurons. Therefore, Jasplakinolide, CytochalasinD as well as a peptide consisting of the first 16 residues of Ser3-phosphorylated Cof1 (pCof1) which functions as an inhibitor of endogenous Cof1 were utilized and the specific drugs were applied either already together with glycine or starting after the cLTP inducing stimulus (Figure 16).

In *fmr1* WT neurons, while structural plasticity could reliably be induced by glycine application as indicated by a significant increase in the average spine head diameter of all analyzed neurons, CytochalasinD or the pCof1 peptide completely prevented an increase in spine head diameter independently of the time-point of application (Figure 16A). Interestingly, a stabilization of actin via Jasplakinolide during and after the glycine stimulus led to a further but not significant increase in spine head diameter when compared to cLTP alone. This effect could not be observed when Jasplakinolide was applied after cLTP induction (Figure 16A).

In *fmr1* KO cells, where glycine application was not sufficient to induce an increase in spine head diameter, also neither application of Jasplakinolide nor CytochalasinD led to any significant spine head diameter changes in comparison to controls (Figure 16A). However, when Cof1 activity was specifically decreased after the glycine stimulus using the pCof1 peptide - which mimicked the activity-dependent modulation we observed in WT cells - a significant increase in spine head diameter was detectable (Figure 16A, B). Importantly, this effect was abolished when we applied the pCof1 peptide already during cLTP induction (Figure 16A).

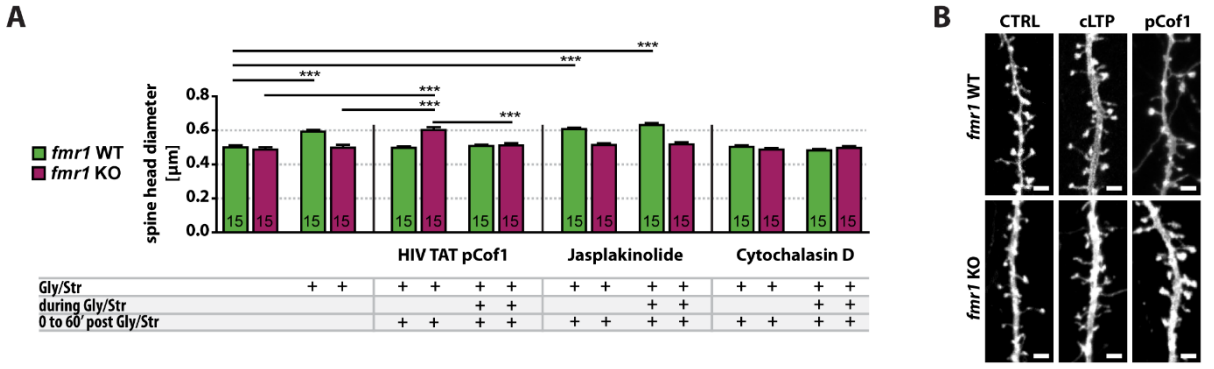

Figure 16 - Structural plasticity deficits in *fmr1* KO neurons can be rescued by manipulation of Cof1 activity. A) Spine head diameter analysis of *fmr1* WT and *fmr1* KO neurons where actin dynamics were modulated either after the stimulation period or during and after the stimulation period. **B)** Shown are representative images of *fmr1* WT and *fmr1* KO dendrites under basal conditions (CTRL), 60 min after induction of cLTP (cLTP) and 60 min after LTP induction where additionally Cof1 activity was blocked via the HIV TAT pCof1 peptide after the stimulation period (pCof1). Note that the application of the HIV TAT pCof1 peptide rescued structural plasticity after NMDAR-dependent LTP in *fmr1* KO neurons. Scale bars – 2 µm. All data is presented as mean ± SEM. Significances are indicated by *p value < 0.05, **p value < 0.01 and ***p value < 0.001. A list of all values and statistics can be seen in paragraph 9.1.

All in all, these data offer clear evidence for the importance of Cof1 activity for structural plasticity following NMDAR-dependent LTP in hippocampal neurons. In *fmr1* WT mice, application of the pCof1 peptide completely abolished structural plasticity indicating that a certain level of Cof1 activity is crucial for morphological changes to occur. In line with this, in *fmr1* KO mice, where structural plasticity was originally absent, a modulation of Cof1 activity which mimicked the regulation of Cof1 seen in *fmr1* WT neurons was able to rescue this defect. In addition, showing that the modulation of ABPs is tightly regulated in time and is specifically taking place after induction of LTP, application of the pCof1 peptide also during the cLTP inducing stimulus was not sufficient to rescue the structural plasticity defect in *fmr1* KO neurons.

5.9 Analysis of ABP mRNA localization after mGluR-dependent LTD in the hippocampus

So far, it could be shown that structural plasticity is absent in the hippocampus of *fmr1* KO mice following NMDAR-dependent LTP because a crucial modulation of actin via Cof1 is missing in a specific time window after neuronal activity. Importantly, this phenotype could be rescued by specifically decreasing Cof1 activity following the LTP stimulus. However, apart from the NMDAR-dependent LTP, also the mGluR-dependent LTD was shown to be dysregulated in FXS (Bear et al., 2004; Huber et al., 2002), namely, it was found to be exaggerated. As FMRP was found to specifically suppress local translation of a subset of proteins which are needed for the mediation of mGluR-dependent LTD and previous work offered evidence that FXS phenotypes might be rescued by specifically inhibiting mGluR-dependent LTD (Dolen et al., 2007), this form of synaptic plasticity had been in the focus of FXS research so far. Nevertheless, while most studies focused on the functional aspects of LTD dysfunction in FXS, the molecular pathways mediating actin-dependent structural changes at dendritic spines upon mGluR-dependent LTD are yet not completely understood. Therefore, to analyze whether similar to what could be shown for NMDAR-dependent LTP, mRNAs of neuronal Pfn isoforms as well as Cof1 are mediated in an activity-dependent manner following mGluR-dependent LTD, the mRNA distribution of these proteins was analyzed in DIV21 primary embryonic hippocampal *fmr1* WT and *fmr1* KO neurons 20, 40 and 60 min upon cLTD induction via DHPG (Figure 17).

5.9.1 ABP mRNA localization after cLTD induction in *fmr1* WT mice

To confirm that cLTD was properly induced, the average spine head diameter (from neurons which were used for the mRNA distribution analysis) was analyzed and as expected, a significant decrease in the average spine head diameter could be observed over time (Figure 17E). While the decrease was not yet significant 20 min after stimulation, a significant reduction was detectable 40 and 60 min after mGluR-dependent LTD induction in *fmr1* WT neurons.

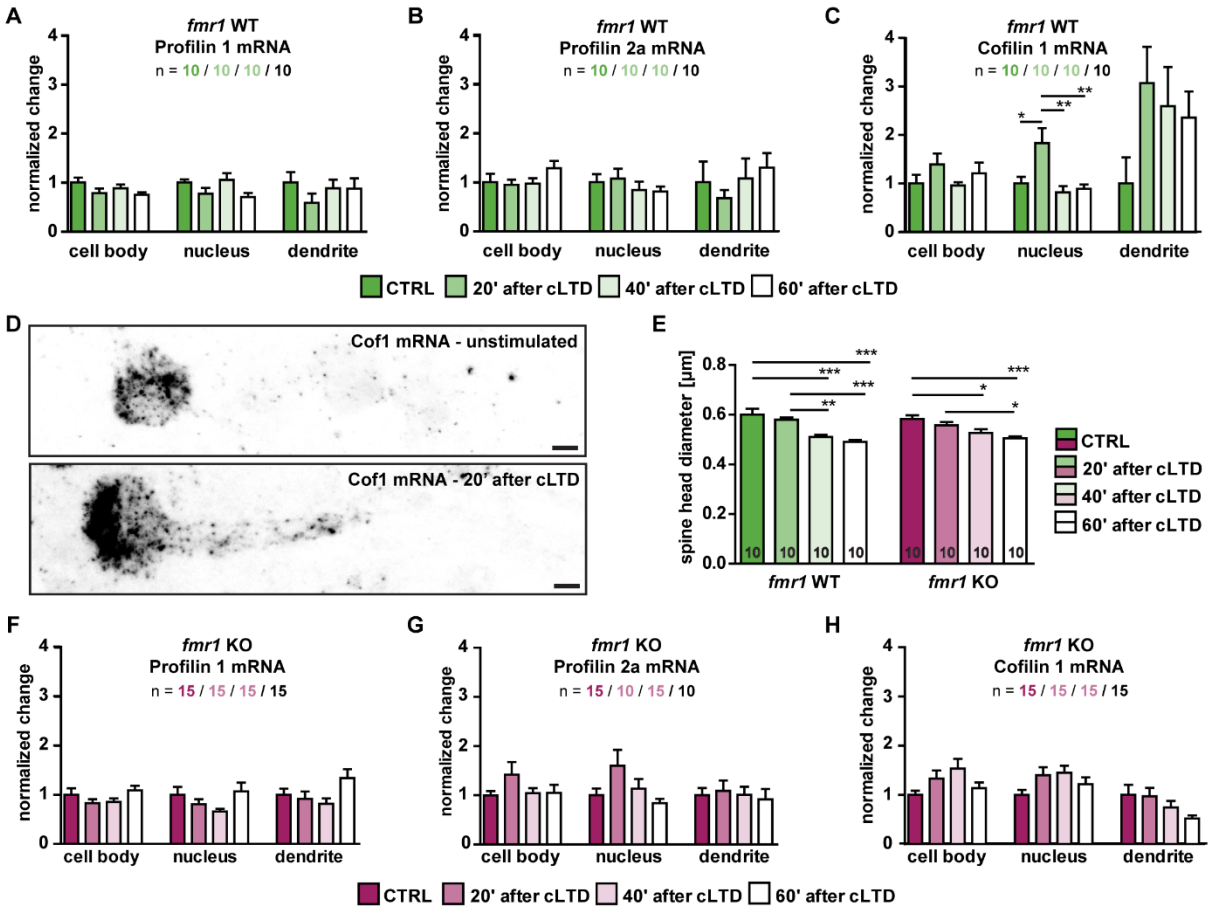

Figure 17 - Analysis of Pfn1, Pfn2a and Cof1 mRNA availability after chemically-induced mGluR-dependent LTD. A,B,C) Analysis of Pfn1, Pfn2a and Cof1 mRNA distribution in hippocampal *fmr1* WT neurons before and 20, 40 and 60 minutes after chemical induction of mGluR-dependent LTD. **D)** Example images showing a FISH against Cof1 mRNAs in unstimulated hippocampal neurons as well as in stimulated neurons 20 minutes after the induction of cLTD. Scale bars – 5 µm. **E)** Average spine head diameter in unstimulated hippocampal *fmr1* WT and *fmr1* KO neurons as well as 20, 40 and 60 minutes after cLTD. **F,G,H)** Pfn1, Pfn2a and Cof1 mRNA distribution in hippocampal *fmr1* KO neurons before and 20, 40 and 60 minutes after chemical induction of mGluR-dependent LTD. All data is presented as mean ± SEM. Significances are indicated by *p value < 0.05, **p value < 0.01 and ***p value < 0.001. A list of all values and statistics can be seen in paragraph 9.1.

Via FISH, in hippocampal *fmr1* WT neurons, the amount of detectable Pfn1, Pfn2a and Cof1 mRNA puncta in the nucleus, the cell body and proximal dendrites was manually counted and normalized to the size of the cellular compartment analyzed. Notably, the chemical induction of mGluR-dependent LTD did not cause any significant changes in the overall level of Pfn1 mRNAs per compartment at any of the different time-points analyzed (20, 40 and 60 min following the stimulus) (Figure 17A). Similarly, no changes in the localization of Pfn2a mRNAs were found (Figure 17B). However, in the nucleus, the overall level of Cof1 mRNA significantly increased 20 min after cLTD induction (Figure 17C, D) while it was back to basal levels again 40 and 60 min after the stimulus. Surprisingly, this increase could not be observed in the cell body as here, no alterations in Cof1 mRNA amount were detectable 20, 40 as well as 60 min after cLTD. In proximal dendrites, however, an increase in Cof1 mRNA levels was clearly

visible starting 20 min after cLTD which was then gradually decreasing over time (Figure 17C). Nevertheless, due to high variations between individual neurons, the dendritic increase in Cof1 mRNA was not statistically significant when compared towards the dendritic amount of Cof1 mRNA under basal conditions.

Collectively, these data suggest that the overall distribution and availability of Pfn1 and Pfn2a mRNAs is not mediated by mGluR-dependent LTD. Contrarily, it could be shown that the induction of LTD leads to a nuclear as well as dendritic increase in Cof1 mRNA, thereby indicating a time specific modulation.

5.9.2 ABP mRNA localization after cLTD induction in *fmr1* KO mice

To confirm that mGluR-dependent LTD was properly induced also in *fmr1* KO neurons (which were used for the analysis of mRNA distribution), the average spine head diameter was analyzed (Figure 17E). As expected, the induction of cLTD led to a decrease in the average spine head diameter over time which was significant 40 and 60 min after the cLTD-inducing stimulus when compared to the average spine head diameter in unstimulated *fmr1* KO control neurons.

Interestingly, the chemical induction of mGluR-dependent LTD did not lead to changes in the distribution of Pfn1 mRNAs in hippocampal neurons. Analysis of the overall mRNA amount in the nucleus, the cell body as well as proximal dendrites revealed no significant alterations in the distribution of Pfn1 mRNAs 20, 40 as well as 60 min after induction of mGluR-dependent LTD (Figure 17F). Similarly, also the FISH analysis of Pfn2a mRNAs could show that the induction of cLTD is not significantly affecting the overall Pfn2a mRNA distribution in *fmr1* KO neurons (Figure 17G). Interestingly, also the cellular distribution of Cof1 mRNAs was found to be unaffected by the chemical induction of mGluR-dependent LTD as overall, no significant alterations in the nuclear, the cell body as well as the dendritic distribution were detected in any of the time-points analyzed (Figure 17H).

Taken together, neither the amount nor the overall distribution of Pfn1, Pfn2a or Cof1 mRNAs was altered after mGluR-dependent LTD in hippocampal *fmr1* KO neurons. Hence, in these neurons, an activity-dependent modulation of Cof1 mRNAs is missing as in comparison, a significant increase in nuclear as well as dendritic availability of Cof1 mRNAs was shown in *fmr1* WT cells. This is especially surprising as on the one hand, spine shrinkage following LTD is known to crucially involve Cof1 activity (Fukazawa et al., 2003) and in addition, previous studies could show that mGluR-dependent LTD is significantly increased in hippocampal *fmr1*

KO neurons (Bear et al., 2004; Huber et al., 2002). Yet, although significant spine shrinkage was observable, an activity-dependent modulation of Cof1 mRNAs seems to be absent in FXS.

5.10 Outlook: Analysis of ABP mRNA transport

Collectively, so far, all experiments hinted towards the fact that ABP mRNAs are regulated in an activity-mediated manner following synaptic activity. Both, NMDAR-dependent LTP as well as mGluR-dependent LTD led to modulations of local ABP mRNA availability in hippocampal *fmr1* WT neurons which might potentially already be sufficient to modulate local translation rates. In line with this, an activity-dependent modulation of local Cof1 translation and ultimately, Cof1 expression upon cLTP confirmed the activity-dependency of local ABP translation in hippocampal neurons. However, how the dendritic availability of ABP mRNAs is actually regulated is yet unknown. Although the experiments described above confirmed that the mRNAs of Pfn1 and Cof1 both can be bound by FMRP (Feuge et al., 2019; Michaelsen-Preusse et al., 2016), one would have expected a clear deficit in the mRNA distribution in *fmr1* KO neurons as here, FMRP is absent. However, both mRNAs were still present in dendrites as well as directly at dendritic spines in *fmr1* KO cells, thereby indicating that apart from FMRP, other mRNA-binding proteins seem to be involved in the transport of those mRNAs. Therefore, in FXS, dysregulations in mRNA localization, at least for the mRNAs observed here, must not necessarily derive from the direct loss of FMRP but might be due to different reasons e.g. changes in mRNA transport in general. Therefore, to visualize and directly analyze the mRNA transport of ABP mRNAs, the MS2 vector system (Bertrand et al., 1998) was utilized (Figure 18).

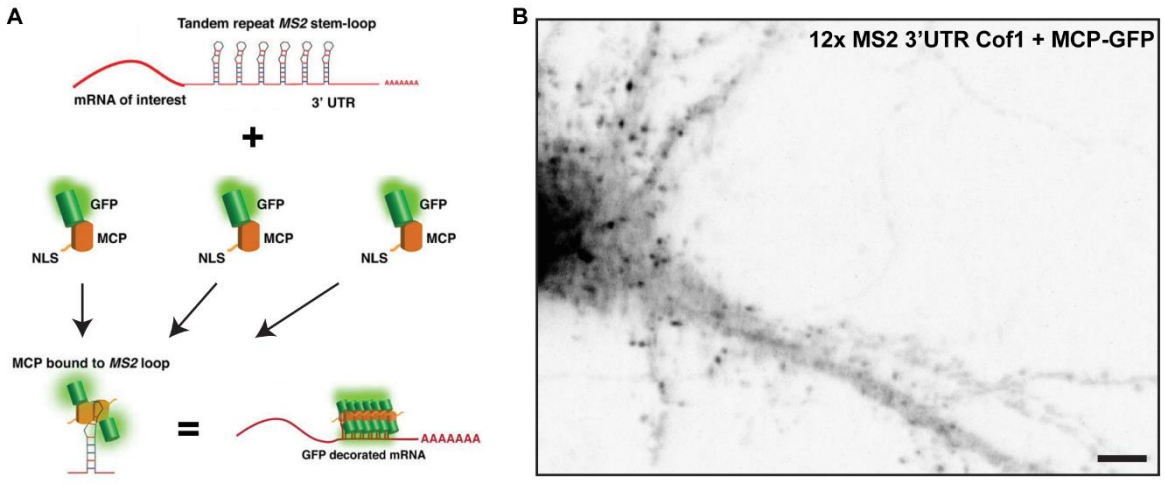

Figure 18 – Analysis of dendritic mRNA transport utilizing the MS2 vector system. A) Scheme of the MS2 vector system. The mRNA (or the UTR) of interest is fused to tandem repeat MS2 stem-loops which can be recognized and bound by GFP-tagged MCP. Hence, the MS2 stem-loops in the mRNA of interest get decorated with GFP and the mRNA can be tracked via live-imaging. **B)** Co-expression of MCP-GFP and 12x MS2 stem-loops fused to the 3'UTR of Cof1 in a hippocampal *fmr1* WT neuron. Note the punctated GFP-staining of individual mRNAs. Scale bar – 5 µm

Here, twelve tandem repeat stem-loops of the MS2 protein were fused to the 3'UTR of Cof1, thereby generating the ‚mRNA of interest'. This construct was co-expressed in DIV21 primary embryonic hippocampal *fmr1* WT neurons together with GFP-tagged MCP which specifically binds to MS2 stem-loops. Hence, in theory, the mRNA of interest gets decorated with GFP-tagged MCP which generates a visible GFP signal (whose strength is dependent on the amount of stem-loops) that allows the live-tracking of mRNAs along dendrites (schematically shown in Figure 18A). Here, specific focus was put on the construct containing the 3'UTR of Cof1 as earlier experiments suggested that the dendritic targeting of Cof1 mRNAs is remarkably strong in comparison to Pfn1 or Pfn2a mRNAs.

However, unfortunately, first experiments did not offer any conclusive results as several sets of experiments were needed to identify the right transfection ratio between the 'mRNA of interest' containing the MS2 stem-loops and the GFP-tagged MCP. In addition, although finally a punctuated GFP staining could be observed (Figure 18B), it turned out that the GFP puncta were not moving. Hence, future experiments need to be carried out to establish this vector system as a reliable method to analyze mRNA transport. Nevertheless, once established, this system could be used to analyze the dendritic transport of Pfn1, Pfn2a as well as Cof1 mRNAs and identify potential alterations in transport speed, transport distance or transport orientation following NMDAR-dependent LTP or mGluR-dependent LTD in hippocampal *fmr1* WT and *fmr1* KO neurons.

6 Discussion

Modifications in the efficacy of individual synaptic connections upon neuronal activity, as LTP and LTD, are believed to play a key role in the process of memory formation (for a review see McGaugh, 2000). Interestingly, both, long-lasting functional as well as structural aspects of LTP and LTD have been shown to be crucially dependent on *de novo* protein synthesis (Flexner et al., 1963; Krug et al., 1984; Linden, 1996; Montarolo et al., 1986; Stanton and Sarvey, 1984) which can occur locally, directly at the dendritic spine (for a review see Holt et al., 2019). As early phases of LTP and LTD are independent of protein synthesis (for a review see Sutton and Schuman, 2006), however, it is believed that locally translated proteins are especially needed for the maintenance of changes in the receptor composition at the postsynaptic density as well as a stabilization of synapse morphology, both via actin-dependent mechanisms. Since actin properties are mediated by a large number of actin-binding proteins (for a review see Lin and Webb, 2009), it can therefore be hypothesized that during the late phases of LTP and LTD, actin regulators are locally synthesized in an input-specific manner at the synapse and then help to maintain structural as well as functional adaptations which were initiated in the early phases.

Notably, the importance of local *de novo* protein synthesis is especially highlighted by the fact that translational dysregulations are a pathological key feature of various neurological diseases. A prime example is the Fragile X Syndrome, the most-frequent heritable form of mental retardation, where the neuropathological phenotype is characterized by a hyperabundance of long and thin dendritic spines (Hinton et al., 1991; Irwin et al., 2000; Irwin et al., 2001) as well as synaptic plasticity deficits (Bear et al., 2004; Huber et al., 2002; Lauterborn et al., 2007; Shang et al., 2009), which are believed to arise from heavy dysregulations in local protein synthesis (Feng et al., 1997). As abnormal dendritic spine shapes indicate a crucial involvement of the actin cytoskeleton, the question arises whether an abnormal local synthesis of actin-binding proteins is contributing to the synaptic phenotypes seen in FXS. However, as so far, the activity-dependency of local ABP translation had not been confirmed, this work aimed at unravelling the role of local ABP translation for hippocampal LTP and LTD in more detail and to shed light on a possible contribution of dysregulated ABP synthesis to the neuropathology of FXS.

Analyzing healthy hippocampal neurons of *fmr1* WT mice, this work for the first time provides evidence that ABPs are locally translated in an activity-dependent manner in a crucial time window for the induction of long-term synaptic plasticity *in vitro,* thereby highlighting their importance for proper neuronal function. In addition, the data indicates that not only local ABP mRNA translation but also mRNA localization and thereby local mRNA availability is activity-dependent. Finally, analysis of *fmr1* WT mice trained in the Morris Water Maze suggests that

the mRNA regulations observed *in vitro* are potentially relevant for learning and memory formation.

In contrast, hippocampal neurons from the mouse model of the Fragile X Syndrome (*fmr1* KO) showed heavy dysregulations in local ABP translation as well as local ABP mRNA availability in response to NMDAR-dependent LTP and mGluR-dependent LTD in the hippocampus. Intriguingly, in case of LTP, this was accompanied by a complete lack of structural plasticity. In addition, *fmr1* KO mice showed impaired spatial memory formation in the Morris Water Maze, accompanied by an absence of experience-dependent modulations of ABPs. Most importantly, *in vitro*, structural plasticity could be rescued by a targeted manipulation of ABP activity implying that the role of ABPs for the neuropathology in FXS might be more profound than previously thought and suggesting that alterations in the regulation of actin could even be a cause rather than a consequence of synaptic phenotypes seen in FXS.

6.1 Local translation of actin-binding proteins in the healthy central nervous system

Although long-term structural modifications at synapses following LTP or LTD induction have been shown to be dependent on the actin cytoskeleton (Chen et al., 2007; Fukazawa et al., 2003; Matsuzaki et al., 2004; Okamoto et al., 2004) as well as *de novo* protein synthesis (Flexner et al., 1963; Linden, 1996; Stanton and Sarvey, 1984), the spatiotemporal regulation of actin is yet opaque for the largest parts. Especially the fact that regulations of synaptic actin seem to be spatially restricted to certain compartments even within an individual dendritic spine (for reviews see Chazeau and Giannone, 2016; Hotulainen and Hoogenraad, 2010) and in addition involve a vast number of actin modulating proteins, exacerbates a detailed understanding of the process. In addition, increasing the complexity even more, specific ABPs might be locally synthesized upon need with a high temporal resolution. As the activity-dependent local synthesis of ABPs had not been shown yet, this work aimed at analyzing the potential local translation of neuronal profilins as well as cofilin 1 following neuronal activity as these proteins have been shown to be involved in mediating both, LTP and LTD (Ackermann and Matus, 2003; Bosch et al., 2014; Fukazawa et al., 2003).

6.1.1 Neuronal profilins and cofilin 1 are locally translated in dendrites

The hypothesis that neurons synthesize proteins locally was postulated already more than 30 years ago as the dendritic presence of ribosomes was discovered (Bodian, 1965; Steward and Levy, 1982). Nevertheless, the potential importance of locally translated proteins for

proper neuronal function became more and more clear just over the last few years and therefore, global interest in understanding the concrete molecular mechanisms arose only recently. So far, barely anything is known about the local translation or the distribution and regulation of ABP mRNAs in neurons in general and therefore, in this work, firstly, the distribution of neuronal profilin as well as cofilin mRNAs was analyzed via Fluorescence *in situ* Hybridization (FISH) in individual hippocampal neurons from healthy *fmr1* WT mice.

As expected, *in vitro* as well as in hippocampal slices, the majority of mRNA puncta of Pfn1, Pfn2a as well as Cof1 was present in the soma as here, the main part of protein synthesis is occurring. However, mRNA puncta of all three ABPs were also clearly visible in dendrites and occasionally even directly in dendritic spines not only *in vitro* but also in hippocampal slices, thereby offering first evidence that these proteins might be locally translated in dendrites. The FISH data presented here suggests that dendrites contain less ABP mRNAs than the soma as the ratio between somatic and dendritic mRNAs was approximately 1:10 for all ABP mRNAs analyzed. In line with this, various earlier studies focusing on *in situ* Hybridization experiments in neurons showed a similar, sparse distribution of mRNAs. Importantly, in comparison towards the cell body, a 10-fold drop-off in dendritic mRNA copy number was predicted already previously (Kosik, 2016), thereby indicating that the overall ratios of mRNA levels between the different cellular compartments that were analyzed in this study allow for a trustworthy assessment of mRNA abundance.

Interestingly, when comparing the *in vitro* mRNA distribution of profilins and Cof1 to each other, the distribution of both Pfn isoform mRNAs in hippocampal *fmr1* WT neurons was identical as the overall amount of detectable mRNAs was similar in all cellular compartments analyzed. This is especially interesting as it could be shown by previous studies that in the hippocampus, Pfn1 is predominantly expressed during development and expression decreases steadily with increasing age in mice (Michaelsen-Preusse et al., 2016). As in contrast, Pfn2a was shown to be predominantly involved in synaptic plasticity processes with a stable expression level in the hippocampus independent of the age (Michaelsen-Preusse et al., 2016), it is unexpected that nevertheless, mRNAs of both isoforms are equally distributed in dendrites. Thus, apart from developmental importance, Pfn1 might either have an important housekeeping role or a neuron-specific function as due to the high energy demands of active mRNA transport one might expect that a dendritic localization of mRNAs is selective only to those with crucial functions. Important to note is, however, that the mRNA distribution was analyzed in DIV21 primary embryonic hippocampal cultures which were derived from E18.5 embryos and as the hippocampal Pfn1 expression steadily decreases with increasing age in mice (Michaelsen-Preusse et al., 2016), future experiments will be needed to unravel whether Pfn1 mRNA levels and hence also the ratio between dendritic Pfn1 and Pfn2a mRNAs changes in mature

hippocampal neurons. However, as the hippocampal cell lysates which were used for the analysis of Pfn expression contained not only neurons but also other cell types, including astrocytes and microglia, it will be important to analyze first whether the observed age-dependent drop in Pfn1 expression indeed is a neuron-specific effect or whether it derives from a different cell type.

In comparison to the mRNA abundance of neuronal profilins, Cof1 mRNAs were detectable at significantly higher amounts in *fmr1* WT neurons, especially in the nucleus as well as the cell body which is in line with earlier work showing that abundances of mRNAs vary profoundly over up to three orders of magnitude in neurons (Cajigas et al., 2012). In contrast to this, however, also Cof1 mRNAs were only sparsely distributed in dendrites and dendritic levels of Cof1 mRNA were similar to those of neuronal Pfn isoforms. Based on these observations and previous work that suggested that even abundant mRNAs are diffusely distributed over the dendritic tree (Cajigas et al., 2012; for a review see Kosik, 2016), the question arises how dendrites and dendritic spines manage with comparably few ABP mRNA amounts. Surprisingly, sparse mRNA numbers might even be beneficial for the fine-tuning of the synaptic proteome as by this, changes in mRNA numbers represent larger fold differences and thus, already minor modulations of synaptic mRNA content could lead to significant consequences. However, statistically, the probability of multiple different sparsely distributed mRNAs being present at the same localization is extremely small which suggests that dendritic spines do not have access to a fixed subset of mRNAs at all times. Supporting this hypothesis, earlier work described a mechanism of mRNA anchoring in dendrites where dendritic mRNAs were shown to undergo limited bidirectional movements which sum up to a total displacement of zero (Knowles et al., 1996). This would indicate that on the one hand, mRNAs might be shared by several dendritic spines of a certain dendritic segment and on the other hand, that mRNAs or newly translated proteins might be ‘patrolling’ in dendrites just to be captured by a dendritic spine (in a yet unknown mechanism, ‘synaptic tagging and capture’ hypothesis (Frey and Morris, 1997)) that undergoes some form of synaptic plasticity. In line with the fact that many synapses do not contain polyribosomes and thus are not able to synthesize proteins locally (Steward and Levy, 1982), this would imply that a certain proportion of synapses might not be able to undergo long-term synaptic plasticity in response to an incoming signal because they either lack crucial proteins, mRNAs or polyribosomes. Although this may appear contradicting at first, a mechanism like this might secure that only a certain group of synapses will get potentiated, namely those which are equipped with ribosomes and possess the correct set of mRNAs. If all activated synapses would equally strengthen in response to an incoming action potential, noise would be indistinguishable and neuronal coding would become inefficient. In light of this, a mechanism like this might additionally be able to keep the general excitability of the whole neuron stable. Theoretically, a synapse that underwent LTP should have a higher

probability to undergo further LTP as it has a higher chance to depolarize the postsynaptic neuron, which would lead to unconstrained strengthening of the synapse. However, generally described under the term homeostatic plasticity, neurons were shown to be able to keep key parameters like average firing rates stable through various mechanisms including synaptic scaling (Davis, 2006; Turrigiano and Nelson, 2004) or balancing of excitation and inhibition in the whole neuronal network (Gonzalez-Islas and Wenner, 2006; Maffei et al., 2004). If dendritic mRNAs indeed are a limiting factor and are captured only by those spines which underwent synaptic plasticity, this might automatically destabilize other spines which are not able to synthesize proteins locally, thereby automatically leading to a certain degree of homeostasis. Therefore, one might even speculate that dendritic RNA abundance could have properties of a code that reflects the past activity of synapses, however, future studies focusing on granular mRNA transport as well as local mRNA regulation in dendrites on a more molecular level will be needed to fully understand how dendritic mRNA distribution is regulated.

While the FISH technique offered reliable information about the intracellular localization of Pfn and Cof1 mRNAs and could confirm the dendritic presence of these mRNAs, it has the limitation that it only represents a static image of mRNA localization and does not confirm that dendritically localized mRNAs indeed are locally translated. Therefore, as it was shown previously that dendritic localization motifs are often encoded in the untranslated regions (Mayford et al., 1996; Muslimov et al., 1997), a membrane bound eGFP version (MYR-eGFP) (Rathod et al., 2012) was utilized to elegantly confirm not only the presence of dendritic localization motifs in the UTRs of neuronal profilins as well as Cof1 but also the local translation of all three ABPs. While expression of the plain MYR-eGFP construct which was lacking a dendritic localization sequence was restricted only to the cell body, addition of the 3'UTRs of either Pfn1 or Cof1 or the 5'UTR of Pfn2a led to a clear GFP expression also in dendrites. As myristoylation of the myristoylation site of the construct results in immediate membrane insertion after translation (Yasuda et al., 2000), it can be excluded that dendritic GFP signals resulted from active transport of somatically translated proteins and thus, the different UTRs were clearly sufficient not only to induce a dendritic targeting of the mRNA but also to induce local translation of the respective MYR-eGFP construct. Theoretically, already the presence of dendritic GFP signals confirmed the local translation of both Pfn isoforms as well as Cof1 but, as a proof of principle, local ABP synthesis was confirmed by a Fluorescence Recovery after Photobleaching approach utilizing the construct with the strongest dendritic expression: MYR-eGFP 3'UTR Cof1. Under basal conditions, a clear recovery of the GFP signal could be observed which was completely abolished when performing the same experiment in the presence of the translational blocker anisomycin. Hence, fluorescence recovery clearly resulted from *de novo* local translation of the MYR-eGFP 3'UTR Cof1 construct and overall,

these data confirm that Cof1 and potentially also Pfn1 and Pfn2a are locally synthesized even under basal conditions in dendrites.

As so far, only very few ABPs were shown to be locally translated (Steward et al., 2014; Troca-Marin et al., 2010) it is surprising that indeed, all three analyzed ABPs were found to be dendritically synthesized. Therefore, the amount of locally translated actin modulators might be significantly higher than previously anticipated. In light of the spatial as well as temporal aspects of actin modulation at synapses, this adds a whole new layer of complexity as newly synthesized ABPs might show only minimal posttranslational modifications and thus, could behave differently and serve a different function than the pool of ABPs that was originally present at the synapse. Supporting this hypothesis, previous studies could show that local ABP concentrations at the synapse during the early plasticity phases are modulated by protein translocations and not by protein synthesis as various ABPs, including profilins as well as Cof1, were shown to undergo activity-dependent translocations in or out of the dendritic spine especially during the early stages of active actin-remodeling (Bosch et al., 2014). In line with this, e-LTP and e-LTD cannot be blocked via application of protein synthesis inhibitors (Frey and Morris, 1997; Sajikumar and Frey, 2004) which is why the current hypothesis states that newly synthesized ABPs are especially important for the long-term stabilization of structural as well as functional changes that occurred during the early phases of LTP or LTD respectively. This is surprising as theoretically, local protein synthesis would have the power to shape the local proteome on a rapid timescale also during early-plasticity since on the one hand, small proteins like Cof1 (166 amino acids) or neuronal Pfn isoforms (140 amino acids each), could be synthesized in a suitable time-window (in about 30-35s) as mammalian translation occurs at approximately 5 amino acids per second (Wu et al., 2016) and on the other hand, the experiments done here show that local ABP synthesis also occurs under basal conditions and hence, a pool of newly generated ABPs should exist at all times anyways. Yet, both, e-LTP and e-LTD are independent of *de novo* protein synthesis (Frey and Morris, 1997; Sajikumar and Frey, 2004) suggesting that there is a constitutive local translation of ABPs that is unrelated to plasticity. Intriguingly, this implies that rather than switching local protein synthesis on or off, neuronal activity is likely to modulate local translation efficacy. As the net amount of local protein translation, however, crucially depends on parameters which have a spatial but also a temporal component, including ribosomal quantity, ribosomal availability or the amount of freely accessible mRNAs, a more detailed understanding of translational dynamics at the synapse is needed. Therefore, to unravel whether neuronal activity is mediating ABP mRNA availability as well as local translation in an activity-dependent manner, in this work the mRNA localization as well as the expression of neuronal profilins and Cof1 was analyzed following NMDAR-dependent LTP as well mGluR-dependent LTD in hippocampal neurons *in vitro*.

6.1.2 Local translation of ABPs is actively modulated during NMDAR-dependent LTP

To gain an insight into the fine-tuning of ABP function during NMDAR-dependent LTP, the spatial as well as temporal organization of ABP mRNA localization as well as ABP translation was analyzed in a time-frame of up to 1 h following cLTP in hippocampal neurons of *fmr1* WT mice. The time-window was specifically chosen as long-term changes in synapse morphology, synapse function and even new synapse formation were shown to occur within 1 hour following neuronal activity (Toni et al., 1999). Confirming that structural plasticity was reliably induced, a significant increase in spine head diameter following the induction of cLTP 40 as well as 60 min after the stimulus was visible in all hippocampal neurons that were analyzed. Notably, additional experiments in the same culture system will be needed in order to confirm that these changes are accompanied by an increase in synaptic strength e.g. via electrophysiological measurements or by analysis of AMPAR trafficking utilizing super-ecliptic pHluorin (SEP) fused to the N terminus of glutamate receptor 1 (SEP-GluR1) (Kopec et al., 2007). However, several studies could already show that glycine application is sufficient to induce AMPAR insertion (Fortin et al., 2010), increased AMPAR function (Musleh et al., 1997) and an increase in amplitude of miniature excitatory postsynaptic currents (Feuge et al., 2019; Lu et al., 2001) thereby suggesting that the morphological changes observed here are coupled to functional adaptations as well.

Previous work suggested that from the two neuronal Pfn isoforms, Pfn2a is the isoform that is predominantly involved in mediating synaptic plasticity processes (Michaelsen-Preusse et al., 2016). Further supporting this hypothesis, the data shown here clearly indicate that neither Pfn1 mRNA localization nor local or global Pfn1 expression are modulated during NMDAR-dependent LTP in the hippocampus. Following cLTP, there were no significant changes in the amount of Pfn1 mRNAs detectable in any of the cellular compartments for up to 60 min after the stimulus. In line with these observations, hippocampal Pfn1 expression was found to be unchanged 60 min after cLTP, thereby further reinforcing that Pfn1 is not the isoform involved in synaptic plasticity and that neither transcription nor Pfn1 translation are mediated in an activity-dependent manner following NMDAR-dependent LTP. Furthermore, the results presented here clearly support the proposed role of Pfn2a in mediating synaptic plasticity processes (Michaelsen-Preusse et al., 2016). Analysis of the Pfn2a mRNA distribution revealed no changes in Pfn2a mRNA localization 20 min following cLTP induction but a clear and significant increase in the amount of Pfn2a mRNAs in the cell body as well as in dendrites 40 min following the stimulus. Interestingly, no changes were visible in the nucleus at any given time-point, indicating that the effect itself is not resulting from an increase in transcription. Proposedly, it may result from an active release of Pfn2a mRNA from RNA-transport granules in which mRNAs might not have been accessible for FISH detection pre-release. However,

future experiments will be needed to unravel whether a granular release of Pfn2a mRNAs indeed causes the effect seen in the experimental setup analyzed here. Most strikingly, however, the heavy increase in Pfn2a abundance which was especially dominant in dendrites was found to be very time-specific as the mRNA amount was back to baseline levels 60 min following cLTP induction in all cellular compartments analyzed again indicating a very specific and short-lived temporal regulation. Interestingly, Pfn2a was shown to be translocating into dendritic spines in the first 30 min upon LTP induction previously (Ackermann and Matus, 2003), thereby indicating that both, Pfn2a mRNA localization and protein localization are locally mediated in a temporal fashion following LTP induction. However, the time-frame of mRNA regulations that was identified in this work suggests that protein translocations precede mRNA modulations. Further supporting the hypothesis that Pfn2a is important for memory formation is also the fact that Pfn2a protein level were increased after cLTP induction in hippocampal slices *in vitro* as well as after spatial learning in the Morris Water Maze. These results indicate that Pfn2a is playing an important role in the mediation of plasticity processes in response to LTP as Pfn2a mRNA localization, protein localization as well as global protein expression are regulated in an activity-dependent manner. Therefore, one might speculate that also the local translation of Pfn2a is activity-dependent. However, as dendritic expression of the membrane-targeted eGFP fused to the UTRs of Pfn2a was too low to analyze the temporal modulation of local Pfn2a synthesis following NMDAR-dependent LTP, additional experiments analyzing the local translation of Pfn2a in greater detail will be needed.

Overall, the observations discussed above suggest the following role for Pfn2a in the mediation of NMDAR-dependent LTP: As primarily, Pfn2a catalyzes the exchange of ADP to ATP at actin monomers and the addition of ATP-actin to existing actin filaments (Goldschmidt-Clermont et al., 1992; reviewed in Jockusch et al., 2007), it is likely that during NMDAR-dependent LTP, Pfn2a's main function is to modulate F-actin polymerization rates. Previous work could show that in the first 4 min following LTP induction, the relative concentration of Pfn2a but also other actin stabilizing proteins in the dendritic spines decreases, suggesting an active translocation out of the dendritic spine (Bosch et al., 2014). In line with this, this first phase of actin modulation is characterized by a rapid breakdown of the actin filament system and a net decrease in actin polymerization (Ouyang et al., 2005), predominantly at the tip of the dendritic spine where the PSD is located. Subsequently, the PSD is remodeled in an activity-dependent manner and new AMPAR's are inserted into the membrane (Plant et al., 2006). In the next phase, up to 30 min following the induction stimulus, Pfn2a and other actin stabilizers like CamKIIß, alpha-Actinin or drebrin A are driven back into the dendritic spine leading to an increase in F-actin polymerization, thereby stabilizing and maintaining the receptor composition at the PSD (Bosch et al., 2014). However, as l-LTP cannot be induced without *de novo* protein synthesis (Stanton and Sarvey, 1984), this stabilization might be insufficient to

keep the newly inserted receptors in place in the long-term. Therefore, around 40 min after LTP induction, the amount of translationally available Pfn2a mRNAs in dendrites increases, presumably leading to a rise of local Pfn2a synthesis which ultimately further enhances the Pfn2a concentration in the dendritic spine. Thus, in this third phase, the local translation of ABPs might be actively modulated to create a milieu that is beneficial for additional F-actin stabilization which allows for a long-term maintenance of the remodeled PSD and a stabilization of the grown dendritic spine. Finally, 60 min after LTP induction, the mRNA availability of Pfn2a mRNAs as well as the local translation of Pfn2a is decreased back to baseline levels which might then restore original protein concentrations in the long-term and thus might allow for a faster response to future stimuli.

Although further experiments will be needed to identify the exact underlying molecular mechanisms, the temporal resolution in which Pfn2a as well as Pfn2a mRNAs are upregulated as well as downregulated during NMDAR-dependent LTP suggests the involvement of an active degradation mechanism that allows for a fast degradation of proteins as well as mRNAs. Indeed, evidence exists that indicates the importance of activity-dependent degradation as NMDAR activation was found to induce a redistribution of proteasomes from dendrites into dendritic spines (Bingol and Schuman, 2006) and in line with this, a decreased proteasome exit rate from dendritic spines could be observed (Bingol and Schuman, 2006). Additionally, processing-bodies (p-bodies), containing decapping enzymes as well as miRNAs and components of the RISC machinery which actively degrades mRNAs were shown to be located directly beneath dendritic spines (Cougot et al., 2008) indicating their competence for active mRNA degradation. Therefore, it is likely that the interplay between local, activity-dependent protein synthesis as well as local, activity-dependent protein and mRNA degradation is necessary to generate the highest possible spatial and temporal resolution of the local proteome.

Interestingly, apart from an activity-dependent modulation of F-actin polymerization by Pfn2a, the data presented here suggests that also F-actin depolymerization is modulated in an activity-dependent fashion during NMDAR-dependent LTP, however, in a different time-frame. For the F-actin-severing protein Cof1, a downregulation in the amount of Cof1 mRNA was detectable in the cell body and the nucleus 60 min following cLTP induction as well as in dendrites indicating an overall decrease of Cof1 mRNA availability at later stages of NMDAR-dependent LTP in hippocampal neurons. Supporting this observation, hippocampal Cof1 expression was found to be significantly decreased 60 min following LTP induction *in vitro* as well as *in vivo* after spatial memory formation suggesting that also Cof1 translation is activity-dependent. Noteworthy, not only for Cof1 but also for Pfn1 and Pfn2a, the analysis of hippocampal protein expression *in vitro* and *in vivo* revealed the same trend that was seen in

the analysis of mRNA distribution, indicating that the mRNA level might indeed reflect the overall protein level. However, protein expression was analyzed in lysates and therefore offers no information about alterations in local translation of the respective proteins which is why in case of Cof1, local translation was directly analyzed in this work. Notably, in line with a decrease in Cof1 mRNA availability and global hippocampal Cof1 expression, local Cof1 synthesis was found to be significantly reduced in a specific time-window at 10 to 40 min following LTP induction indicating that also local Cof1 synthesis is activity-dependent and negatively modulated during NMDAR-dependent LTP. Notably, in comparison with the slow decrease in Cof1 mRNA availability in dendrites, the local translation rate of Cof1 was found to be modulated earlier after induction of LTP suggesting that both mechanisms are regulated by different pathways. Various studies could show that in order to maximize the efficient use of resources, translation initiation is the rate limiting step for protein synthesis (Shah et al., 2013) and hence, mRNA availability can become a limiting factor if it drops below a certain threshold. However, although the available amount of ABP mRNAs is actively modulated following LTP induction, it seems not to be the rate limiting factor for local translation as otherwise, a modulation of mRNA availability would have preceded observable changes in the local translation rate. In this respect, other variables, including the availability of ribosomes, the availability of initiation and elongation factors, mRNA secondary structure, the occurrence of poly-proline stretches in the mRNA as well as the structure of the ribosomal binding site, need to be considered (for a review see Sonenberg and Hinnebusch, 2009). Therefore, to completely understand the complex modulation of local ABP synthesis during processes of synaptic plasticity, additional experiments focusing on the temporal interplay of multiple of these factors will be needed.

The experiments done in this work clearly show that upon LTP induction, local Cof1 mRNA availability and local Cof1 translation are negatively modulated and thereby suggest an important role of Cof1 for NMDAR-dependent LTP. Previous work could show that in the early phase of LTP induction, in the first 5 min, Cof1 is actively translocating into the dendritic spine supporting the assumption that it is crucial for initial F-actin breakdown (Bosch et al., 2014). Therefore, similar to what could also be shown for Pfn2a, in the early-phase of LTP, the local concentration of Cof1 seems to be actively modulated via protein localization changes. Supporting this hypothesis, local translation of Cof1 was found to be negatively modulated at a later time point, starting at 10 min and prolonging up to 40 min after the stimulus. Proposedly, in this second phase, a stabilization of F-actin is needed in order to maintain the receptor composition at the newly remodelled PSD and therefore, a higher concentration of active Cof1 could potentially be disadvantageous. As a result from a decrease in local Cof1 translation and local Cof1 mRNA availability, the Cof1 concentration in spines might decrease and thus, in line with the predicted function and regulation of Pfn2a at this stage, the overall ABP composition

might support a shift towards increased F-actin polymerization and F-actin stabilization, thereby favoring spine growth. Finally, around 60 min after the original stimulus, the local translation rate normalizes which in the long-term might also restore local Cof1 concentrations.

Overall, the data set nicely supports a mode of bidirectional regulation for Pfn2a and Cof1 on the mRNA as well as on the protein level during NMDAR-dependent LTP. Given the fact that in terms of energy efficiency, ABPs would not be synthesized with such a sharp spatial and temporal regulation if their mutual activity and immediate action would not be crucial, these results suggest that also the general activity of these ABPs might follow the same regulatory trend. However, neuronal profilins and Cof1 are not constantly active but are regulated via phosphorylation (Sathish et al., 2004; Yang et al., 1998). Therefore, it will be important to additionally analyze the activation states of these ABPs at different time-points following NMDAR-dependent LTP in future experiments.

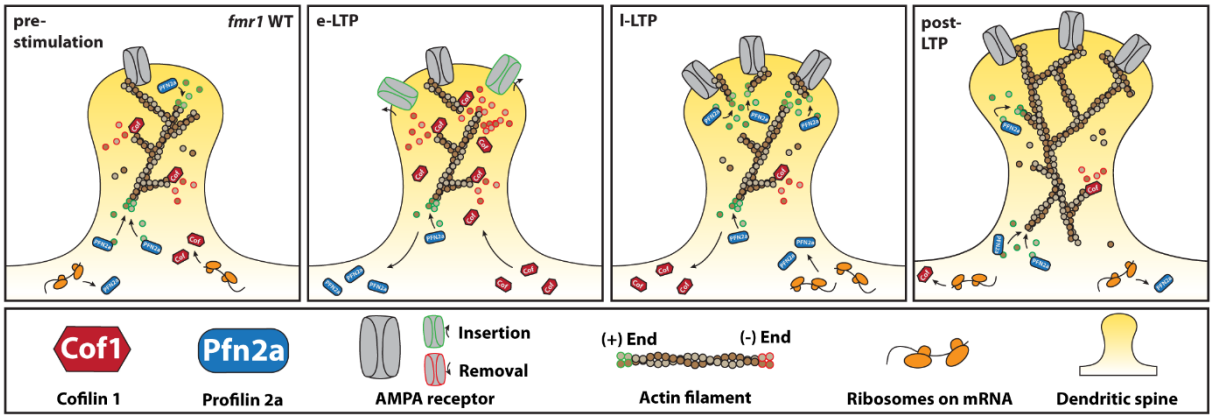

Figure 19 – Schematic model of bidirectional modulations of Pfn2a and Cof1 activity following NMDAR-dependent LTP. Pre-stimulation, the local synthesis of Cof1 and Pfn2a as well as local concentrations of Pfn2a and Cof1 are in balance. Following induction of NMDAR-dependent LTP, in the early phase (e-LTP), Pfn2a is translocating out of the spine while Cof1 enters the spine, thereby shifting the F-/G-actin ratio towards G-actin. This leads to a partial destabilization of the PSD which allows the insertion of new AMPA receptors. During late-LTP (l-LTP), the local translation of Cof1 decreases and Cof1 leaves the spine while in addition, Pfn2a is driven back into the spine, thereby creating a milieu that favors F-actin polymerization. As a result, newly inserted AMPA receptors are stabilized and the dendritic spine grows. Finally, post-LTP, local translation rates as well as protein concentrations are back to basal levels.

In summary, the *in vitro* and the *in vivo* data presented here for the first time offer evidence of an activity-dependent local synthesis of ABPs in dendrites. In addition, they provide a more detailed understanding of the temporal modulation of different ABPs during synaptic plasticity comparing alterations during the early with the late phase of NMDAR-dependent-LTP (Figure 19). Overall, they support a model where in the early-phase, local ABP concentrations are changed as a result of active protein translocations and not by modulations of local ABP synthesis. This leads to a reduced concentration of F-actin stabilizing proteins like Pfn2a and an increase in the local concentration of F-actin destabilizing proteins like Cof1, thereby

inducing a rapid breakdown of the actin cytoskeleton. Following this first phase of rapid F-actin depolymerization, now as a result of translocations of preexisting proteins in combination with an active modulation of local protein synthesis, the set of synaptic ABPs can specifically be modulated. Intriguingly, concluding from the bidirectional modulations of Pfn2a and Cof1 that could be shown in this work, in the late-phase of LTP induction, the concentration of promotors of F-actin polymerization increases while the concentration of F-actin destabilizers decreases. This creates a milieu that favors F-actin polymerization and leads to additional spine growth and helps to stabilize the remodeled receptor composition at the PSD in the long-term.

6.1.3 The localization of ABP mRNAs is regulated in an activity-dependent manner following mGluR-dependent LTD

Neuronal profilins as well as Cof1 were shown not only to be crucially involved in mediating LTP but also LTD (Ackermann and Matus, 2003; Bosch et al., 2014; Fukazawa et al., 2003; Zhou et al., 2004). Importantly, previous work suggests that both these forms of synaptic plasticity at least in parts share common molecular mechanisms (Kandel, 2001; Korte and Schmitz, 2016; Sajikumar and Frey, 2004). On the one hand, destabilizing ABPs like Cof1 were shown to be essential for LTD (Zhou et al., 2004), indicating that the initial F-actin breakdown might be based on the same regulatory mechanism that initiates LTP. On the other hand, 30 min after induction of LTD, profilins were found to be actively targeted to dendritic spines (Ackermann and Matus, 2003), thereby suggesting that also F-actin stabilization at later stages might depend on similar mechanisms and in addition might follow a comparable temporal modulation. Intriguingly, various results from the experiments presented in this work strengthen and even expand this model.

For the analysis of LTD-dependent effects *in vitro*, the Gp1 mGluR agonist DHPG was used to reliably induce mGluR-dependent LTD chemically. Confirming the induction of structural plasticity, a significant decrease in the spine head diameter of hippocampal neurons was detected 40 and 60 min following the stimulus. Notably, additional electrophysiological experiments will be needed to confirm that also functional plasticity was reliably induced. However, various previous studies could confirm that an application of DHPG leads to long-lasting AMPAR removal (Snyder et al., 2001; Xiao et al., 2001) and a depression of synaptic evoked responses (Huber et al., 2001) for up to 120 min after application (Fitzjohn et al., 2001), thereby indicating that structural modifications are not uncoupled from functional plasticity following DHPG-induced mGluR-dependent LTD. When analyzing the intracellular mRNA distribution of neuronal Pfn isoforms as well as Cof1 20 min, 40 min as well as 60 min following LTD induction, the mRNA of Cof1 was found to be mediated in an LTD-dependent manner as after 20 min a rapid increase in dendritic Cof1 mRNA puncta was observable which was then

steadily declining. Contrarily, Pfn1 as well as Pfn2 mRNA amounts were completely unchanged in all cellular compartments at all time-points analyzed. Although additional experiments analyzing the activation states as well as the global and local translation of ABPs upon LTD induction will be needed in order to completely understand the complex regulatory mechanisms, the following course of action for profilins and Cof1 during mGluR-dependent LTD can be hypothesized from the results:

In the first minutes after the LTD-inducing stimulus, the local concentration of Cof1 increases, thereby favoring F-actin depolymerization. Whether this initial modification of the local proteome, however, is mediated by active protein translocations (as described for LTP in Bosch et al., 2014) which might then also include Pfn2a still needs to be elucidated. Especially Cof1 activity was found to be crucial for this initial phase (Fukazawa et al., 2003) and it is proposed that in comparison towards the initial phase of LTP, Cof1 is kept active for a longer time-period, thereby prolonging the phase of F-actin destabilization and promoting AMPAR retraction from the PSD. Supporting this assumption, 20 min after the stimulus, the amount of dendritically localized Cof1 mRNAs was found to be increased which might cause a rise in local Cof1 translation and an increased amount of locally active Cof1 which ultimately might promote spine shrinkage. Lastly, to stabilize structural changes at the spine, promotors of F-actin polymerization like Pfn2a might be driven back into the spine, shifting the G/F-actin ratio towards F-actin.

Interestingly, the data suggest that the mRNA of Pfn2a is not mediated in an LTD-dependent manner, although the protein itself seems to be involved (Ackermann and Matus, 2003). One might speculate that if locally synthesized ABPs that stabilize F-actin indeed are primarily important for the long-term maintenance of newly inserted receptors in the PSD, they might not be needed during LTD as here, receptors are removed from the membrane and the remaining ones might already be anchored sufficiently. However, l-LTD cannot be induced when protein synthesis is blocked indicating that newly generated proteins must serve a crucial function that otherwise could not be fulfilled. Therefore, to understand the complex regulation of mGluR-LTD in more detail, future studies will have to focus on identifying the exact role of locally translated LTD-dependent proteins and their time frame of action at the synapse.

6.2 Local translation of actin-binding proteins in the diseased central nervous system

For the first time, this work provides evidence for an activity-dependent regulation of local ABP translation in response to LTP as well as LTD, highlighting the relevance of actin modulators for proper neuronal function. Given the importance of local protein synthesis for l-LTP and l-

LTD (Flexner et al., 1963; Krug et al., 1984; Linden, 1996; Montarolo et al., 1986; Stanton and Sarvey, 1984), one might speculate that a disruption of local ABP translation or a disruption of local actin modulation in general would have a tremendous influence on neuronal function and might even completely abolish their ability to undergo synaptic plasticity. As LTP and LTD are believed to represent the cellular correlates of learning and memory processes, this could potentially lead to severe impairments of brain function in the affected individual. Supporting this hypothesis, several forms of mental retardation, especially some of the more severe forms were shown to be linked to dysregulations in actin modulatory pathways (Allen et al., 1998; Billuart et al., 1998; Tassabehji et al., 1996). Intriguingly, of special interest in this regard is the most common heritable form of mental retardation, the Fragile X Syndrome which is characterized by heavy dysregulations of local protein translation resulting from the loss of the RNA-binding protein FMRP (for a review see Bagni and Oostra, 2013).

In FXS, the lack of FMRP heavily influences signal processing at individual synapses (Hu et al., 2008; Huber et al., 2002; Lauterborn et al., 2007; Shang et al., 2009), thereby impairing synaptogenesis, spine maturation and synaptic as well as circuit plasticity (Contractor et al., 2015). While onset and maintenance of these phenotypes are controversial in the literature (He and Portera-Cailliau, 2013), they share the common observation of an overall immature dendritic spine profile (Rudelli et al., 1985). Strikingly, all these processes are crucially dependent on precisely timed modulations of the actin cytoskeleton, mediated by distinct sets of ABPs (reviewed in Lin and Webb, 2009) indicating a potentially important role of the actin cytoskeleton in the neuropathology of the disease. In this regard, direct interactions between FMRP and mRNAs of ABPs have been described, however, the number of validated FMRP target ABP mRNAs is surprisingly low. Notably, previous work could show that FMRP is directly interacting with the mRNA of the Pfn1 *Drosophila* homologue Chikadee (Reeve et al., 2005) and evidence exists that Cof1 expression and activity is dysregulated in *fmr1* KO mice, thereby indicating a potential direct link to FMRP (Pyronneau et al., 2017). Hence, as the experiments done in *fmr1* WT mice could confirm the local translation of neuronal Pfn isoforms and Cof1 and highlighted their importance for the proper induction of LTP and LTD in the hippocampus, an *in silico* analysis was done to identify possible FMRP-binding sites in the mRNAs of these proteins.

6.2.1 Pfn1 and Cof1 mRNAs are direct targets of FMRP and hippocampal expression is altered in *fmr1* KO mice

The RNA-binding motifs of FMRP allow for high affinity binding of WGGA-motifs (TGGA, AGGA) as well as stem-g-quartet loops and U-rich RNA (Ashley et al., 1993a; Siomi et al., 1993). Therefore, the mRNA sequences of neuronal Pfn isoforms and Cof1 were scanned for

regions that are likely to serve an FMRP-binding function. Interestingly, in line with the fact that FMRP was shown to bind the *Drosophila* homologue of Pfn1 (Reeve et al., 2005), a high occurrence of guanine bases indicating a potential stem-g-quartet loop in close proximity to two TGGA-motifs could be found in the mouse and the human mRNA of Pfn1, thereby indicating potential FMRP binding in this region. Notably, the identified sequence was similar compared to the already validated FMRP-target mRNA of PSD-95 (Zalfa et al., 2007), thereby further strengthening the likelihood of a direct interaction between FMRP and the mRNA of Pfn1. Contrarily, neither in the human nor in the mouse mRNA sequence of Pfn2a, any regions could be identified that indicate FMRP-binding. Thus, FMRP binding to Pfn seems to be specific to Pfn1, due to a conserved binding-site in mice and humans. In addition, in human as well as murine mRNAs of Cof1, a sequence with multiple repetitive guanine repeats was found, thereby suggesting that also the mRNAs of human and mouse Cof1 contain a conserved FMRP-binding motif. Finally, to confirm these *in silico* results, an RNA immunoprecipitation was performed and indeed, a direct interaction between FMRP and the murine mRNAs of Pfn1 and Cof1 could be confirmed, while no interaction with the mRNA of Pfn2a was detectable (data not shown as the RIP was performed by a different PhD-student, data is published in Feuge et al., 2019; Michaelsen-Preusse et al., 2016).

As FMRP is involved in the transport of mRNAs and the regulation of local translation (Dictenberg et al., 2008; Feng et al., 1997), these results opened the possibility that the translation of Pfn1 and Cof1 is dysregulated in FXS. Therefore, hippocampal expression of these ABPs was analyzed and since Pfn1 was shown to be predominantly expressed during development with a decreasing expression level in aging mice (Michaelsen-Preusse et al., 2016), expression levels were analyzed at different developmental stages: during development at P0 and P14 as well as in adult mice at P120. Importantly, indicating a direct influence of FMRP on the expression of its targets, in *fmr1* KO mice, Pfn1 expression was found to be significantly reduced at P0 where its expression is usually at its peak in the WT hippocampus (Michaelsen-Preusse et al., 2016). Interestingly, however, Pfn1 expression was normal at P14 and also at P120, suggesting that this defect is restricted to the phase of early development. In line with this, additional work from the lab of Martin Korte could link the dysregulation of Pfn1 to spine maturation deficits and the occurrence of long and thin spines during development in *fmr1* KO mice (Michaelsen-Preusse et al., 2016) and Pfn1 overexpression was even able to completely rescue this phenotype (Michaelsen-Preusse et al., 2016), thereby further supporting the hypothesis that rather than being a consequence, dysregulations of ABPs could be a cause for synaptic phenotypes in FXS. Highlighting the fact that this defect indeed is specific to Pfn1, hippocampal Pfn2a expression was unchanged at all developmental stages analyzed. Strikingly, while in adult mice Pfn expression was normal, hippocampal Cof1 levels were significantly decreased at this stage, thereby confirming general changes in the

expression of ABPs in adult *fmr1* KO mice. In line with this, FRAP experiments could confirm that basal actin dynamics are slower in mature hippocampal *fmr1* KO neurons as the turn-over time of actin filaments was shown to be significantly increased (Feuge et al., 2019). Given the F-actin severing function of Cof1 (for a review see Moon and Drubin, 1995), this effect might be directly caused by a decreased expression and reduced action of Cof1, however, experimental evidence confirming a causal relationship is still missing.

Surprisingly, both, hippocampal Pfn1 as well as Cof1 expression were found to be reduced in the absence of FMRP although FMRP is primarily known to suppress translation of its target mRNAs and therefore, an increase in expression might be expected. However, almost all large scale studies suggest that FMRP can also have an enhancing effect on the translation of a subset of its targets (for a review see Maurin and Bardoni, 2018) but the detailed molecular mechanism how FMRP is able to function as a repressor as well as an enhancer of translation simultaneously is yet not completely understood. Based on the observations that the RNA binding specificity of FMRP can be modulated by the binding to several interaction partners including FXR1P (Siomi et al., 1995), FXR2P (Zhang et al., 1995), CYFIP1 and CYFIP2 (Schenck et al., 2001) or by post-translational modifications e.g. by sumoylation (Khayachi et al., 2018), it is believed that these modulations might be crucially involved, however, direct evidence for this is missing. Nevertheless, from the data shown here it can be assumed that in case of Pfn1 and Cof1 mRNAs, FMRP seems to exert an enhancing rather than a suppressing action. Whether FMRP directly modulates translation rates or has a stabilizing effect on these mRNAs which might prolong the overall time-period in which these mRNAs can be translated (which might indirectly increase the amount of new protein) still needs to be elucidated.

Overall, the data shown here point towards the fact that the commonly observed immature spine profile in FXS might indeed be caused by a dysregulation of actin dynamics, mediated by ABPs. Intriguingly, the fact that Pfn1 was found to be differentially expressed during development but not in adult mice where instead Cof1 expression was altered suggests that dependent on the type of ABPs involved, the neuropathological mechanisms causing dysregulated actin dynamics during development seem to be different than those involved in mature *fmr1* KO neurons. A model like this would nicely explain why observations of dendritic spine phenotypes in *fmr1* KO mice are varying substantially (reviewed in He and Portera-Cailliau, 2013). If the set of ABPs that is dysregulated during the critical period of synaptogenesis consists of proteins which are mainly expressed during development e.g. Pfn1 (Michaelsen-Preusse et al., 2016), the phenotype in adult *fmr1* KO mice might be caused by a different set of ABPs, e.g. Cof1 (Feuge et al., 2019). Therefore, as the data presented in this work suggest that the local translation as well as the mRNA localization of ABPs is mediated

following NMDAR-LTP as well as mGluR-LTD and both of these forms of synaptic plasticity were previously shown to be dysregulated in the hippocampus of *fmr1* KO mice, additional experiments were carried out to analyze whether these activity-dependent mRNA modulations are differentially regulated in *fmr1* KO mice.

6.2.2 ABP mRNA availability and local translation are dysregulated following synaptic plasticity in hippocampal *fmr1* KO neurons

The fact that FMRP has a well-described function in the dendritic transport of mRNAs (Dictenberg et al., 2008) opened the possibility that the loss of FMRP in FXS leads to an altered distribution of ABPs and potentially, a lack of dendritically localized ABP mRNAs. Therefore, at first, the mRNA distribution of neuronal Pfn isoforms as well as Cof1 was analyzed in hippocampal neurons from *fmr1* KO mice. Surprisingly, however, in the overall cellular distribution only minor changes were detectable. In the soma, where the main proportion of mRNAs is located, the overall amount of Pfn1, Pfn2a as well as Cof1 mRNAs was completely unchanged in comparison to *fmr1* WT neurons. In line with the fact that phenotypes in FXS are believed to derive from translational dysregulations and not from transcriptional deficits (Feng et al., 1997) this suggests that changes in ABP expression levels indeed are caused by alterations in translation and not gene transcription. Interestingly, however, for both Pfn isoforms, the dendritic abundance of mRNAs was found to be decreased in *fmr1* KO neurons, indicating that the loss of FMRP indeed might lead to decreased levels of ABP mRNAs in dendrites which in turn could influence the local translation of ABPs and the neuronal ability to undergo synaptic plasticity. Nevertheless, it will be important to study the underlying molecular mechanism of Pfn mRNA transport in more detail in future experiments as decreased dendritic levels of Pfn1 mRNAs might be directly related to the loss of FMRP, however, in case of Pfn2a they have to be indirect as FMRP is not able to bind to the mRNA to Pfn2a. In addition, apart from FMRP, other mRNA transporters have to be involved in the transport process of these mRNAs as otherwise, in the absence of FMRP, Pfn mRNAs would not have been detectable in dendrites in the first place. Intriguingly, the same holds true for the mRNA of Cof1 as the analysis revealed that the overall amount and distribution of Cof1 mRNAs is equal in *fmr1* WT and *fmr1* KO neurons and also dendritic mRNA levels are unaffected by the loss of FMRP although the Cof1 mRNA was shown to be a direct target of FMRP. These observations suggest that at least for neuronal Pfn isoforms and Cof1 mRNAs, mRNA transport is not heavily affected by the loss of FMRP and that *fmr1* KO neurons do not lack dendritically localized ABP mRNAs. Based on these findings, the next set of experiments focused on investigating the possibility that the loss of FMRP negatively affects the activity-dependent regulation and the local translation of mRNAs that could originally be seen in *fmr1* WT neurons.

In FXS, the best-studied form of synaptic plasticity is the mGluR-dependent LTD as several studies could show that the loss of FMRP leads to an increased basal translation of LTD-dependent proteins, thereby causing an exaggerated LTD in the hippocampus (Bear et al., 2004; Huber et al., 2002). Interestingly, however, when analyzing the average spine head diameter of hippocampal *fmr1* KO neurons in which mGluR-dependent LTD had been induced, spine shrinkage was not exaggerated. Hence, in *fmr1* KO neurons, spine shrinkage seems to be independent from the amount of AMPAR's that are removed from the PSD in response to the stimulus which is unexpected as AMPAR trafficking is directly linked to modulations of synaptic actin (Gu et al., 2010; for a review see Hanley, 2014; Zhou et al., 2001). Previous work could show that either application of Latrunculin A, an F-actin assembly inhibitor, or application of Jasplakinolide, an F-actin stabilizer, can block AMPAR insertion following cLTP (Gu et al., 2010), thereby suggesting that for AMPAR trafficking a very tight regulation of synaptic actin is crucial. Therefore, one might have expected that as a result from an increased AMPAR removal, which would suggest a prolonged period of destabilized actin, spine shrinkage is exaggerated, too. Nevertheless, the data shown here suggest that spine shrinkage following mGluR-dependent LTD is uncoupled from functional changes at the synapse which raised the question whether the local translation of ABPs is mediated in an activity-dependent manner in *fmr1* KO neurons at all.

The experiments done in *fmr1* WT cells could show that the dendritic availability of Cof1 mRNAs is increased in an activity-dependent manner following mGluR-dependent LTD while the mRNAs of Pfn1 and Pfn2a are unaffected by the stimulation. In line with this, also in *fmr1* KO neurons, the induction of LTD had no effect on the overall distribution of Pfn1 and Pfn2a mRNAs. Interestingly, however, an LTD-dependent modulation of Cof1 mRNA localization was completely absent, too, suggesting that at least for the mRNAs analyzed here, an activity-dependent regulation is missing. Notably, in FXS, the mGluR-dependent LTD has been shown to be independent of *de novo* protein synthesis as l-LTD cannot be blocked via application of translation inhibitors (Hou et al., 2006; Todd et al., 2003; Westmark and Malter, 2007). While the underlying regulatory mechanisms are not completely understood it is believed that either the basal translation rates of LTD-dependent proteins are already at their maximum in *fmr1* KO mice and thus, stimulation becomes ineffective or that Gq coupled receptor-dependent translation is not initiated following mGluR5 stimulation (Ronesi and Huber, 2008). Supporting this hypothesis, in *fmr1* KO mice, a decreased association between mGluR5 and the scaffold and signaling protein Homer could be observed (Ronesi et al., 2012). An interaction between mGluR5 and Homer is needed to activate the translational machinery via the PI3K kinase-mTOR pathway, however, in FXS, this mechanism might be perturbed as in *fmr1* KO neurons, mGluR activation fails to stimulate PI3K (Ronesi and Huber, 2008). In line with this, previous work could show that in case of PSD-95 which is rapidly translated in response to mGluR

activation in *fmr1* WT mice, an mGluR-dependent change in PSD-95 expression is missing in *fmr1* KO neurons (Todd et al., 2003). Therefore, an activity-dependent modulation of mRNAs might be missing simply because *de novo* protein synthesis is not initiated in response to mGluR-dependent LTD. Nevertheless, in order to confirm that a modulation of local *de novo* protein translation upon mGluR-LTD indeed is absent, additional experiments focusing on the local translation of ABPs, e.g. of Cof1 in response to mGluR-LTD in *fmr1* KO neurons will be needed.

While so far, most studies focused on analyzing the mGluR-dependent LTD in the context of FXS, several publications suggest that also the NMDAR-dependent LTP is defective in the hippocampus of *fmr1* KO mice as a long-term maintenance of this form of LTP is absent (Feuge et al., 2019; Lauterborn et al., 2007; Shang et al., 2009). However, whether these functional alterations are accompanied or even caused by deficits in structural plasticity had not been studied yet. Interestingly, the experiments presented here clearly show that activity-dependent spine growth is missing in *fmr1* KO neurons as no changes in the average spine head diameter were detectable for a time course of up to 60 min following LTP induction, thereby hinting towards the fact that following NMDAR-LTP, a modulation of synaptic actin is lacking. Intriguingly, supporting this observation, an activity-dependent regulation of dendritic ABP mRNA availability as could be shown for Pfn2a and Cof1 mRNAs in *fmr1* WT neurons was missing, too. In addition, the fact that no significant changes in the hippocampal expression of Pfn1, Pfn2a or Cof1 were detectable 60 min after LTP induction as well suggests that not only a modulation of synaptic actin but also a modulation of activity-dependent local translation is missing. Notably, in contrast to the regulation that was seen in the *fmr1* WT, expression of Cof1 was found to be slightly increased upon NMDAR-LTP induction, indicating that even if local ABP translation rates are modified in response to the stimulus, the mechanism is perturbed. Therefore, to unravel whether an LTP-dependent modulation of local ABP translation is impaired or completely absent, the local translation of Cof1 in response to NMDAR-LTP was analyzed in more detail. Intriguingly, further strengthening the previously discussed observation that hippocampal Cof1 expression is significantly decreased in adult *fmr1* KO mice which indicated that FMRP might function as a translational enhancer on Cof1 mRNA, the local translation of Cof1 was found to be reduced already under basal conditions. After induction of NMDAR-dependent LTP, however, in contrast to *fmr1* WT neurons, the local translation of Cof1 increased, thereby offering a possible explanation why the hippocampal expression of Cof1 was found to be upregulated following LTP induction in the *fmr1* KO.

In sum, the overall dataset suggests that upon induction of NMDAR-dependent LTP local translation of Cof1 is dysregulated and an activity-dependent modulation of dendritic mRNA availability is missing. Together with the fact that structural plasticity was completely absent,

this indicates that *fmr1* KO neurons lose their ability to control the synaptic proteome on a rapid temporal resolution. This would imply that on the one hand, actin-dependent remodeling processes during e-LTP might be disturbed as a result of altered basal synaptic ABP concentrations and on the other hand, that a long-term maintenance of LTP is not possible because the translation-based modification of the local ABP proteome is dysregulated. Hence, the results presented here suggest for the first time that the lack of structural and ultimately, also functional plasticity in *fmr1* KO neurons might be attributable to a disturbed regulation of synaptic actin.

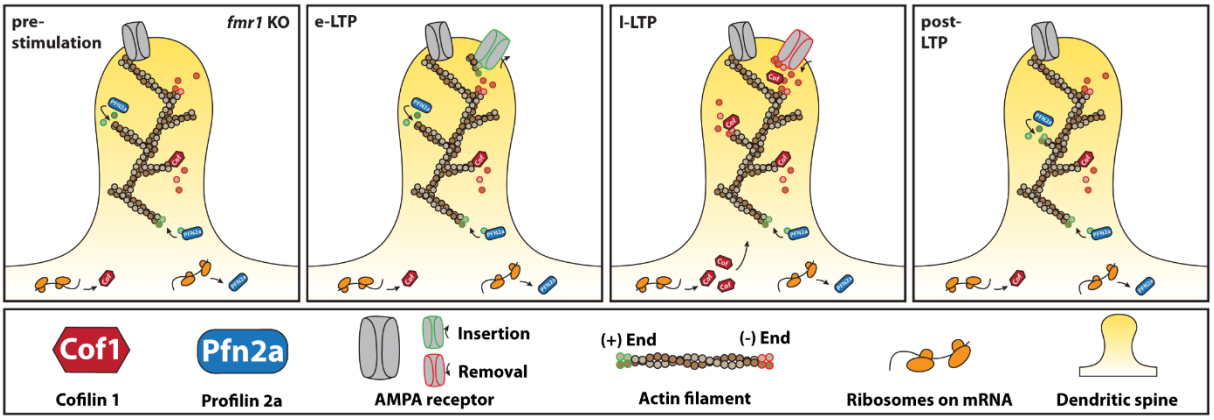

Figure 20 – Schematic model of actin dysregulations during NMDAR-dependent LTP in *fmr1* KO neurons. Already pre-stimulation synaptic actin is dysregulated as indicated by decreased local synthesis rates of Cof1 and increased F-actin turnover rates (Feuge et al., 2019). During e-LTP, Cof1 levels might be too low to allow for an immediate F-actin remodeling in response to the stimulus. Hence, although AMPA receptors might be newly inserted into the PSD in the intial phase, they might not be maintainable over time as during l-LTP, the local synthesis of Cof1 enhances which might increase local Cof1 concentrations and thus, promote F-actin depolymerization. Hence, newly inserted AMPA receptors can not be stabilized and might be lost again. In addition, as F-actin polymerization is unfavored, the dendritic spine is not growing in response to the stimulus. Therefore, post-LTP, neither structural plasticity nor functional plasticity changes are detectable.

Although future experiments will be needed that determine the amount of active ABP isoforms on the level of single synapses in order to understand the complex regulation of actin following LTP in *fmr1* KO neurons, from the results shown here, the following course of actin modulations can be predicted: In the *fmr1* WT it was shown that during e-LTP, the local proteome is shaped by protein translocations (Bosch et al., 2014) that lead to an enrichment of F-actin destabilizing proteins including Cof1 which then induce a rapid breakdown of the synaptic actin cytoskeleton (Bosch et al., 2014). Although the experiments done here offer no information whether these input-specific translocations are dysregulated in FXS, the fact that basal local Cof1 translation is significantly reduced in *fmr1* KO neurons would suggest that potentially, Cof1 levels are too low to allow for an active remodeling on a rapid time-scale. In line with this, it could be shown recently that synaptic actin filaments are more stable in the *fmr1* KO (Feuge et al., 2019) which

might hinder a proper induction of NMDAR-dependent LTP already in the initial phase. In addition, in the late and translation-dependent phase of LTP, *fmr1* KO neurons might not be able to alter the local ABP proteome in order to create a milieu that favors spine growth and overall F-actin stabilization. As predicted in this work, the long-term maintenance of functional and structural changes upon LTP proposedly involves a translation-dependent increase in the local concentrations of actin stabilizers like Pfn2a and a decrease in destabilizing proteins like Cof1 in the *fmr1* WT. In *fmr1* KO neurons, however, an activity-dependent modulation of Pfn2a mRNA was missing completely and the local translation of Cof1 was found to be dysregulated, leading to an increase in local Cof1 synthesis. Hence, it can be anticipated that even if e-LTP is properly induced, as a result, functional and structural changes cannot be stabilized in an activity-dependent manner and thus are not maintained in the long-term which could explain why structural plasticity upon NMDAR-dependent LTP induction is missing and why dendritic spines appear to be immature in *fmr1* KO mice. Nevertheless, this work primarily focused on the analysis of structural plasticity and functional aspects of synapse dysfunction where not assessed. Therefore, it will be important to perform electrophysiological measurements or calcium-imaging (which would allow a readout on a single synapse level (Siegel and Lohmann, 2013)) to characterize the relationship between structural and functional plasticity in greater detail. This would help to unravel whether structural adaptations are uncoupled from functional plasticity which might still be properly induced or whether structural plasticity is absent because functional plasticity is missing, too (or vice versa).

6.2.3 *fmr1* KO mice show deficits in memory formation and an experience-dependent modulation of ABP expression is missing

This work could show that in the *fmr1* WT, ABP expression is mediated in an activity-dependent manner *in vitro* as well as *in vivo* and that this modulation is dysregulated in *fmr1* KO neurons *in vitro*, leading to a complete lack of structural plasticity following NMDAR-dependent LTP. These results support the previous observation that functional plasticity following NMDAR-dependent LTP is absent in the hippocampus of *fmr1* KO mice (Lauterborn et al., 2007; Shang et al., 2009) and they indicate a direct link between dysregulated actin dynamics, LTP and LTD deficits and ultimately, behavioral phenotypes of FXS. The majority of FXS patients suffers from a learning disability (Hall et al., 2008; Skinner et al., 2005) and therefore, to test whether also *in vivo* an experience-dependent modulation of ABP expression levels is missing, hippocampal ABP expression in *fmr1* KO mice was analyzed following spatial memory formation in the Morris Water Maze (Morris, 1984). Notably, the performance of *fmr1* KO mice in the Morris Water Maze is described controversially in the literature (Baker et al., 2010; D'Hooge et al., 1997; Dobkin et al., 2000; Kooy et al., 1996; Leach et al., 2016), however, most

studies reported normal trial performance but observed memory acquisition or reversal learning deficits, interestingly not only in *fmr1* KO mice (Baker et al., 2010; D'Hooge et al., 1997; Kooy et al., 1996) but also *fmr1* KO rats (Tian et al., 2017) thereby indicating hippocampal dysfunction. In line with this, in the Morris Water Maze performed here, an, albeit mild, impairment in spatial memory formation in *fmr1* KO mice could be observed. In general, *fmr1* KO mice learned to locate and recall the position of the hidden platform in a hippocampus-dependent manner as indicated by a significant target quadrant preference during the probe trials as well as a significantly decreasing training latency and an increase in hippocampus-dependent search strategies over the course of the training. In comparison with the *fmr1* WT, however, *fmr1* KO mice learned slower and were less precise in memory recall, suggesting an impaired ability to obtain and maintain spatial memory. Importantly, in addition, while hippocampal expression of Pfn2a and Cof1 was significantly altered in *fmr1* WT mice following training in the Morris Water Maze, neither Pfn1, nor Pfn2a or Cof1 were differently expressed in the hippocampus of *fmr1* KO mice following training, thereby indicating that indeed an experience-dependent modulation of ABP expression is missing. Intriguingly, the hippocampal ABP expression profile following spatial memory formation completely mirrored the ABP expression profile in hippocampal slices of *fmr1* KO mice after chemical induction of NMDAR-dependent LTP, proposing that the dysregulation of ABPs that could be observed *in vitro* is of physiological relevance also *in vivo* and that behavioral phenotypes in FXS indeed might be linked to dysregulated actin-dynamics.

6.3 Actin modulators as a potential treatment for the Fragile X Syndrome

So far, the experiments presented here could show that the local modulation of Pfn2a and Cof1 that is needed to precisely time actin filament stabilization/destabilization for structural plasticity and memory formation to occur in *fmr* WT neurons is missing in *fmr1* KO cells. As up until now, a small number of studies provided evidence that a possible treatment to alleviate autism-like symptoms in FXS could be a targeted manipulation of the actin cytoskeleton (Bongmba et al., 2011; Dolan et al., 2013; reviewed in Michaelsen-Preusse et al., 2018), this hypothesis was tested by specifically interfering with actin dynamics during/after the induction of NMDAR-dependent LTP either by generally modulating actin polymerization or by direct manipulation of Cof1 activity. Here, focus was put specifically on the action of Cof1 as on the one hand, its mRNA was shown to be regulated upon NMDAR-dependent LTP as well as mGluR-dependent LTD and on the other hand, the mRNA of Cof1 was identified as a direct target of FMRP while the mRNA of Pfn2a was not. If indeed the decrease in Cof1 expression observed in *fmr1* WT neurons is crucial for structural plasticity and if the absence of this regulation is responsible for the plasticity impairment in *fmr1* KO cells, partially blocking Cof1

should be able to rescue this defect. Indeed, partial block of Cof1 activity in *fmr1* KO neurons rescued structural plasticity, however, only if the blocking peptide was applied after the stimulation period thereby confirming the time specific action of Cof1. In addition, this effect could be specifically attributed to Cof1 as a general stabilization of the actin network did not lead to the same result. This is interesting as application of Jasplakinolide has been shown to enhance memory formation (Huang et al., 2013) but seems not to exert an effect in *fmr1* KO neurons. In *fmr1* WT neurons, either blockage of F-actin polymerization via Cytochalasin D or an additional decrease in Cof1 activity (on top of the decrease of Cof1 activity that occurs in response to LTP induction) completely blocked spine head diameter changes, thereby supporting the hypothesis that a precisely timed modulation of Cof1 activity and F-actin polymerization/depolymerization is crucial for structural plasticity to occur.

These observations suggest that a targeted manipulation of actin dynamics indeed might be able to rescue synaptic phenotypes in FXS. However, the experiments done here only focused on structural aspects of synapse dysfunction and it will be important to confirm in future experiments, e.g. by electrophysiological measurements, that not only structural but also functional plasticity can be rescued by an approach like this. Interestingly, evidence indicating that an interference with actin dynamics, especially via modification of the Rac1-PAK-Cof1 pathway is able to rescue functional plasticity deficits and even behavioral phenotypes in FXS already exists. On the one hand, pharmacological inhibition of Rac1, which is typically found to be overactive in *fmr1* KO mice, was able to reduce the exaggerated mGluR-dependent LTD in the hippocampus (Bongmba et al., 2011). On the other hand, pharmacological reduction of PAK activity was shown to rescue functional synaptic deficits in the somatosensory cortex (Pyronneau et al., 2017), to rescue spine morphology phenotypes in layer 2/3 cortical neurons and to reverse hyperactivity as well as repetitive behaviors in *fmr1* KO mice (Dolan et al., 2013). Hence, the targeted manipulation of ABPs might indeed provide a potential treatment strategy for FXS.

Importantly, indicating a general relevance, spine phenotypes seem to be not only a key feature of FXS but of autism spectrum disorders in general (for a review see Joensuu et al., 2018) and pharmacological blocking of Cof1 activity could prevent repetitive behaviors, autism-like social phenotypes as well as functional plasticity deficits also in a different mouse model for autism spectrum disorders (Shank3 KO mice) (Duffney et al., 2015). However, although the work presented here as well as the studies described above indicate that synaptic defects in autism disorders may be reversible by normalizing excessive activity in pathways that modulate the actin cytoskeleton, it is important to note that a therapeutic approach like this will certainly carry risks. The results presented here clearly show that especially the timing and the location of actin modulations is of crucial importance for neuronal function. In addition, they

suggest that the mechanisms mediating synaptic actin polymerization in response to LTP and LTD might be mediated by similar mechanisms as indicated by the fact that Cof1 and Pfn2a seem to be involved in both, NMDAR-dependent LTP as well as mGluR-dependent LTD. Therefore, simply decreasing or increasing the activity of individual ABPs pharmacologically may not be beneficial in the long-term as it needs to be taken care that they are regulated solely in the brain, potentially in a brain region specific manner, in the correct neuronal population and in addition at the right time without causing any side effects that might destroy the balance between synapse strengthening, synapse weakening and homeostatic plasticity mechanisms. In this regard, however, it is of benefit that there are brain specific isoforms of actin which might help to identify potential therapeutic targets with reduced risks of peripheral side effects.

7 Final conclusions and Outlook

The work presented here aimed at offering a more detailed understanding of the spatial and temporal aspects of dendritic ABP mRNA regulations which allow neurons to modulate the synaptic proteome and ultimately, synaptic actin, on a rapid timescale in response to neuronal activity as these modulations might well be the underlying mechanism of structural plasticity in the brain and might be crucially important for long-term memory storage.

In hippocampal neurons from *fmr1* WT mice, this study could show for the first time that in response to NMDAR-dependent LTP as well as mGluR-dependent LTD, the localization and thereby the local availability of ABP mRNAs as well as the local translation of ABPs is mediated in an activity-dependent manner *in vitro* and potentially also *in vivo*. Intriguingly, the results indicate that over a time course of up to 60 min, the synaptic concentrations of ABPs are rapidly altered in order to shift between phases of F-actin polymerization (actin stabilization) and F-actin depolymerization (actin destabilization) which might allow for rapid actin remodeling processes and promote spine growth or spine shrinkage, respectively.

In hippocampal neurons from *fmr1* KO mice, the mouse model of the Fragile X Syndrome, however, ABP expression was found to be altered already under basal conditions and activity-dependent modulations of local ABP mRNA availability were found to be completely absent in response to either NMDAR-dependent LTP or mGluR-dependent LTD *in vitro*. Intriguingly, in case of NMDAR-dependent LTP, this defect was accompanied by a total lack of activity-dependent structural plasticity which could be directly linked to a missing regulation of the ABP Cof1. In addition, this work could show that also *in vivo*, in *fmr1* KO mice which showed deficits in spatial memory formation in the Morris Water Maze, an activity-dependent modulation of ABPs is missing. Remarkably, underlining the general importance of actin modulators for proper neuronal function, these data for the first time connect learning and memory deficits in FXS to plasticity deficits derived from dysregulations of ABP expression, ABP mRNA localization and local ABP translation.

Most importantly, the experiments presented here could show that structural plasticity defects in the mouse model of FXS can be rescued by a targeted modulation of Cof1 activity. However, so far only a rescue of structural phenotypes could be confirmed and it will be important to show via electrophysiological measurements or calcium-imaging that the chemical protocols used in this study indeed cause long-term strengthening or weakening of synapses, respectively. Here, only structural changes of dendritic spines were analyzed and a significant increase or decrease in the average spine head diameter was interpreted as a confirmation that synaptic plasticity was properly induced. Thus, although several studies already confirmed that functional plasticity is induced after chemical LTP and LTD induction (Feuge et al., 2019;

Fitzjohn et al., 2001; Fortin et al., 2010; Huber et al., 2001; Lu et al., 2001; Musleh et al., 1997; Snyder et al., 2001; Xiao et al., 2001), a proof-of-principle experiment should be done. Notably, if functional plasticity defects occur, it will be important to test whether also these are rescuable by a targeted modulation of Cof1. If so, it could be tested whether learning and memory deficits can be prevented too. Therefore, *in vivo* experiments could be performed where HIV TAT pCof1 injected animals are trained in the Morris Water Maze to unravel whether the spatial memory deficits observed in this work can be rescued as well. Interestingly, the same peptide that was utilized in this study was already used for *in vivo* experiments in a previous study (Duffney et al., 2015) where a low dose (15 pmol/g) of HIV TAT pCof1 was injected into Shank3-deficient mice (a mouse model of autism). While no side-effects were reported, the peptide was able to rescue social deficits of these mice and led to a significantly increased NMDAR-to-AMPAR ratio in prefrontal cortex neurons for up to 5 days post-injection.

Notably, multiple central statements of this work are based on the analysis of ABP mRNA distributions done via Fluorescence *in situ* Hybridizations (FISH). However, the quantification of exact mRNA numbers in the dendritic compartment is challenging because mRNAs are commonly incorporated into RNA granules (reviewed in Thomas et al., 2011) and thus are not easily accessible for *in situ* Hybridization. While a certain fraction of single mRNA molecules might be below the detection limit, in other cases multiple mRNA signals might overlap and occur as one. Hence, it should be noted that the amount of detectable mRNA puncta analyzed in this study is not reflecting the amount of dendritic ABP mRNAs to the full extent and therefore, additional experiments will be needed that allow for a detection of single mRNA strands. Here, sense and antisense riboprobes were prepared in the lab. By an approach like this only one riboprobe at a time can bind to the target-mRNA and in addition, individual charges of synthesized riboprobes show variations in riboprobe length and thus, potentially also in specificity. Therefore, a single-molecule FISH approach utilizing ~40 company-designed riboprobes against one individual target mRNA would help to increase specificity as well as achieve a fluorophore-to-mRNA ratio that might allow for the detection and quantification of individual mRNA strands in dendrites (for reviews see Buxbaum et al., 2015; Kwon and Sabatini, 2011). For a single molecule analysis like this, however, also an increase in resolution will be needed. In this study, conventional confocal microscopy with a resolution limit of ~200 nm allowed for a reliable analysis of overall mRNA distribution in hippocampal neurons. However, it becomes more and more clear that very small numbers of dendritically localized mRNAs can be of crucial importance and therefore, it will be important to couple a single-molecule FISH approach with super-resolution microscopy e.g. Stimulated emission depletion microscopy (STED) or Structured illumination microscopy (SIM) in order to identify the exact localization of individual mRNA molecules in dendrites and dendritic spines.

An additional limitation of FISH is that it only offers a static image of the current mRNA distribution which is why in this work, several time-points following LTP or LTD induction were analyzed in order to gain a basic overview of mRNA distribution changes over time. However, if mRNAs are still in the process of being transported or kept in place cannot be anticipated from the FISH. Therefore, future experiments should include more time-points in order to increase the temporal resolution of the results. In addition, they should specifically focus on the analysis of live mRNA transport especially in the FXS mouse model as FMRP has a well-known function as an mRNA transporter (Dictenberg et al., 2008). As described in the Results section, first experiments with the aim of analyzing the mRNA transport of Cof1 were already done in this work, however, the MS2 vector system that was used for these experiments (Bertrand et al., 1998) has to be optimized. Especially the low fluorophore-to-mRNA ratio makes it challenging to detect individual single mRNAs in live neurons using this system, however, once established, the analysis of ABP mRNA transport will offer valuable results which will help to better understand the molecular mechanisms of ABP dysregulations in FXS.

Next, to further strengthen the results presented here, FISH experiments and single cell analysis should be repeated in hippocampal slices where the hippocampal architecture is kept intact and which represent the *in vivo* situation better than primary embryonic hippocampal cultures. This will be especially important as phenotypes in FXS might be brain region specific and even different regions of the hippocampus might be differentially affected by the syndrome. The results shown here could already confirm that also in hippocampal slices, Pfn1, Pfn2a as well as Cof1 mRNAs are present in the *stratum oriens* as well as the *stratum radiatum* and therefore, experiments could easily be repeated. An interesting approach would be to either induce LTP or LTD chemically or electrically in acute hippocampal slices while performing electrophysiological measurements. Afterwards, at a given time-point after the stimulus, acute slices could be taken out of the setup and fixed in order to perform FISH. By this, information about *in vivo* mRNA localization, spine morphology and functional plasticity would be assessable in one experiment.

Finally, future work might consider to focus on analyzing the activity-dependent spatial and temporal modulations of other ABPs at the synapse in greater detail. Given the multifarious functions of actin in dendritic spines, the amount of actin modulators that are involved in the mediation of synaptic plasticity is large and a more detailed understanding of the local regulations of all these ABPs will be crucial to understand the molecular mechanisms underlying memory formation. In addition, knowledge concerning the spatial and temporal modulations not only of ABPs but also of other proteins and mRNAs at the synapse will help to identify future therapeutic targets that might help to develop new treatment strategies against FXS or even autism spectrum disorders in general.

8 References

Abe, K., Chisaka, O., Van Roy, F., and Takeichi, M. (2004). Stability of dendritic spines and synaptic contacts is controlled by alpha N-catenin. Nature neuroscience 7, 357-363.

Ackermann, M., and Matus, A. (2003). Activity-induced targeting of profilin and stabilization of dendritic spine morphology. Nature neuroscience 6, 1194-1200.

Adrian, M., Kusters, R., Storm, C., Hoogenraad, C.C., and Kapitein, L.C. (2017). Probing the Interplay between Dendritic Spine Morphology and Membrane-Bound Diffusion. Biophysical journal 113, 2261-2270.

Alarcon, J.M., Hodgman, R., Theis, M., Huang, Y.S., Kandel, E.R., and Richter, J.D. (2004). Selective modulation of some forms of schaffer collateral-CA1 synaptic plasticity in mice with a disruption of the CPEB-1 gene. Learning & memory 11, 318-327.

Allen, K.M., Gleeson, J.G., Bagrodia, S., Partington, M.W., MacMillan, J.C., Cerione, R.A., Mulley, J.C., and Walsh, C.A. (1998). PAK3 mutation in nonsyndromic X-linked mental retardation. Nature genetics 20, 25-30.

Andersen, P., Moser, E., Moser, M.B., and Trommald, M. (1996). Cellular correlates to spatial learning in the rat hippocampus. Journal of physiology, Paris 90, 349.

Andreassi, C., and Riccio, A. (2009). To localize or not to localize: mRNA fate is in 3'UTR ends. Trends in cell biology 19, 465-474.

Andrianantoandro, E., and Pollard, T.D. (2006). Mechanism of actin filament turnover by severing and nucleation at different concentrations of ADF/cofilin. Molecular cell 24, 13-23.

Antar, L.N., Li, C., Zhang, H., Carroll, R.C., and Bassell, G.J. (2006). Local functions for FMRP in axon growth cone motility and activity-dependent regulation of filopodia and spine synapses. Molecular and cellular neurosciences 32, 37-48.

Araya, R., Jiang, J., Eisenthal, K.B., and Yuste, R. (2006). The spine neck filters membrane potentials. Proceedings of the National Academy of Sciences of the United States of America 103, 17961-17966.

Ascano, M., Jr., Mukherjee, N., Bandaru, P., Miller, J.B., Nusbaum, J.D., Corcoran, D.L., Langlois, C., Munschauer, M., Dewell, S., Hafner, M.*, et al.* (2012). FMRP targets distinct mRNA sequence elements to regulate protein expression. Nature 492, 382-386.

Ashley, C.T., Jr., Wilkinson, K.D., Reines, D., and Warren, S.T. (1993a). FMR1 protein: conserved RNP family domains and selective RNA binding. Science 262, 563-566.

Ashley, C.T., Sutcliffe, J.S., Kunst, C.B., Leiner, H.A., Eichler, E.E., Nelson, D.L., and Warren, S.T. (1993b). Human and murine FMR-1: alternative splicing and translational initiation downstream of the CGG-repeat. Nature genetics 4, 244-251.

Bagni, C., and Oostra, B.A. (2013). Fragile X syndrome: From protein function to therapy. American journal of medical genetics Part A 161A, 2809-2821.

Baker, K.B., Wray, S.P., Ritter, R., Mason, S., Lanthorn, T.H., and Savelieva, K.V. (2010). Male and female Fmr1 knockout mice on C57 albino background exhibit spatial learning and memory impairments. Genes, brain, and behavior 9, 562-574.

Bamburg, J.R., and Bernstein, B.W. (2010). Roles of ADF/cofilin in actin polymerization and beyond. F1000 biology reports 2, 62.

Bardoni, B., Mandel, J.L., and Fisch, G.S. (2000). FMR1 gene and fragile X syndrome. American journal of medical genetics 97, 153-163.

Bear, M.F., Huber, K.M., and Warren, S.T. (2004). The mGluR theory of fragile X mental retardation. Trends in neurosciences 27, 370-377.

Bertrand, E., Chartrand, P., Schaefer, M., Shenoy, S.M., Singer, R.H., and Long, R.M. (1998). Localization of ASH1 mRNA particles in living yeast. Molecular cell 2, 437-445.

Bienenstock, E.L., Cooper, L.N., and Munro, P.W. (1982). Theory for the development of neuron selectivity: orientation specificity and binocular interaction in visual cortex. The Journal of neuroscience : the official journal of the Society for Neuroscience 2, 32-48.

Billuart, P., Bienvenu, T., Ronce, N., des Portes, V., Vinet, M.C., Zemni, R., Carrie, A., Beldjord, C., Kahn, A., Moraine, C., and Chelly, J. (1998). Oligophrenin 1 encodes a rho-GAP protein involved in X-linked mental retardation. Pathologie-biologie 46, 678.

Bilousova, T.V., Dansie, L., Ngo, M., Aye, J., Charles, J.R., Ethell, D.W., and Ethell, I.M. (2009). Minocycline promotes dendritic spine maturation and improves behavioural performance in the fragile X mouse model. Journal of medical genetics 46, 94-102.

Bingol, B., and Schuman, E.M. (2006). Activity-dependent dynamics and sequestration of proteasomes in dendritic spines. Nature 441, 1144-1148.

Birbach, A. (2008). Profilin, a multi-modal regulator of neuronal plasticity. BioEssays : news and reviews in molecular, cellular and developmental biology 30, 994-1002.

Birbach, A., Verkuyl, J.M., and Matus, A. (2006). Reversible, activity-dependent targeting of profilin to neuronal nuclei. Experimental cell research 312, 2279-2287.

Bliss, T.V., and Collingridge, G.L. (1993). A synaptic model of memory: long-term potentiation in the hippocampus. Nature 361, 31-39.

Bliss, T.V., and Lomo, T. (1973). Long-lasting potentiation of synaptic transmission in the dentate area of the anaesthetized rabbit following stimulation of the perforant path. The Journal of physiology 232, 331-356.

Boda, B., Mendez, P., Boury-Jamot, B., Magara, F., and Muller, D. (2014). Reversal of activity-mediated spine dynamics and learning impairment in a mouse model of Fragile X syndrome. The European journal of neuroscience 39, 1130-1137.

Bodian, D. (1965). A Suggestive Relationship of Nerve Cell Rna with Specific Synaptic Sites. Proceedings of the National Academy of Sciences of the United States of America 53, 418-425.

Bongmba, O.Y., Martinez, L.A., Elhardt, M.E., Butler, K., and Tejada-Simon, M.V. (2011). Modulation of dendritic spines and synaptic function by Rac1: a possible link to Fragile X syndrome pathology. Brain research 1399, 79-95.

Bosch, M., Castro, J., Saneyoshi, T., Matsuno, H., Sur, M., and Hayashi, Y. (2014). Structural and molecular remodeling of dendritic spine substructures during long-term potentiation. Neuron 82, 444-459.

Bozdagi, O., Shan, W., Tanaka, H., Benson, D.L., and Huntley, G.W. (2000). Increasing numbers of synaptic puncta during late-phase LTP: N-cadherin is synthesized, recruited to synaptic sites, and required for potentiation. Neuron 28, 245-259.

Braun, A., Aszodi, A., Hellebrand, H., Berna, A., Fassler, R., and Brandau, O. (2002). Genomic organization of profilin-III and evidence for a transcript expressed exclusively in testis. Gene 283, 219-225.

Braun, K., and Segal, M. (2000). FMRP involvement in formation of synapses among cultured hippocampal neurons. Cerebral cortex 10, 1045-1052.

Briz, V., Zhu, G., Wang, Y., Liu, Y., Avetisyan, M., Bi, X., and Baudry, M. (2015). Activity-dependent rapid local RhoA synthesis is required for hippocampal synaptic plasticity. The Journal of neuroscience : the official journal of the Society for Neuroscience 35, 2269-2282.

Brown, V., Jin, P., Ceman, S., Darnell, J.C., O'Donnell, W.T., Tenenbaum, S.A., Jin, X., Feng, Y., Wilkinson, K.D., Keene, J.D*., et al.* (2001). Microarray identification of FMRP-associated brain mRNAs and altered mRNA translational profiles in fragile X syndrome. Cell 107, 477-487.

Buxbaum, A.R., Yoon, Y.J., Singer, R.H., and Park, H.Y. (2015). Single-molecule insights into mRNA dynamics in neurons. Trends in cell biology 25, 468-475.

Cajigas, I.J., Tushev, G., Will, T.J., tom Dieck, S., Fuerst, N., and Schuman, E.M. (2012). The local transcriptome in the synaptic neuropil revealed by deep sequencing and high-resolution imaging. Neuron 74, 453-466.

Ceman, S., O'Donnell, W.T., Reed, M., Patton, S., Pohl, J., and Warren, S.T. (2003). Phosphorylation influences the translation state of FMRP-associated polyribosomes. Human molecular genetics 12, 3295-3305.

Chang, F., Woollard, A., and Nurse, P. (1996). Isolation and characterization of fission yeast mutants defective in the assembly and placement of the contractile actin ring. Journal of cell science 109 (Pt 1), 131-142.

Chazeau, A., and Giannone, G. (2016). Organization and dynamics of the actin cytoskeleton during dendritic spine morphological remodeling. Cellular and molecular life sciences : CMLS 73, 3053-3073.

Chen, J.H., Kellner, Y., Zagrebelsky, M., Grunwald, M., Korte, M., and Walla, P.J. (2015). Two-Photon Correlation Spectroscopy in Single Dendritic Spines Reveals Fast Actin Filament Reorganization during Activity-Dependent Growth. PloS one 10, e0128241.

Chen, L.Y., Rex, C.S., Casale, M.S., Gall, C.M., and Lynch, G. (2007). Changes in synaptic morphology accompany actin signaling during LTP. The Journal of neuroscience : the official journal of the Society for Neuroscience 27, 5363-5372.

Chiurazzi, P., and Oostra, B.A. (2000). Genetics of mental retardation. Current opinion in pediatrics 12, 529-535.

Cohen, L.D., and Ziv, N.E. (2017). Recent insights on principles of synaptic protein degradation. F1000Research 6, 675.

Comery, T.A., Harris, J.B., Willems, P.J., Oostra, B.A., Irwin, S.A., Weiler, I.J., and Greenough, W.T. (1997). Abnormal dendritic spines in fragile X knockout mice: maturation and pruning deficits. Proceedings of the National Academy of Sciences of the United States of America 94, 5401-5404.

Contractor, A., Klyachko, V.A., and Portera-Cailliau, C. (2015). Altered Neuronal and Circuit Excitability in Fragile X Syndrome. Neuron 87, 699-715.

Cougot, N., Bhattacharyya, S.N., Tapia-Arancibia, L., Bordonne, R., Filipowicz, W., Bertrand, E., and Rage, F. (2008). Dendrites of mammalian neurons contain specialized P-body-like structures that respond to neuronal activation. The Journal of neuroscience : the official journal of the Society for Neuroscience 28, 13793-13804.

Cruz-Martin, A., Crespo, M., and Portera-Cailliau, C. (2010). Delayed stabilization of dendritic spines in fragile X mice. The Journal of neuroscience : the official journal of the Society for Neuroscience 30, 7793-7803.

Czaplinski, K., and Singer, R.H. (2006). Pathways for mRNA localization in the cytoplasm. Trends in biochemical sciences 31, 687-693.

D'Hooge, R., Nagels, G., Franck, F., Bakker, C.E., Reyniers, E., Storm, K., Kooy, R.F., Oostra, B.A., Willems, P.J., and De Deyn, P.P. (1997). Mildly impaired water maze performance in male Fmr1 knockout mice. Neuroscience 76, 367-376.

Darnell, J.C., Van Driesche, S.J., Zhang, C., Hung, K.Y., Mele, A., Fraser, C.E., Stone, E.F., Chen, C., Fak, J.J., Chi, S.W*., et al.* (2011). FMRP stalls ribosomal translocation on mRNAs linked to synaptic function and autism. Cell 146, 247-261.

Davis, G.W. (2006). Homeostatic control of neural activity: from phenomenology to molecular design. Annual review of neuroscience 29, 307-323.

Derkach, V.A., Oh, M.C., Guire, E.S., and Soderling, T.R. (2007). Regulatory mechanisms of AMPA receptors in synaptic plasticity. Nature reviews Neuroscience 8, 101-113.

Di Nardo, A., Gareus, R., Kwiatkowski, D., and Witke, W. (2000). Alternative splicing of the mouse profilin II gene generates functionally different profilin isoforms. Journal of cell science 113 Pt 21, 3795-3803.

Dictenberg, J.B., Swanger, S.A., Antar, L.N., Singer, R.H., and Bassell, G.J. (2008). A direct role for FMRP in activity-dependent dendritic mRNA transport links filopodial-spine morphogenesis to fragile X syndrome. Developmental cell 14, 926-939.

Dobkin, C., Rabe, A., Dumas, R., El Idrissi, A., Haubenstock, H., and Brown, W.T. (2000). Fmr1 knockout mouse has a distinctive strain-specific learning impairment. Neuroscience 100, 423-429.

Dolan, B.M., Duron, S.G., Campbell, D.A., Vollrath, B., Shankaranarayana Rao, B.S., Ko, H.Y., Lin, G.G., Govindarajan, A., Choi, S.Y., and Tonegawa, S. (2013). Rescue of fragile X syndrome phenotypes in Fmr1 KO mice by the small-molecule PAK inhibitor FRAX486. Proceedings of the National Academy of Sciences of the United States of America 110, 5671-5676.

Dolen, G., Osterweil, E., Rao, B.S., Smith, G.B., Auerbach, B.D., Chattarji, S., and Bear, M.F. (2007). Correction of fragile X syndrome in mice. Neuron 56, 955-962.

Duffney, L.J., Zhong, P., Wei, J., Matas, E., Cheng, J., Qin, L., Ma, K., Dietz, D.M., Kajiwara, Y., Buxbaum, J.D., and Yan, Z. (2015). Autism-like Deficits in Shank3-Deficient Mice Are Rescued by Targeting Actin Regulators. Cell reports 11, 1400-1413.

Dutch-Belgian Fragile X Consortium (1994). Fmr1 knockout mice: a model to study fragile X mental retardation. Cell 78, 23-33.

Eberhart, D.E., Malter, H.E., Feng, Y., and Warren, S.T. (1996). The fragile X mental retardation protein is a ribonucleoprotein containing both nuclear localization and nuclear export signals. Human molecular genetics 5, 1083-1091.

Ebrahimi, S., and Okabe, S. (2014). Structural dynamics of dendritic spines: molecular composition, geometry and functional regulation. Biochimica et biophysica acta 1838, 2391-2398.

Feig, S., and Lipton, P. (1993). Pairing the cholinergic agonist carbachol with patterned Schaffer collateral stimulation initiates protein synthesis in hippocampal CA1 pyramidal cell dendrites via a muscarinic, NMDA-dependent mechanism. The Journal of neuroscience : the official journal of the Society for Neuroscience 13, 1010-1021.

Feng, Y., Absher, D., Eberhart, D.E., Brown, V., Malter, H.E., and Warren, S.T. (1997). FMRP associates with polyribosomes as an mRNP, and the I304N mutation of severe fragile X syndrome abolishes this association. Molecular cell 1, 109-118.

Feuge, J., Scharkowski, F., Michaelsen-Preusse, K., and Korte, M. (2019). FMRP Modulates Activity-Dependent Spine Plasticity by Binding Cofilin1 mRNA and Regulating Localization and Local Translation. Cerebral cortex.

Firat-Karalar, E.N., and Welch, M.D. (2011). New mechanisms and functions of actin nucleation. Current opinion in cell biology 23, 4-13.

Fitzjohn, S.M., Palmer, M.J., May, J.E., Neeson, A., Morris, S.A., and Collingridge, G.L. (2001). A characterisation of long-term depression induced by metabotropic glutamate receptor activation in the rat hippocampus in vitro. The Journal of physiology 537, 421-430.

Flexner, J.B., Flexner, L.B., and Stellar, E. (1963). Memory in mice as affected by intracerebral puromycin. Science 141, 57-59.

Fortin, D.A., Davare, M.A., Srivastava, T., Brady, J.D., Nygaard, S., Derkach, V.A., and Soderling, T.R. (2010). Long-term potentiation-dependent spine enlargement requires synaptic Ca2+-permeable

AMPA receptors recruited by CaM-kinase I. The Journal of neuroscience : the official journal of the Society for Neuroscience 30, 11565-11575.

Frankland, P.W., and Bontempi, B. (2005). The organization of recent and remote memories. Nature reviews Neuroscience 6, 119-130.

Frey, U., Huang, Y.Y., and Kandel, E.R. (1993). Effects of cAMP simulate a late stage of LTP in hippocampal CA1 neurons. Science 260, 1661-1664.

Frey, U., and Morris, R.G. (1997). Synaptic tagging and long-term potentiation. Nature 385, 533-536.

Fukazawa, Y., Saitoh, Y., Ozawa, F., Ohta, Y., Mizuno, K., and Inokuchi, K. (2003). Hippocampal LTP is accompanied by enhanced F-actin content within the dendritic spine that is essential for late LTP maintenance in vivo. Neuron 38, 447-460.

Gaiarsa, J.L., Caillard, O., and Ben-Ari, Y. (2002). Long-term plasticity at GABAergic and glycinergic synapses: mechanisms and functional significance. Trends in neurosciences 25, 564-570.

Gholizadeh, S., Halder, S.K., and Hampson, D.R. (2015). Expression of fragile X mental retardation protein in neurons and glia of the developing and adult mouse brain. Brain research 1596, 22-30.

Godfraind, J.M., Reyniers, E., De Boulle, K., D'Hooge, R., De Deyn, P.P., Bakker, C.E., Oostra, B.A., Kooy, R.F., and Willems, P.J. (1996). Long-term potentiation in the hippocampus of fragile X knockout mice. American journal of medical genetics 64, 246-251.

Goldschmidt-Clermont, P.J., Furman, M.I., Wachsstock, D., Safer, D., Nachmias, V.T., and Pollard, T.D. (1992). The control of actin nucleotide exchange by thymosin beta 4 and profilin. A potential regulatory mechanism for actin polymerization in cells. Molecular biology of the cell 3, 1015-1024.

Goldstein, L.S., and Yang, Z. (2000). Microtubule-based transport systems in neurons: the roles of kinesins and dyneins. Annual review of neuroscience 23, 39-71.

Gomez-Mancilla, B. (2012). Tweaking the social network. Science translational medicine 4, 131fs139.

Gonzalez-Islas, C., and Wenner, P. (2006). Spontaneous network activity in the embryonic spinal cord regulates AMPAergic and GABAergic synaptic strength. Neuron 49, 563-575.

Gonzalez, I., Buonomo, S.B., Nasmyth, K., and von Ahsen, U. (1999). ASH1 mRNA localization in yeast involves multiple secondary structural elements and Ash1 protein translation. Current biology : CB 9, 337-340.

Gordon, M.W. (1969). Neuronal plasticity and memory. The American journal of orthopsychiatry 39, 578-594.

Gorlich, A., Zimmermann, A.M., Schober, D., Bottcher, R.T., Sassoe-Pognetto, M., Friauf, E., Witke, W., and Rust, M.B. (2012). Preserved morphology and physiology of excitatory synapses in profilin1-deficient mice. PloS one 7, e30068.

Grossman, A.W., Aldridge, G.M., Lee, K.J., Zeman, M.K., Jun, C.S., Azam, H.S., Arii, T., Imoto, K., Greenough, W.T., and Rhyu, I.J. (2010). Developmental characteristics of dendritic spines in the dentate gyrus of Fmr1 knockout mice. Brain research 1355, 221-227.

Grossman, A.W., Elisseou, N.M., McKinney, B.C., and Greenough, W.T. (2006). Hippocampal pyramidal cells in adult Fmr1 knockout mice exhibit an immature-appearing profile of dendritic spines. Brain research 1084, 158-164.

Gu, J., Lee, C.W., Fan, Y., Komlos, D., Tang, X., Sun, C., Yu, K., Hartzell, H.C., Chen, G., Bamburg, J.R., and Zheng, J.Q. (2010). ADF/cofilin-mediated actin dynamics regulate AMPA receptor trafficking during synaptic plasticity. Nature neuroscience 13, 1208-1215.

Gungabissoon, R.A., and Bamburg, J.R. (2003). Regulation of growth cone actin dynamics by ADF/cofilin. The journal of histochemistry and cytochemistry : official journal of the Histochemistry Society 51, 411-420.

Gurel, P.S., A, M., Guo, B., Shu, R., Mierke, D.F., and Higgs, H.N. (2015). Assembly and turnover of short actin filaments by the formin INF2 and profilin. The Journal of biological chemistry 290, 22494-22506.

Hall, S.S., Burns, D.D., Lightbody, A.A., and Reiss, A.L. (2008). Longitudinal changes in intellectual development in children with Fragile X syndrome. Journal of abnormal child psychology 36, 927-939.

Halpain, S., Hipolito, A., and Saffer, L. (1998). Regulation of F-actin stability in dendritic spines by glutamate receptors and calcineurin. The Journal of neuroscience : the official journal of the Society for Neuroscience 18, 9835-9844.

Hanley, J.G. (2014). Actin-dependent mechanisms in AMPA receptor trafficking. Frontiers in cellular neuroscience 8, 381.

Hanson, J., and Lowy, J. (1964). The Structure of Actin Filaments and the Origin of the Axial Periodicity in the I-Substance of Vertebrate Striated Muscle. Proceedings of the Royal Society of London Series B, Biological sciences 160, 449-460.

Harlow, E.G., Till, S.M., Russell, T.A., Wijetunge, L.S., Kind, P., and Contractor, A. (2010). Critical period plasticity is disrupted in the barrel cortex of FMR1 knockout mice. Neuron 65, 385-398.

Harreveld, A.V., and Fifkova, E. (1975). Rapid freezing of deep cerebral structures for electron microscopy. The Anatomical record 182, 377-385.

Hayama, T., Noguchi, J., Watanabe, S., Takahashi, N., Hayashi-Takagi, A., Ellis-Davies, G.C., Matsuzaki, M., and Kasai, H. (2013). GABA promotes the competitive selection of dendritic spines by controlling local Ca2+ signaling. Nature neuroscience 16, 1409-1416.

Hayashi-Takagi, A., Yagishita, S., Nakamura, M., Shirai, F., Wu, Y.I., Loshbaugh, A.L., Kuhlman, B., Hahn, K.M., and Kasai, H. (2015). Labelling and optical erasure of synaptic memory traces in the motor cortex. Nature 525, 333-338.

Hayashi, M.L., Rao, B.S., Seo, J.S., Choi, H.S., Dolan, B.M., Choi, S.Y., Chattarji, S., and Tonegawa, S. (2007). Inhibition of p21-activated kinase rescues symptoms of fragile X syndrome in mice. Proceedings of the National Academy of Sciences of the United States of America 104, 11489-11494.

He, C.X., and Portera-Cailliau, C. (2013). The trouble with spines in fragile X syndrome: density, maturity and plasticity. Neuroscience 251, 120-128.

Hebb, D.O. (1949). The Organization of Behavior. A Neuropsychological Theory. New York: John Wiley & Sons, Inc.

Hering, H., and Sheng, M. (2003). Activity-dependent redistribution and essential role of cortactin in dendritic spine morphogenesis. The Journal of neuroscience : the official journal of the Society for Neuroscience 23, 11759-11769.

Hinton, V.J., Brown, W.T., Wisniewski, K., and Rudelli, R.D. (1991). Analysis of neocortex in three males with the fragile X syndrome. American journal of medical genetics 41, 289-294.

Hirokawa, N. (2006). mRNA transport in dendrites: RNA granules, motors, and tracks. The Journal of neuroscience : the official journal of the Society for Neuroscience 26, 7139-7142.

Hofmann, W.A., and de Lanerolle, P. (2006). Nuclear actin: to polymerize or not to polymerize. The Journal of cell biology 172, 495-496.

Holt, C.E., Martin, K.C., and Schuman, E.M. (2019). Local translation in neurons: visualization and function. Nature structural & molecular biology 26, 557-566.

Honkura, N., Matsuzaki, M., Noguchi, J., Ellis-Davies, G.C., and Kasai, H. (2008). The subspine organization of actin fibers regulates the structure and plasticity of dendritic spines. Neuron 57, 719-729.

Honore, B., Madsen, P., Andersen, A.H., and Leffers, H. (1993). Cloning and expression of a novel human profilin variant, profilin II. FEBS letters 330, 151-155.

Hotulainen, P., and Hoogenraad, C.C. (2010). Actin in dendritic spines: connecting dynamics to function. The Journal of cell biology 189, 619-629.

Hotulainen, P., Llano, O., Smirnov, S., Tanhuanpaa, K., Faix, J., Rivera, C., and Lappalainen, P. (2009). Defining mechanisms of actin polymerization and depolymerization during dendritic spine morphogenesis. The Journal of cell biology 185, 323-339.

Hou, L., Antion, M.D., Hu, D., Spencer, C.M., Paylor, R., and Klann, E. (2006). Dynamic translational and proteasomal regulation of fragile X mental retardation protein controls mGluR-dependent long-term depression. Neuron 51, 441-454.

Hu, E., Chen, Z., Fredrickson, T., and Zhu, Y. (2001). Molecular cloning and characterization of profilin-3: a novel cytoskeleton-associated gene expressed in rat kidney and testes. Experimental nephrology 9, 265-274.

Hu, H., Qin, Y., Bochorishvili, G., Zhu, Y., van Aelst, L., and Zhu, J.J. (2008). Ras signaling mechanisms underlying impaired GluR1-dependent plasticity associated with fragile X syndrome. J Neurosci 28, 7847-7862.

Huang, W., Zhu, P.J., Zhang, S., Zhou, H., Stoica, L., Galiano, M., Krnjevic, K., Roman, G., and Costa-Mattioli, M. (2013). mTORC2 controls actin polymerization required for consolidation of long-term memory. Nature neuroscience 16, 441-448.

Huber, K.M., Gallagher, S.M., Warren, S.T., and Bear, M.F. (2002). Altered synaptic plasticity in a mouse model of fragile X mental retardation. Proceedings of the National Academy of Sciences of the United States of America 99, 7746-7750.

Huber, K.M., Roder, J.C., and Bear, M.F. (2001). Chemical induction of mGluR5- and protein synthesis--dependent long-term depression in hippocampal area CA1. Journal of neurophysiology 86, 321-325.

Irwin, S.A., Galvez, R., and Greenough, W.T. (2000). Dendritic spine structural anomalies in fragile-X mental retardation syndrome. Cerebral cortex 10, 1038-1044.

Irwin, S.A., Patel, B., Idupulapati, M., Harris, J.B., Crisostomo, R.A., Larsen, B.P., Kooy, F., Willems, P.J., Cras, P., Kozlowski, P.B., *et al.* (2001). Abnormal dendritic spine characteristics in the temporal and visual cortices of patients with fragile-X syndrome: a quantitative examination. American journal of medical genetics 98, 161-167.

Jockusch, B.M., Murk, K., and Rothkegel, M. (2007). The profile of profilins. Reviews of physiology, biochemistry and pharmacology 159, 131-149.

Joensuu, M., Lanoue, V., and Hotulainen, P. (2018). Dendritic spine actin cytoskeleton in autism spectrum disorder. Progress in neuro-psychopharmacology & biological psychiatry 84, 362-381.

Kaech, S., Fischer, M., Doll, T., and Matus, A. (1997). Isoform specificity in the relationship of actin to dendritic spines. The Journal of neuroscience : the official journal of the Society for Neuroscience 17, 9565-9572.

Kandel, E.R. (2001). The molecular biology of memory storage: a dialogue between genes and synapses. Science 294, 1030-1038.

Kang, H., and Schuman, E.M. (1996). A requirement for local protein synthesis in neurotrophin-induced hippocampal synaptic plasticity. Science 273, 1402-1406.

Kapitein, L.C., and Hoogenraad, C.C. (2011). Which way to go? Cytoskeletal organization and polarized transport in neurons. Molecular and cellular neurosciences 46, 9-20.

Kaufmann, W.E., and Moser, H.W. (2000). Dendritic anomalies in disorders associated with mental retardation. Cerebral cortex 10, 981-991.

Khayachi, A., Gwizdek, C., Poupon, G., Alcor, D., Chafai, M., Casse, F., Maurin, T., Prieto, M., Folci, A., De Graeve, F.*, et al.* (2018). Sumoylation regulates FMRP-mediated dendritic spine elimination and maturation. Nature communications 9, 757.

Kiebler, M.A., and Bassell, G.J. (2006). Neuronal RNA granules: movers and makers. Neuron 51, 685-690.

Kim, K., Lakhanpal, G., Lu, H.E., Khan, M., Suzuki, A., Hayashi, M.K., Narayanan, R., Luyben, T.T., Matsuda, T., Nagai, T.*, et al.* (2015). A Temporary Gating of Actin Remodeling during Synaptic Plasticity Consists of the Interplay between the Kinase and Structural Functions of CaMKII. Neuron 87, 813-826.

Knierim, J.J. (2006). Neural representations of location outside the hippocampus. Learning & memory 13, 405-415.

Knowles, R.B., Sabry, J.H., Martone, M.E., Deerinck, T.J., Ellisman, M.H., Bassell, G.J., and Kosik, K.S. (1996). Translocation of RNA granules in living neurons. The Journal of neuroscience : the official journal of the Society for Neuroscience 16, 7812-7820.

Kondrashov, N., Pusic, A., Stumpf, C.R., Shimizu, K., Hsieh, A.C., Ishijima, J., Shiroishi, T., and Barna, M. (2011). Ribosome-mediated specificity in Hox mRNA translation and vertebrate tissue patterning. Cell 145, 383-397.

Kooy, R.F., D'Hooge, R., Reyniers, E., Bakker, C.E., Nagels, G., De Boulle, K., Storm, K., Clincke, G., De Deyn, P.P., Oostra, B.A., and Willems, P.J. (1996). Transgenic mouse model for the fragile X syndrome. American journal of medical genetics 64, 241-245.

Kopec, C.D., Real, E., Kessels, H.W., and Malinow, R. (2007). GluR1 links structural and functional plasticity at excitatory synapses. The Journal of neuroscience : the official journal of the Society for Neuroscience 27, 13706-13718.

Korte, M., and Schmitz, D. (2016). Cellular and System Biology of Memory: Timing, Molecules, and Beyond. Physiological reviews 96, 647-693.

Kosik, K.S. (2016). Life at Low Copy Number: How Dendrites Manage with So Few mRNAs. Neuron 92, 1168-1180.

Koskinen, M., Bertling, E., Hotulainen, R., Tanhuanpaa, K., and Hotulainen, P. (2014). Myosin IIb controls actin dynamics underlying the dendritic spine maturation. Molecular and cellular neurosciences 61, 56-64.

Krug, M., Lossner, B., and Ott, T. (1984). Anisomycin blocks the late phase of long-term potentiation in the dentate gyrus of freely moving rats. Brain research bulletin 13, 39-42.

Kwon, H.B., and Sabatini, B.L. (2011). Glutamate induces de novo growth of functional spines in developing cortex. Nature 474, 100-104.

Laggerbauer, B., Ostareck, D., Keidel, E.M., Ostareck-Lederer, A., and Fischer, U. (2001). Evidence that fragile X mental retardation protein is a negative regulator of translation. Human molecular genetics 10, 329-338.

Lambrechts, A., Braun, A., Jonckheere, V., Aszodi, A., Lanier, L.M., Robbens, J., Van Colen, I., Vandekerckhove, J., Fassler, R., and Ampe, C. (2000). Profilin II is alternatively spliced, resulting in profilin isoforms that are differentially expressed and have distinct biochemical properties. Molecular and cellular biology 20, 8209-8219.

Lambrechts, A., Verschelde, J.L., Jonckheere, V., Goethals, M., Vandekerckhove, J., and Ampe, C. (1997). The mammalian profilin isoforms display complementary affinities for PIP2 and proline-rich sequences. The EMBO journal 16, 484-494.

Larson, J., Jessen, R.E., Kim, D., Fine, A.K., and du Hoffmann, J. (2005). Age-dependent and selective impairment of long-term potentiation in the anterior piriform cortex of mice lacking the fragile X mental retardation protein. The Journal of neuroscience : the official journal of the Society for Neuroscience 25, 9460-9469.

Lashley, K.S. (1950). In Search of the Engram. Society for Experimental Biology, Physiological mechanisms in animal behavior. (Society's Symposium IV.), 454-482.

Lassing, I., and Lindberg, U. (1985). Specific interaction between phosphatidylinositol 4,5-bisphosphate and profilactin. Nature 314, 472-474.

Lauterborn, J.C., Rex, C.S., Kramar, E., Chen, L.Y., Pandyarajan, V., Lynch, G., and Gall, C.M. (2007). Brain-derived neurotrophic factor rescues synaptic plasticity in a mouse model of fragile X syndrome. The Journal of neuroscience : the official journal of the Society for Neuroscience 27, 10685-10694.

Leach, P.T., Hayes, J., Pride, M., Silverman, J.L., and Crawley, J.N. (2016). Normal Performance of Fmr1 Mice on a Touchscreen Delayed Nonmatching to Position Working Memory Task. eNeuro 3.

Lee, A., Li, W., Xu, K., Bogert, B.A., Su, K., and Gao, F.B. (2003). Control of dendritic development by the Drosophila fragile X-related gene involves the small GTPase Rac1. Development 130, 5543-5552.

Leuner, B., Falduto, J., and Shors, T.J. (2003). Associative memory formation increases the observation of dendritic spines in the hippocampus. The Journal of neuroscience : the official journal of the Society for Neuroscience 23, 659-665.

Levenga, J., de Vrij, F.M., Buijsen, R.A., Li, T., Nieuwenhuizen, I.M., Pop, A., Oostra, B.A., and Willemsen, R. (2011). Subregion-specific dendritic spine abnormalities in the hippocampus of Fmr1 KO mice. Neurobiology of learning and memory 95, 467-472.

Li, J., Pelletier, M.R., Perez Velazquez, J.L., and Carlen, P.L. (2002). Reduced cortical synaptic plasticity and GluR1 expression associated with fragile X mental retardation protein deficiency. Molecular and cellular neurosciences 19, 138-151.

Lightbody, A.A., and Reiss, A.L. (2009). Gene, brain, and behavior relationships in fragile X syndrome: evidence from neuroimaging studies. Developmental disabilities research reviews 15, 343-352.

Lin, W.H., and Webb, D.J. (2009). Actin and Actin-Binding Proteins: Masters of Dendritic Spine Formation, Morphology, and Function. The open neuroscience journal 3, 54-66.

Linden, D.J. (1996). A protein synthesis-dependent late phase of cerebellar long-term depression. Neuron 17, 483-490.

Liu, Z.H., Chuang, D.M., and Smith, C.B. (2011). Lithium ameliorates phenotypic deficits in a mouse model of fragile X syndrome. The international journal of neuropsychopharmacology 14, 618-630.

Lorente De Nó, R. (1934). Studies on the structure of the cerebral cortex. II. Continuation of the study of the ammonic system. Journal für Psychologie und Neurologie 46, 113-177.

Lu, W., Man, H., Ju, W., Trimble, W.S., MacDonald, J.F., and Wang, Y.T. (2001). Activation of synaptic NMDA receptors induces membrane insertion of new AMPA receptors and LTP in cultured hippocampal neurons. Neuron 29, 243-254.

Luo, L., Hensch, T.K., Ackerman, L., Barbel, S., Jan, L.Y., and Jan, Y.N. (1996). Differential effects of the Rac GTPase on Purkinje cell axons and dendritic trunks and spines. Nature 379, 837-840.

Luscher, C., and Huber, K.M. (2010). Group 1 mGluR-dependent synaptic long-term depression: mechanisms and implications for circuitry and disease. Neuron 65, 445-459.

Lynch, M.A. (2004). Long-term potentiation and memory. Physiological reviews 84, 87-136.

Maass, W., and Zador, A.M. (1999). Dynamic stochastic synapses as computational units. Neural computation 11, 903-917.

Maffei, A., Nelson, S.B., and Turrigiano, G.G. (2004). Selective reconfiguration of layer 4 visual cortical circuitry by visual deprivation. Nature neuroscience 7, 1353-1359.

Mammoto, A., Sasaki, T., Asakura, T., Hotta, I., Imamura, H., Takahashi, K., Matsuura, Y., Shirao, T., and Takai, Y. (1998). Interactions of drebrin and gephyrin with profilin. Biochemical and biophysical research communications 243, 86-89.

Manns, J.R., and Eichenbaum, H. (2006). Evolution of declarative memory. Hippocampus 16, 795-808.

Martin, J.P., and Bell, J. (1943). A Pedigree of Mental Defect Showing Sex-Linkage. Journal of neurology and psychiatry 6, 154-157.

Matsuzaki, M., Honkura, N., Ellis-Davies, G.C., and Kasai, H. (2004). Structural basis of long-term potentiation in single dendritic spines. Nature 429, 761-766.

Maurin, T., and Bardoni, B. (2018). Fragile X Mental Retardation Protein: To Be or Not to Be a Translational Enhancer. Frontiers in molecular biosciences 5, 113.

Mayford, M., Baranes, D., Podsypanina, K., and Kandel, E.R. (1996). The 3'-untranslated region of CaMKII alpha is a cis-acting signal for the localization and translation of mRNA in dendrites. Proceedings of the National Academy of Sciences of the United States of America 93, 13250-13255.

McGaugh, J.L. (2000). Memory--a century of consolidation. Science 287, 248-251.

Meredith, R.M., Holmgren, C.D., Weidum, M., Burnashev, N., and Mansvelder, H.D. (2007). Increased threshold for spike-timing-dependent plasticity is caused by unreliable calcium signaling in mice lacking fragile X gene FMR1. Neuron 54, 627-638.

Michaelsen-Preusse, K., Feuge, J., and Korte, M. (2018). Imbalance of synaptic actin dynamics as a key to fragile X syndrome? The Journal of physiology 596, 2773-2782.

Michaelsen-Preusse, K., Zessin, S., Grigoryan, G., Scharkowski, F., Feuge, J., Remus, A., and Korte, M. (2016). Neuronal profilins in health and disease: Relevance for spine plasticity and Fragile X syndrome. Proceedings of the National Academy of Sciences of the United States of America 113, 3365-3370.

Michaelsen, K., Murk, K., Zagrebelsky, M., Dreznjak, A., Jockusch, B.M., Rothkegel, M., and Korte, M. (2010). Fine-tuning of neuronal architecture requires two profilin isoforms. Proceedings of the National Academy of Sciences of the United States of America 107, 15780-15785.

Miki, H., Suetsugu, S., and Takenawa, T. (1998). WAVE, a novel WASP-family protein involved in actin reorganization induced by Rac. The EMBO journal 17, 6932-6941.

Milner, B. (1972). Disorders of learning and memory after temporal lobe lesions in man. Clinical neurosurgery 19, 421-446.

Montarolo, P.G., Goelet, P., Castellucci, V.F., Morgan, J., Kandel, E.R., and Schacher, S. (1986). A critical period for macromolecular synthesis in long-term heterosynaptic facilitation in Aplysia. Science 234, 1249-1254.

Moon, A., and Drubin, D.G. (1995). The ADF/cofilin proteins: stimulus-responsive modulators of actin dynamics. Molecular biology of the cell 6, 1423-1431.

Morris, R. (1984). Developments of a water-maze procedure for studying spatial learning in the rat. Journal of neuroscience methods 11, 47-60.

Morris, R.G., Anderson, E., Lynch, G.S., and Baudry, M. (1986). Selective impairment of learning and blockade of long-term potentiation by an N-methyl-D-aspartate receptor antagonist, AP5. Nature 319, 774-776.

Moser, M.B., Trommald, M., and Andersen, P. (1994). An increase in dendritic spine density on hippocampal CA1 pyramidal cells following spatial learning in adult rats suggests the formation of new synapses. Proceedings of the National Academy of Sciences of the United States of America 91, 12673-12675.

Murase, S., Mosser, E., and Schuman, E.M. (2002). Depolarization drives beta-Catenin into neuronal spines promoting changes in synaptic structure and function. Neuron 35, 91-105.

Murk, K., Wittenmayer, N., Michaelsen-Preusse, K., Dresbach, T., Schoenenberger, C.A., Korte, M., Jockusch, B.M., and Rothkegel, M. (2012). Neuronal profilin isoforms are addressed by different signalling pathways. PloS one 7, e34167.

Musleh, W., Bi, X., Tocco, G., Yaghoubi, S., and Baudry, M. (1997). Glycine-induced long-term potentiation is associated with structural and functional modifications of alpha-amino-3-hydroxyl-5-methyl-4-isoxazolepropionic acid receptors. Proceedings of the National Academy of Sciences of the United States of America 94, 9451-9456.

Muslimov, I.A., Santi, E., Homel, P., Perini, S., Higgins, D., and Tiedge, H. (1997). RNA transport in dendrites: a cis-acting targeting element is contained within neuronal BC1 RNA. The Journal of neuroscience : the official journal of the Society for Neuroscience 17, 4722-4733.

Nagerl, U.V., Eberhorn, N., Cambridge, S.B., and Bonhoeffer, T. (2004). Bidirectional activity-dependent morphological plasticity in hippocampal neurons. Neuron 44, 759-767.

Nagerl, U.V., Willig, K.I., Hein, B., Hell, S.W., and Bonhoeffer, T. (2008). Live-cell imaging of dendritic spines by STED microscopy. Proceedings of the National Academy of Sciences of the United States of America 105, 18982-18987.

Nakayama, A.Y., Harms, M.B., and Luo, L. (2000). Small GTPases Rac and Rho in the maintenance of dendritic spines and branches in hippocampal pyramidal neurons. The Journal of neuroscience : the official journal of the Society for Neuroscience 20, 5329-5338.

Narayanan, U., Nalavadi, V., Nakamoto, M., Pallas, D.C., Ceman, S., Bassell, G.J., and Warren, S.T. (2007). FMRP phosphorylation reveals an immediate-early signaling pathway triggered by group I mGluR and mediated by PP2A. The Journal of neuroscience : the official journal of the Society for Neuroscience 27, 14349-14357.

Narayanan, U., Nalavadi, V., Nakamoto, M., Thomas, G., Ceman, S., Bassell, G.J., and Warren, S.T. (2008). S6K1 phosphorylates and regulates fragile X mental retardation protein (FMRP) with the neuronal protein synthesis-dependent mammalian target of rapamycin (mTOR) signaling cascade. The Journal of biological chemistry 283, 18478-18482.

Neuhoff, H., Sassoe-Pognetto, M., Panzanelli, P., Maas, C., Witke, W., and Kneussel, M. (2005). The actin-binding protein profilin I is localized at synaptic sites in an activity-regulated manner. The European journal of neuroscience 21, 15-25.

Nimchinsky, E.A., Oberlander, A.M., and Svoboda, K. (2001). Abnormal development of dendritic spines in FMR1 knock-out mice. The Journal of neuroscience : the official journal of the Society for Neuroscience 21, 5139-5146.

Nimchinsky, E.A., Sabatini, B.L., and Svoboda, K. (2002). Structure and function of dendritic spines. Annual review of physiology 64, 313-353.

Niwa, R., Nagata-Ohashi, K., Takeichi, M., Mizuno, K., and Uemura, T. (2002). Control of actin reorganization by Slingshot, a family of phosphatases that dephosphorylate ADF/cofilin. Cell 108, 233-246.

Nosyreva, E.D., and Huber, K.M. (2005). Developmental switch in synaptic mechanisms of hippocampal metabotropic glutamate receptor-dependent long-term depression. The Journal of neuroscience : the official journal of the Society for Neuroscience 25, 2992-3001.

Nusser, Z., Hajos, N., Somogyi, P., and Mody, I. (1998). Increased number of synaptic GABA(A) receptors underlies potentiation at hippocampal inhibitory synapses. Nature 395, 172-177.

Okamoto, K., Nagai, T., Miyawaki, A., and Hayashi, Y. (2004). Rapid and persistent modulation of actin dynamics regulates postsynaptic reorganization underlying bidirectional plasticity. Nature neuroscience 7, 1104-1112.

Oliet, S.H., Malenka, R.C., and Nicoll, R.A. (1997). Two distinct forms of long-term depression coexist in CA1 hippocampal pyramidal cells. Neuron 18, 969-982.

Ouyang, Y., Wong, M., Capani, F., Rensing, N., Lee, C.S., Liu, Q., Neusch, C., Martone, M.E., Wu, J.Y., Yamada, K.*, et al.* (2005). Transient decrease in F-actin may be necessary for translocation of proteins into dendritic spines. The European journal of neuroscience 22, 2995-3005.

Pan, F., Aldridge, G.M., Greenough, W.T., and Gan, W.B. (2010). Dendritic spine instability and insensitivity to modulation by sensory experience in a mouse model of fragile X syndrome. Proceedings of the National Academy of Sciences of the United States of America 107, 17768-17773.

Paradee, W., Melikian, H.E., Rasmussen, D.L., Kenneson, A., Conn, P.J., and Warren, S.T. (1999). Fragile X mouse: strain effects of knockout phenotype and evidence suggesting deficient amygdala function. Neuroscience 94, 185-192.

Pavlov, D., Muhlrad, A., Cooper, J., Wear, M., and Reisler, E. (2007). Actin filament severing by cofilin. Journal of molecular biology 365, 1350-1358.

Peters, A., and Kaiserman-Abramof, I.R. (1970). The small pyramidal neuron of the rat cerebral cortex. The perikaryon, dendrites and spines. The American journal of anatomy 127, 321-355.

Pilo Boyl, P., Di Nardo, A., Mulle, C., Sassoe-Pognetto, M., Panzanelli, P., Mele, A., Kneussel, M., Costantini, V., Perlas, E., Massimi, M.*, et al.* (2007). Profilin2 contributes to synaptic vesicle exocytosis, neuronal excitability, and novelty-seeking behavior. The EMBO journal 26, 2991-3002.

Plant, K., Pelkey, K.A., Bortolotto, Z.A., Morita, D., Terashima, A., McBain, C.J., Collingridge, G.L., and Isaac, J.T. (2006). Transient incorporation of native GluR2-lacking AMPA receptors during hippocampal long-term potentiation. Nature neuroscience 9, 602-604.

Polet, D., Lambrechts, A., Vandepoele, K., Vandekerckhove, J., and Ampe, C. (2007). On the origin and evolution of vertebrate and viral profilins. FEBS letters 581, 211-217.

Pyronneau, A., He, Q., Hwang, J.Y., Porch, M., Contractor, A., and Zukin, R.S. (2017). Aberrant Rac1-cofilin signaling mediates defects in dendritic spines, synaptic function, and sensory perception in fragile X syndrome. Science signaling 10.

Qin, M., Entezam, A., Usdin, K., Huang, T., Liu, Z.H., Hoffman, G.E., and Smith, C.B. (2011). A mouse model of the fragile X premutation: effects on behavior, dendrite morphology, and regional rates of cerebral protein synthesis. Neurobiology of disease 42, 85-98.

Racz, B., and Weinberg, R.J. (2006). Spatial organization of cofilin in dendritic spines. Neuroscience 138, 447-456.

Rathod, R., Havlicek, S., Frank, N., Blum, R., and Sendtner, M. (2012). Laminin induced local axonal translation of beta-actin mRNA is impaired in SMN-deficient motoneurons. Histochemistry and cell biology 138, 737-748.

Reeve, S.P., Bassetto, L., Genova, G.K., Kleyner, Y., Leyssen, M., Jackson, F.R., and Hassan, B.A. (2005). The Drosophila fragile X mental retardation protein controls actin dynamics by directly regulating profilin in the brain. Current biology : CB 15, 1156-1163.

Reinhard, M., Giehl, K., Abel, K., Haffner, C., Jarchau, T., Hoppe, V., Jockusch, B.M., and Walter, U. (1995). The proline-rich focal adhesion and microfilament protein VASP is a ligand for profilins. The EMBO journal 14, 1583-1589.

Rex, C.S., Chen, L.Y., Sharma, A., Liu, J., Babayan, A.H., Gall, C.M., and Lynch, G. (2009). Different Rho GTPase-dependent signaling pathways initiate sequential steps in the consolidation of long-term potentiation. The Journal of cell biology 186, 85-97.

Ronesi, J.A., Collins, K.A., Hays, S.A., Tsai, N.P., Guo, W., Birnbaum, S.G., Hu, J.H., Worley, P.F., Gibson, J.R., and Huber, K.M. (2012). Disrupted Homer scaffolds mediate abnormal mGluR5 function in a mouse model of fragile X syndrome. Nature neuroscience 15, 431-440, S431.

Ronesi, J.A., and Huber, K.M. (2008). Metabotropic glutamate receptors and fragile x mental retardation protein: partners in translational regulation at the synapse. Science signaling 1, pe6.

Rudelli, R.D., Brown, W.T., Wisniewski, K., Jenkins, E.C., Laure-Kamionowska, M., Connell, F., and Wisniewski, H.M. (1985). Adult fragile X syndrome. Clinico-neuropathologic findings. Acta neuropathologica 67, 289-295.

Rust, M.B., Gurniak, C.B., Renner, M., Vara, H., Morando, L., Gorlich, A., Sassoe-Pognetto, M., Banchaabouchi, M.A., Giustetto, M., Triller, A.*, et al.* (2010). Learning, AMPA receptor mobility and synaptic plasticity depend on n-cofilin-mediated actin dynamics. The EMBO journal 29, 1889-1902.

Sajikumar, S., and Frey, J.U. (2004). Late-associativity, synaptic tagging, and the role of dopamine during LTP and LTD. Neurobiology of learning and memory 82, 12-25.

Samuels, I. (1972). Hippocampal lesions in the rat: effects on spatial and visual habits. Physiology & behavior 8, 1093-1097.

Sathish, K., Padma, B., Munugalavadla, V., Bhargavi, V., Radhika, K.V., Wasia, R., Sairam, M., and Singh, S.S. (2004). Phosphorylation of profilin regulates its interaction with actin and poly (L-proline). Cellular signalling 16, 589-596.

Scheetz, A.J., Nairn, A.C., and Constantine-Paton, M. (2000). NMDA receptor-mediated control of protein synthesis at developing synapses. Nature neuroscience 3, 211-216.

Schenck, A., Bardoni, B., Moro, A., Bagni, C., and Mandel, J.L. (2001). A highly conserved protein family interacting with the fragile X mental retardation protein (FMRP) and displaying selective interactions with FMRP-related proteins FXR1P and FXR2P. Proceedings of the National Academy of Sciences of the United States of America 98, 8844-8849.

Schultz, S.R., and Rolls, E.T. (1999). Analysis of information transmission in the Schaffer collaterals. Hippocampus 9, 582-598.

Scoville, W.B., and Milner, B. (1957). Loss of recent memory after bilateral hippocampal lesions. Journal of neurology, neurosurgery, and psychiatry 20, 11-21.

Segal, M., Kreher, U., Greenberger, V., and Braun, K. (2003). Is fragile X mental retardation protein involved in activity-induced plasticity of dendritic spines? Brain research 972, 9-15.

Semon, R. (1904) Die Mneme als erhaltendes Prinzip im Wechsel des organischen Geschehens. Leipzig: Wilhelm Engelmann.

Serano, T.L., and Cohen, R.S. (1995). A small predicted stem-loop structure mediates oocyte localization of Drosophila K10 mRNA. Development 121, 3809-3818.

Shah, P., Ding, Y., Niemczyk, M., Kudla, G., and Plotkin, J.B. (2013). Rate-limiting steps in yeast protein translation. Cell 153, 1589-1601.

Shang, Y., Wang, H., Mercaldo, V., Li, X., Chen, T., and Zhuo, M. (2009). Fragile X mental retardation protein is required for chemically-induced long-term potentiation of the hippocampus in adult mice. Journal of neurochemistry 111, 635-646.

Shepherd, G.M. (1996). The dendritic spine: a multifunctional integrative unit. Journal of neurophysiology 75, 2197-2210.

Siegel, F., and Lohmann, C. (2013). Probing synaptic function in dendrites with calcium imaging. Experimental neurology 242, 27-32.

Siomi, H., Matunis, M.J., Michael, W.M., and Dreyfuss, G. (1993). The pre-mRNA binding K protein contains a novel evolutionarily conserved motif. Nucleic acids research 21, 1193-1198.

Siomi, M.C., Siomi, H., Sauer, W.H., Srinivasan, S., Nussbaum, R.L., and Dreyfuss, G. (1995). FXR1, an autosomal homolog of the fragile X mental retardation gene. The EMBO journal 14, 2401-2408.

Sit, S.T., and Manser, E. (2011). Rho GTPases and their role in organizing the actin cytoskeleton. Journal of cell science 124, 679-683.

Skinner, M., Hooper, S., Hatton, D.D., Roberts, J., Mirrett, P., Schaaf, J., Sullivan, K., Wheeler, A., and Bailey, D.B., Jr. (2005). Mapping nonverbal IQ in young boys with fragile X syndrome. American journal of medical genetics Part A 132A, 25-32.

Smith, W.B., Starck, S.R., Roberts, R.W., and Schuman, E.M. (2005). Dopaminergic stimulation of local protein synthesis enhances surface expression of GluR1 and synaptic transmission in hippocampal neurons. Neuron 45, 765-779.

Snyder, E.M., Philpot, B.D., Huber, K.M., Dong, X., Fallon, J.R., and Bear, M.F. (2001). Internalization of ionotropic glutamate receptors in response to mGluR activation. Nature neuroscience 4, 1079-1085.

Sonenberg, N., and Hinnebusch, A.G. (2009). Regulation of translation initiation in eukaryotes: mechanisms and biological targets. Cell 136, 731-745.

Stanton, P.K., and Sarvey, J.M. (1984). Blockade of long-term potentiation in rat hippocampal CA1 region by inhibitors of protein synthesis. The Journal of neuroscience : the official journal of the Society for Neuroscience 4, 3080-3088.

Star, E.N., Kwiatkowski, D.J., and Murthy, V.N. (2002). Rapid turnover of actin in dendritic spines and its regulation by activity. Nature neuroscience 5, 239-246.

Steward, O., Farris, S., Pirbhoy, P.S., Darnell, J., and Driesche, S.J. (2014). Localization and local translation of Arc/Arg3.1 mRNA at synapses: some observations and paradoxes. Frontiers in molecular neuroscience 7, 101.

Steward, O., and Levy, W.B. (1982). Preferential localization of polyribosomes under the base of dendritic spines in granule cells of the dentate gyrus. The Journal of neuroscience : the official journal of the Society for Neuroscience 2, 284-291.

Su, T., Fan, H.X., Jiang, T., Sun, W.W., Den, W.Y., Gao, M.M., Chen, S.Q., Zhao, Q.H., and Yi, Y.H. (2011). Early continuous inhibition of group 1 mGlu signaling partially rescues dendritic spine abnormalities in the Fmr1 knockout mouse model for fragile X syndrome. Psychopharmacology 215, 291-300.

Surrey, V., Zoller, C., Lork, A.A., Moradi, M., Balk, S., Dombert, B., Saal-Bauernschubert, L., Briese, M., Appenzeller, S., Fischer, U., and Jablonka, S. (2018). Impaired Local Translation of beta-actin mRNA in Ighmbp2-Deficient Motoneurons: Implications for Spinal Muscular Atrophy with respiratory Distress (SMARD1). Neuroscience 386, 24-40.

Sutton, M.A., and Schuman, E.M. (2006). Dendritic protein synthesis, synaptic plasticity, and memory. Cell 127, 49-58.

Szabo, E.C., Manguinhas, R., and Fonseca, R. (2016). The interplay between neuronal activity and actin dynamics mimic the setting of an LTD synaptic tag. Scientific reports 6, 33685.

Tanaka, J., Horiike, Y., Matsuzaki, M., Miyazaki, T., Ellis-Davies, G.C., and Kasai, H. (2008). Protein synthesis and neurotrophin-dependent structural plasticity of single dendritic spines. Science 319, 1683-1687.

Tassabehji, M., Metcalfe, K., Fergusson, W.D., Carette, M.J., Dore, J.K., Donnai, D., Read, A.P., Proschel, C., Gutowski, N.J., Mao, X., and Sheer, D. (1996). LIM-kinase deleted in Williams syndrome. Nature genetics 13, 272-273.

Teyler, T.J., and DiScenna, P. (1986). The hippocampal memory indexing theory. Behavioral neuroscience 100, 147-154.

Thomas, M.G., Loschi, M., Desbats, M.A., and Boccaccio, G.L. (2011). RNA granules: the good, the bad and the ugly. Cellular signalling 23, 324-334.

Tian, Y., Yang, C., Shang, S., Cai, Y., Deng, X., Zhang, J., Shao, F., Zhu, D., Liu, Y., Chen, G.*, et al.* (2017). Loss of FMRP Impaired Hippocampal Long-Term Plasticity and Spatial Learning in Rats. Frontiers in molecular neuroscience 10, 269.

Todd, P.K., Mack, K.J., and Malter, J.S. (2003). The fragile X mental retardation protein is required for type-I metabotropic glutamate receptor-dependent translation of PSD-95. Proceedings of the National Academy of Sciences of the United States of America 100, 14374-14378.

Tom Dieck, S., Hanus, C., and Schuman, E.M. (2014). SnapShot: local protein translation in dendrites. Neuron 81, 958-958 e951.

Toni, N., Buchs, P.A., Nikonenko, I., Bron, C.R., and Muller, D. (1999). LTP promotes formation of multiple spine synapses between a single axon terminal and a dendrite. Nature 402, 421-425.

Torre, E.R., and Steward, O. (1992). Demonstration of local protein synthesis within dendrites using a new cell culture system that permits the isolation of living axons and dendrites from their cell bodies. The Journal of neuroscience : the official journal of the Society for Neuroscience 12, 762-772.

Troca-Marin, J.A., Alves-Sampaio, A., Tejedor, F.J., and Montesinos, M.L. (2010). Local translation of dendritic RhoA revealed by an improved synaptoneurosome preparation. Molecular and cellular neurosciences 43, 308-314.

Turrigiano, G.G., and Nelson, S.B. (2004). Homeostatic plasticity in the developing nervous system. Nature reviews Neuroscience 5, 97-107.

Verkerk, A.J., Pieretti, M., Sutcliffe, J.S., Fu, Y.H., Kuhl, D.P., Pizzuti, A., Reiner, O., Richards, S., Victoria, M.F., Zhang, F.P., and et al. (1991). Identification of a gene (FMR-1) containing a CGG repeat coincident with a breakpoint cluster region exhibiting length variation in fragile X syndrome. Cell 65, 905-914.

von der Malsburg, C. (1987). Synaptic Plasticity as Basis of Brain Organization. The Neural and Molecular Bases of Learning, John Wiley & Sons Limited (eds. J.-P. Changeux and M. Konishi), 411-432. ©S. Bernhard, Dahlem Konferenzen, 1987

Wang, D.O., Martin, K.C., and Zukin, R.S. (2010). Spatially restricting gene expression by local translation at synapses. Trends in neurosciences 33, 173-182.

Wegner, A. (1976). Head to tail polymerization of actin. Journal of molecular biology 108, 139-150.

Weiler, I.J., Irwin, S.A., Klintsova, A.Y., Spencer, C.M., Brazelton, A.D., Miyashiro, K., Comery, T.A., Patel, B., Eberwine, J., and Greenough, W.T. (1997). Fragile X mental retardation protein is translated near synapses in response to neurotransmitter activation. Proceedings of the National Academy of Sciences of the United States of America 94, 5395-5400.

Weiler, I.J., Spangler, C.C., Klintsova, A.Y., Grossman, A.W., Kim, S.H., Bertaina-Anglade, V., Khaliq, H., de Vries, F.E., Lambers, F.A., Hatia, F.*, et al.* (2004). Fragile X mental retardation protein is necessary for neurotransmitter-activated protein translation at synapses. Proceedings of the National Academy of Sciences of the United States of America 101, 17504-17509.

Welshhans, K., and Bassell, G.J. (2011). Netrin-1-induced local beta-actin synthesis and growth cone guidance requires zipcode binding protein 1. The Journal of neuroscience : the official journal of the Society for Neuroscience 31, 9800-9813.

Westmark, C.J., and Malter, J.S. (2007). FMRP mediates mGluR5-dependent translation of amyloid precursor protein. PLoS biology 5, e52.

Wilson, B.M., and Cox, C.L. (2007). Absence of metabotropic glutamate receptor-mediated plasticity in the neocortex of fragile X mice. Proceedings of the National Academy of Sciences of the United States of America 104, 2454-2459.

Witke, W., Podtelejnikov, A.V., Di Nardo, A., Sutherland, J.D., Gurniak, C.B., Dotti, C., and Mann, M. (1998). In mouse brain profilin I and profilin II associate with regulators of the endocytic pathway and actin assembly. The EMBO journal 17, 967-976.

Witke, W., Sutherland, J.D., Sharpe, A., Arai, M., and Kwiatkowski, D.J. (2001). Profilin I is essential for cell survival and cell division in early mouse development. Proceedings of the National Academy of Sciences of the United States of America 98, 3832-3836.

Woolfrey, K.M., and Srivastava, D.P. (2016). Control of Dendritic Spine Morphological and Functional Plasticity by Small GTPases. Neural plasticity 2016, 3025948.

Wu, B., Eliscovich, C., Yoon, Y.J., and Singer, R.H. (2016). Translation dynamics of single mRNAs in live cells and neurons. Science 352, 1430-1435.

Xiao, M.Y., Zhou, Q., and Nicoll, R.A. (2001). Metabotropic glutamate receptor activation causes a rapid redistribution of AMPA receptors. Neuropharmacology 41, 664-671.

y Cajal, S.R. (1894). The Croonian lecture. La fine structure des centres nerveux. Proceedings of the Royal Society of London 55 (331-335), 444-468.

Yang, N., Higuchi, O., Ohashi, K., Nagata, K., Wada, A., Kangawa, K., Nishida, E., and Mizuno, K. (1998). Cofilin phosphorylation by LIM-kinase 1 and its role in Rac-mediated actin reorganization. Nature 393, 809-812.

Yasuda, K., Kosugi, A., Hayashi, F., Saitoh, S., Nagafuku, M., Mori, Y., Ogata, M., and Hamaoka, T. (2000). Serine 6 of Lck tyrosine kinase: a critical site for Lck myristoylation, membrane localization, and function in T lymphocytes. Journal of immunology 165, 3226-3231.

Zalfa, F., Eleuteri, B., Dickson, K.S., Mercaldo, V., De Rubeis, S., di Penta, A., Tabolacci, E., Chiurazzi, P., Neri, G., Grant, S.G., and Bagni, C. (2007). A new function for the fragile X mental retardation protein in regulation of PSD-95 mRNA stability. Nature neuroscience 10, 578-587.

Zhang, H.L., Eom, T., Oleynikov, Y., Shenoy, S.M., Liebelt, D.A., Dictenberg, J.B., Singer, R.H., and Bassell, G.J. (2001a). Neurotrophin-induced transport of a beta-actin mRNP complex increases beta-actin levels and stimulates growth cone motility. Neuron 31, 261-275.

Zhang, Y., O'Connor, J.P., Siomi, M.C., Srinivasan, S., Dutra, A., Nussbaum, R.L., and Dreyfuss, G. (1995). The fragile X mental retardation syndrome protein interacts with novel homologs FXR1 and FXR2. The EMBO journal 14, 5358-5366.

Zhang, Y.Q., Bailey, A.M., Matthies, H.J., Renden, R.B., Smith, M.A., Speese, S.D., Rubin, G.M., and Broadie, K. (2001b). Drosophila fragile X-related gene regulates the MAP1B homolog Futsch to control synaptic structure and function. Cell 107, 591-603.

Zhao, M.G., Toyoda, H., Ko, S.W., Ding, H.K., Wu, L.J., and Zhuo, M. (2005). Deficits in trace fear memory and long-term potentiation in a mouse model for fragile X syndrome. The Journal of neuroscience : the official journal of the Society for Neuroscience 25, 7385-7392.

Zhou, Q., Homma, K.J., and Poo, M.M. (2004). Shrinkage of dendritic spines associated with long-term depression of hippocampal synapses. Neuron 44, 749-757.

Zhou, Q., Xiao, M., and Nicoll, R.A. (2001). Contribution of cytoskeleton to the internalization of AMPA receptors. Proceedings of the National Academy of Sciences of the United States of America 98, 1261-1266.

Zola-Morgan, S.M., and Squire, L.R. (1990). The primate hippocampal formation: evidence for a time-limited role in memory storage. Science 250, 288-290.

Zorio, D.A., Jackson, C.M., Liu, Y., Rubel, E.W., and Wang, Y. (2017). Cellular distribution of the fragile X mental retardation protein in the mouse brain. The Journal of comparative neurology 525, 818-849.

9 Supplement

9.1 List of all means, SEMs, statistic values and statistic tests used

Figure 9

9A	**Legend**		**Rel. expression**	**n**	**Significance**	**Statistic test used**
	Profilin 1	*fmr1* WT	1,000 ± 0,210	n = 3		
		fmr1 KO	0,378 ± 0,060	n = 3	*fmr1* WT p = 0,046	Student's t-test
	Profilin 2a	*fmr1* WT	1,000 ± 0,151	n = 3		
		fmr1 KO	1,232 ± 0,121	n = 3		
9B	**Legend**		**Rel. expression**	**n**	**Significance**	**Statistic test used**
	Profilin 1	*fmr1* WT	1,000 ± 0,047	n = 3		
		fmr1 KO	1,044 ± 0,116	n = 3		
	Profilin 2a	*fmr1* WT	1,000 ± 0,015	n = 3		
		fmr1 KO	1,071 ± 0,062	n = 3		
9C	**Legend**		**Rel. expression**	**n**	**Significance**	**Statistic test used**
	Profilin 1	*fmr1* WT	1,000 ± 0,132	n = 3		
		fmr1 KO	1,079 ± 0,185	n = 3		
	Profilin 2a	*fmr1* WT	1,000 ± 0,015	n = 3		
		fmr1 KO	1,071 ± 0,062	n = 3		
	Cofilin 1	*fmr1* WT	1,000 ± 0,110	n = 3		
		fmr1 KO	0,556 ± 0,091	n = 3	*fmr1* WT p = 0,036	Student's t-test

Figure 11

11E	**Repeated Measures ANOVA:**		MYR-eGFP 3'UTR ß-actin VS Anisomycin			
	Mauchly-Test		non-significant			
	Significant over time?		p < 0,001		F = 15,623	df = 7,21
	Significance time*treatment?		p = 0,002		F = 4,826	df = 7,21
	Legend		**Fluo.-Intens.**	**n**	**Significance**	**Statistic test used**
	3'UTR ß-actin	Pre-bleach	100,0 ± 0,00	n = 3		
		0 min	12,67 ± 0,22	n = 3		
		5 min	23,77 ± 1,42	n = 3		
		10 min	27,20 ± 0,94	n = 3		
		20 min	36,63 ± 2,91	n = 3		
		30 min	44,16 ± 1,41	n = 3		
		40 min	43,11 ± 4,21	n = 3		
		50 min	43,40 ± 3,39	n = 3		
		60 min	44,77 ± 3,74	n = 3		
	Anisomycin	Pre-bleach	100,0 ± 0,00	n = 3		
		0 min	9,79 ± 1,73	n = 3		
		5 min	13,13 ± 0,94	n = 3	CTRL 5' p = 0,005	Student's t-test
		10 min	13,91 ± 0,37	n = 3	CTRL 10' p = 0,003	Student's t-test
		20 min	15,87 ± 2,27	n = 3	CTRL 20' p = 0,028	Student's t-test
		30 min	18,37 ± 2,05	n = 3	CTRL 30' p = 0,001	Student's t-test

		40 min	19,46 ± 2,49	n = 3	CTRL 40‘ p = 0,011	Student’s t-test
		50 min	18,66 ± 3,58	n = 3	CTRL 50‘ p = 0,041	Student’s t-test
		60 min	18,80 ± 2,74	n = 3	CTRL 60‘ p = 0,029	Student’s t-test
11F	**Repeated Measures ANOVA**:		MYR-eGFP 3’UTR Cof1 VS MYR-eGFP Anisomycin			
	Mauchly-Test		non-significant			
	Significant over time?		p ≤ 0,001		F = 69,285	df = 7,42
	Significance time*treatment?		p ≤ 0,001		F = 11,981	df = 7,42
	Legend		**Fluo.-Intens.**	**n**	**Significance**	**Statistic test used**
	3’UTR Cof1	Pre-bleach	100,0 ± 0,00	n = 5		
		0 min	13,55 ± 2,09	n = 5		
		5 min	33,06 ± 3,18	n = 5		
		10 min	40,35 ± 2,54	n = 5		
		20 min	49,33 ± 2,53	n = 5		
		30 min	53,97 ± 1,74	n = 5		
		40 min	56,00 ± 1,34	n = 5		
		50 min	55,80 ± 1,11	n = 5		
		60 min	55,16 ± 1,20	n = 5		
	Anisomycin	Pre-bleach	100,0 ± 0,00	n = 3		
		0 min	9,36 ± 3,40	n = 3		
		5 min	16,27 ± 2,38	n = 3	3’UTR Cof p = 0,024	Student’s t-test
		10 min	21,33 ± 1,93	n = 3	3’UTR Cof p = 0,004	Student’s t-test
		20 min	27,43 ± 3,02	n = 3	3’UTR Cof p = 0,002	Student’s t-test
		30 min	30,49 ± 3,77	n = 3	3’UTR Cof p < 0,001	Student’s t-test
		40 min	31,44 ± 3,97	n = 3	3’UTR Cof p < 0,001	Student’s t-test
		50 min	32,22 ± 3,29	n = 3	3’UTR Cof p < 0,001	Student’s t-test
		60 min	32,44 ± 3,66	n = 3	3’UTR Cof p < 0,001	Student’s t-test

Figure 12

12A	**Legend**		**mRNAs per µm²**	**n**	**Significance**	**Statistic test used**
	cell body	Profilin 1	0,139 ± 0,015	n = 25	Cofilin p < 0,001	One-Way ANOVA
		Profilin 2a	0,121 ± 0,009	n = 25	Cofilin p < 0,001	Post-hoc Tuckey
		Cofilin 1	0,272 ± 0,019	n = 25		
	nucleus	Profilin 1	0,181 ± 0,018	n = 25	Cofilin p < 0,001	One-Way ANOVA
		Profilin 2a	0,151 ± 0,013	n = 25	Cofilin p < 0,001	Post-hoc Tuckey
		Cofilin 1	0,275 ± 0,019	n = 25		
	prox. dendrites	Profilin 1	0,014 ± 0,002	n = 25		
		Profilin 2a	0,010 ± 0,001	n = 25	Cofilin p = 0,042	One-Way ANOVA
		Cofilin 1	0,016 ± 0,002	n = 25		Post-hoc Tuckey
12B	**Legend**		**mRNAs per µm²**	**n**	**Significance**	**Statistic test used**
	cell body	Profilin 1	0,125 ± 0,012	n = 15	Cofilin p < 0,001	One-Way ANOVA
		Profilin 2a	0,109 ± 0,006	n = 15	Cofilin p < 0,001	Post-hoc Tuckey
		Cofilin 1	0,303 ± 0,038	n = 15		
	nucleus	Profilin 1	0,104 ± 0,010	n = 15	Cofilin p = 0,004	One-Way ANOVA
		Profilin 2a	0,090 ± 0,008	n = 15	Cofilin p = 0,001	Post-hoc Tuckey
		Cofilin 1	0,217 ± 0,038	n = 15		

	prox. dendrites	Profilin 1		0,007 ± 0,002	n = 15	Cofilin p = 0,041	One-Way ANOVA
		Profilin 2a		0,004 ± 0,001	n = 15	Cofilin p = 0,001	Post-hoc Tuckey
		Cofilin 1		0,012 ± 0,002	n = 15		
12C	**Legend**			**mRNAs per µm²**	**n**	**Significance**	**Statistic test used**
	Profilin 1	cell body	WT	1,000 ± 0,107	n = 25		
			KO	0,898 ± 0,086	n = 15		
		nucleus	WT	1,000 ± 0,010	n = 25		
			KO	0,572 ± 0,053	n = 15	WT p = 0,003	Student's t-test
		prox.dend.	WT	1,000 ± 0,123	n = 25		
			KO	0,487 ± 0,068	n = 15	WT p = 0,004	Student's t-test
	Profilin2a	cell body	WT	1,000 ± 0,075	n = 25		
			KO	0,902 ± 0,052	n = 15		
		nucleus	WT	1,000 ± 0,084	n = 25		
			KO	0,592 ± 0,052	n = 15	WT p = 0,001	Student's t-test
		prox.dend.	WT	1,000 ± 0,127	n = 25		
			KO	0,365 ± 0,052	n = 15	WT p < 0,001	Student's t-test
	Cofilin 1	cell body	WT	1,000 ± 0,052	n = 25		
			KO	1,112 ± 0,139	n = 15		
		nucleus	WT	1,000 ± 0,068	n = 25		
			KO	0,787 ± 0,140	n = 15		
		prox.dend.	WT	1,000 ± 0,115	n = 25		
			KO	0,737 ± 0,135	n = 15		

Figure 13

13A	**Legend**			**mRNAs per µm²**	**n**	**Significance**	**Statistic test used**
	Profilin 1	cell body	0'	1,000 ± 0,107	n = 25		
			20'	1,218 ± 0,134	n = 16		
			40'	0,938 ± 0,065	n = 15		
			60'	0,779 ± 0,051	n = 17	20' p = 0.023	One-Way ANOVA Post-hoc Tuckey
		nucleus	0'	1,000 ± 0,010	n = 25		
			20'	1,172 ± 0,107	n = 16		
			40'	0,901 ± 0,093	n = 15		
			60'	0,773 ± 0,080	n = 17	20' p = 0.042	One-Way ANOVA Post-hoc Tuckey
		prox.dend.	0'	1,000 ± 0,124	n = 25		
			20'	0,998 ± 0,162	n = 16		
			40'	0,842 ± 0,183	n = 15		
			60'	0,579 ± 0,115	n = 17		
13B	Profilin2a	cell body	0'	1,000 ± 0,075	n = 25	40' p < 0,001	
			20'	1,169 ± 0,071	n = 15	40' p < 0,001	One-Way ANOVA Post-hoc Tuckey
			40'	1,823 ± 0,146	n = 15		
			60'	0,870 ± 0,061	n = 15	40' p < 0,001	
		nucleus	0'	1,000 ± 0,084	n = 25		
			20'	1,075 ± 0,155	n = 15		
			40'	1,005 ± 0,131	n = 15		
			60'	0,794 ± 0,103	n = 15		

		prox.dend.	0’	1,000 ± 0,128	n = 25	40’ p < 0,001	
			20’	0,681 ± 0,137	n = 15	40’ p < 0,001	One-Way ANOVA
			40’	2,371 ± 0,520	n = 15		Post-hoc Tuckey
			60’	0,587 ± 0,093	n = 15	40’ p < 0,001	
13C	Cofilin 1	cell body	0’	1,000 ± 0,052	n = 25		
			20’	0,840 ± 0,062	n = 18		
			40’	0,906 ± 0,064	n = 15	60’ p = 0,037	One-Way ANOVA
			60’	0,658 ± 0,052	n = 15	0’ p < 0,001	Post-hoc Tuckey
		nucleus	0’	1,000 ± 0,068	n = 25		
			20’	0,958 ± 0,072	n = 18	60’ p = 0,029	One-Way ANOVA
			40’	0,669 ± 0,085	n = 15	0’ p = 0,014	Post-hoc Tuckey
			60’	0,634 ± 0,080	n = 15	0’ p = 0,005	
		prox.dend.	0’	1,000 ± 0,116	n = 25		
			20’	1,019 ± 0,111	n = 18		
			40’	1,219 ± 0,217	n = 15		One-Way ANOVA
			60’	0,600 ± 0,100	n = 15	40’ p = 0,026	Post-hoc Tuckey
	Legend			**mRNAs per µm²**	**n**	**Significance**	**Statistic test used**
13E	Profilin 1	cell body	0’	1,000 ± 0,096	n = 15		
			20’	1,063 ± 0,067	n = 15		One-Way ANOVA
			40’	1,324 ± 0,104	n = 15	0’ p = 0,05	Post-hoc Tuckey
			60’	1,104 ± 0,074	n = 15		
		nucleus	0’	1,000 ± 0,092	n = 15		
			20’	0,985 ± 0,129	n = 15		
			40’	1,361 ± 0,220	n = 15		
			60’	1,016 ± 0,091	n = 15		
		prox.dend.	0’	1,000 ± 0,138	n = 15		
			20’	0,997 ± 0,230	n = 15		
			40’	0,942 ± 0,167	n = 15		
			60’	0,650 ± 0,064	n = 15		
13F	Profilin2a	cell body	0’	1,000 ± 0,058	n = 15		
			20’	0,980 ± 0,057	n = 15		
			40’	1,086 ± 0,079	n = 15		
			60’	0,973 ± 0,067	n = 15		
		nucleus	0’	1,000 ± 0,088	n = 15		
			20’	0,996 ± 0,131	n = 15		
			40’	1,024 ± 0,096	n = 15		
			60’	1,205 ± 0,093	n = 15		
		prox.dend.	0’	1,000 ± 0,146	n = 15		
			20’	1,088 ± 0,131	n = 15		
			40’	1,822 ± 0,340	n = 15		
			60’	1,667 ± 0,223	n = 15		
13G	Cofilin 1	cell body	0’	1,000 ± 0,125	n = 15		
			20’	0,887 ± 0,091	n = 15		
			40’	0,804 ± 0,037	n = 15		
			60’	0,998 ± 0,163	n = 15		

		nucleus	0’	1,000 ± 0,177	n = 15		
			20’	1,172 ± 0,161	n = 15		
			40’	0,720 ± 0,076	n = 15		
			60’	1,160 ± 0,211	n = 15		
		prox.dend.	0’	1,000 ± 0,183	n = 15		
			20’	0,831 ± 0,128	n = 15		
			40’	0,675 ± 0,113	n = 15		
			60’	0,828 ± 0,139	n = 15		
13H	**Two-Way ANOVA genotype*stimulation**			F = 13,731		p < 0,001	df = 3,168
	Legend			**Spine head dia.**	**n**	**Significance**	**Statistic test used**
	fmr1 WT	0’		0,472 ± 0,006	n = 50		
		20’		0,476 ± 0,007	n = 21		
		40’		0,571 ± 0,007	n = 30	0’,20’,60’ p < 0,001	One-Way ANOVA
		60’		0,672 ± 0,011	n = 15	0’,20’ p < 0,001	Post-hoc Tuckey
	fmr1 KO	0’		0,503 ± 0,025	n = 15		
		20’		0,512 ± 0,013	n = 15		
		40’		0,526 ± 0,020	n = 15		
		60’		0,560 ± 0,021	n = 15		
13I	**Two-Way ANOVA genotype*stimulation**						
	Profilin 1			F = 0,788		p = 0,401	df = 1,8
	Profilin 2a			F = 4,595		p = 0,064	df = 1,8
	Cofilin 1			F = 12,286		p = 0,008	df = 1,8
	Legend			**Rel. expression**	**n**	**Significance**	**Statistic test used**
	Profilin 1	*fmr1* WT	CTRL	1,000 ± 0,132	n = 3		
		fmr1 WT	cLTP	1,107 ± 0,096	n = 3		
		fmr1 KO	CTRL	1,079 ± 0,185	n = 3		
		fmr1 KO	cLTP	0,956 ± 0,076	n = 3		
	Profilin 2	*fmr1* WT	CTRL	1,000 ± 0,015	n = 3		
		fmr1 WT	cLTP	1,240 ± 0,082	n = 3	WT CTRL p = 0,045	Student’s t-test
		fmr1 KO	CTRL	1,071 ± 0,062	n = 3		
		fmr1 KO	cLTP	0,890 ± 0,167	n = 3		
	Cofilin 1	*fmr1* WT	CTRL	1,000 ± 0,110	n = 3		
		fmr1 WT	cLTP	0,614 ± 0,034	n = 3	WT CTRL p = 0,028	Student’s t-test
		fmr1 KO	CTRL	0,556 ± 0,091	n = 3	WT CTRL p = 0,036	Student’s t-test
		fmr1 KO	cLTP	0,824 ± 0,116	n = 3		

Figure 14

14A	**Repeated Measures ANOVA:**		*fmr1* WT MYR-eGFP 3’UTR Cof1 CTRL VS cLTP			
	Mauchly-Test		non-significant			
	Significant over time?		p ≤ 0,001	F = 157,680		df = 7,42
	Significance time*treatment?		p ≤ 0,001	F = 5,716		df = 7,42
	Legend		**Fluo.-Intens.**	**n**	**Significance**	**Statistic test used**
	3’UTR Cof1	Pre-bleach	100,0 ± 0,00	n = 5		

		0 min	13,55 ± 2,09	n = 5		
		5 min	33,06 ± 3,18	n = 5		
		10 min	40,35 ± 2,54	n = 5		
		20 min	49,33 ± 2,53	n = 5		
		30 min	53,97 ± 1,74	n = 5		
		40 min	56,00 ± 1,34	n = 5		
		50 min	55,80 ± 1,11	n = 5		
		60 min	55,16 ± 1,20	n = 5		
	3'UTRCof1 cLTP	Pre-bleach	100,0 ± 0,00	n = 3		
		0 min	15,49 ± 0,64	n = 3		
		5 min	22,57 ± 0,76	n = 3		
		10 min	27,56 ± 0,13	n = 3	CTRL p = 0,017	Student's t-test
		20 min	37,12 ± 1,59	n = 3	CTRL p = 0,028	Student's t-test
		30 min	43,04 ± 3,16	n = 3	CTRL p = 0,035	Student's t-test
		40 min	47,96 ± 1,83	n = 3	CTRL p = 0,049	Student's t-test
		50 min	52,29 ± 2,30	n = 3		
		60 min	53,63 ± 1,88	n = 3		
14B	**Repeated Measures ANOVA:**		MYR-eGFP 3'UTR Cof1	*fmr1* WT VS *fmr1* KO		
	Mauchly-Test		non-significant			
	Significant over time?		p < 0,001	F = 108,443	df = 7,42	
	Significance time*treatment?		p < 0,001	F = 9,587	df = 7,42	
	Repeated Measures ANOVA:		*fmr1* KO MYR-eGFP 3'UTR Cof1	CTRL VS cLTP		
	Mauchly-Test		non-significant			
	Significant over time?		p < 0,001	F = 96,267	df = 7,28	
	Significance time*treatment?		p < 0,001	F = 7,448	df = 7,28	
	Legend		**Fluo.-Intens.**	**n**	**Significance**	**Statistic test used**
	3'UTR Cof1	Pre-bleach	100,0 ± 0,00	n = 3		
		0 min	19,46 ± 0,92	n = 3		
		5 min	32,57 ± 3,25	n = 3		
		10 min	35,90 ± 3,50	n = 3		
		20 min	40,39 ± 4,32	n = 3		
		30 min	42,13 ± 4,32	n = 3	WT CTRL p = 0,028	Student's t-test
		40 min	43,25 ± 4,91	n = 3	WT CTRL p = 0,021	Student's t-test
		50 min	43,18 ± 5,16	n = 3	WT CTRL p = 0,023	Student's t-test
		60 min	42,77 ± 5,66	n = 3	WT CTRL p = 0,036	Student's t-test
	3'UTRCof1 cLTP	Pre-bleach	100,0 ± 0,00	n = 3		
		0 min	17,41 ± 0,01	n = 3		
		5 min	30,43 ± 1,39	n = 3		
		10 min	38,59 ± 3,12	n = 3		
		20 min	48,01 ± 3,51	n = 3		
		30 min	53,95 ± 1,32	n = 3		
		40 min	54,02 ± 0,81	n = 3		
		50 min	54,34 ± 1,06	n = 3		
		60 min	54,96 ± 0,83	n = 3		

Figure 15

15A	**Repeated Measures ANOVA:**	Pretraining latency *fmr1* WT VS *fmr1* KO		
	Mauchly-Test	non-significant		
	Significant over time?	p ≤ 0,001	F = 24,989	df = 2,36
	Significance time*treatment?	p = 0,362	F = 1,044	df = 2,36

	Legend		**Escape latency**	**n**	**Significance**	**Statistic test used**
	fmr1 WT	Day 1	46,60 ± 6,59 s	n = 3		
		Day 2	20,27 ± 6,07 s	n = 3		
		Day 3	12,09 ± 3,22 s	n = 3		
	fmr1 KO	Day 1	44,66 ± 6,01 s	n = 4		
		Day 2	30,50 ± 8,23 s	n = 4		
		Day 3	9,83 ± 5,57	n = 4		

15B	**Repeated Measures ANOVA:**	Escape latency *fmr1* WT VS *fmr1* KO		
	Mauchly-Test	Significant p = 0,021		
	Significant over time?	p ≤ 0,001	F = 6,687	df = 7,182
	Significance time*treatment?	p = 0,106	F = 1,721	df = 7,182

	Legend		**Escape latency**	**n**	**Significance**	**Statistic test used**
	fmr1 WT	Day 1	26,10 ± 5,23 s	n = 3		
		Day 2	25,63 ± 6,07 s	n = 3		
		Day 3	16,77 ± 3,48 s	n = 3		
		Day 4	12,64 ± 4,86 s	n = 3		
		Day 5	15,42 ± 3,17 s	n = 3		
		Day 6	11,59 ± 3,38 s	n = 3		
		Day 7	8,89 ± 2,91 s	n = 3		
		Day 8	11,59 ± 4,23 s	n = 3		
	fmr1 KO	Day 1	44,26 ± 4,57 s	n = 4	WT CTRL p = 0,015	Student's t-test
		Day 2	22,31 ± 4,48 s	n = 4		
		Day 3	18,14 ± 3,55 s	n = 4		
		Day 4	23,29 ± 4,77 s	n = 4		
		Day 5	11,14 ± 2,97 s	n = 4		
		Day 6	20,43 ± 4,85 s	n = 4		
		Day 7	9,71 ± 2,11 s	n = 4		
		Day 8	22,70 ± 5,67 s	n = 4		

15C	**Legend**		**Escape latency**	**n**	**Significance**	**Statistic test used**
	fmr1 WT	Day 1	26,10 ± 5,23 s	n = 3		
	fmr1 KO	Day 1	44,26 ± 4,57 s	n = 4	WT CTRL p = 0,015	Student's t-test

15D	**Legend**		**Day 1**	**Day 2**	**Day 3**	**Day 4**	**Day 5**	**Day 6**	**Day 7**	**Day 8**
	fmr1 WT	Thigmotaxis	0%	0%	0%	0%	0%	0%	0%	0%
		Random	50%	25%	25%	25%	41,7%	8,3%	8,3%	25%
		Scanning	33,4%	66,7%	58,4%	33,3%	41,7%	58,4%	50%	41,7%
		Chaining	8,3%	8,3%	8,3%	8,4%	16,6%	0%	0%	0%
		Direct	8,3%	0%	8,3%	33,3%	0%	33,3%	41,7%	33,3%
		Total	100%	100%	100%	100%	100%	100%	100%	100%
	fmr1 KO	Thigmotaxis	0%	0%	0%	0%	0%	0%	0%	0%
		Random	87,5%	25%	31,2%	37,5%	25%	31,2%	37,5%	43,8%
		Scanning	12,5%	56,2%	43,8%	50%	37,5%	43,8%	31,2%	18,8%
		Chaining	0%	12,5%	12,5%	0%	12,5%	6,2%	12,5%	0%
		Direct	0%	6,3%	12,5%	12,5%	25%	18,8%	18,8%	37,4%
		Total	100%	100%	100%	100%	100%	100%	100%	100%

	***fmr1* WT**	**Repeated Measures ANOVA Direct Search**				
		Mauchly-Test		non-significant		
		Significant over time?		F = 6,829	df = 7,14	P = 0,001
	***fmr1* KO**	**Repeated Measures ANOVA Direct Search**				
		Mauchly-Test		non-significant		
		Significant over time?		F = 1,265	df = 7,21	p = 0,314
15E	**Two-Way ANOVA genotype*localization**		F = 0,522		p = 0,672	df = 3,20
	Legend		**Time in %**	**n**	**Significance**	**Statistic test used**
	fmr1 WT	Q1	21,04 ± 2,63	n = 3		
		Q2	17,18 ± 5,46	n = 3	TQ p = 0,029	One-Way ANOVA
		Q3	18,30 ± 3,74	n = 3	TQ p = 0,035	Post-hoc Tuckey
		TQ	43,48 ± 7,47	n = 3		
	fmr1 KO	Q1	17,22 ± 7,01	n = 4	TQ p = 0,006	One-Way ANOVA
		Q2	23,17 ± 3,63	n = 4	TQ p = 0,025	Post-hoc Tuckey
		Q3	13,50 ± 1,26	n = 4	TQ p = 0,002	
		TQ	46,11 ± 5,42	n = 4		
15F	**Two-Way ANOVA genotype*localization**		F = 0,207		p = 0,890	df = 3,20
	Legend		**Time in %**	**n**	**Significance**	**Statistic test used**
	fmr1 WT	Q1	6,37 ± 3,08	n = 3	TQ p = 0,014	One-Way ANOVA
		Q2	17,18 ± 5,46	n = 3	TQ p = 0,045	Post-hoc Tuckey
		Q3	15,48 ± 7,71	n = 3	TQ p = 0,037	
		TQ	57,55 ± 14,34	n = 3		
	fmr1 KO	Q1	13,72 ± 6,32	n = 4	TQ p = 0,039	One-Way ANOVA
		Q2	20,45 ± 7,52	n = 4		Post-hoc Tuckey
		Q3	14,11 ± 10,86	n = 4	TQ p = 0,041	
		TQ	51,72 ± 9,11	n = 4		
15H	**Legend**		**Platf. crossings**	**n**	**Significance**	**Statistic test used**
	fmr1 WT		4,67 ± 1,33	n = 3		
	fmr1 KO		1,75 ± 0,25	n = 4	WT p = 0,0527	Student's t-test
15I	**Two-Way ANOVA genotype*training**					
	Profilin 1		F = 1,565		p = 0,246	df = 1,8
	Profilin 2a		F = 2,687		p = 0,140	df = 1,8
	Cofilin 1		F = 13,047		p = 0,007	df = 1,8
	Legend		**Rel. expression**	**n**	**Significance**	**Statistic test used**
	Profilin 1	*fmr1* WT CTRL	1,000 ± 0,086	n = 3		
		fmr1 WT train	0,846 ± 0,065	n = 3		
		fmr1 KO CTRL	0,699 ± 0,133	n = 3		
		fmr1 KO train	0,765 ± 0,039	n = 3		
	Profilin 2	*fmr1* WT CTRL	1,000 ± 0,107	n = 3		
		fmr1 WT train	1,171 ± 0,152	n = 3		
		fmr1 KO CTRL	1,044 ± 0,102	n = 3		

		fmr1 KO	train	0,862 ± 0,041	n = 3		
	Cofilin 1	*fmr1* WT	CTRL	1,000 ± 0,091	n = 3		
		fmr1 WT	train	0,506 ± 0,057	n = 3	WT CTRL p = 0,011	One-Way ANOVA
		fmr1 KO	CTRL	0,554 ± 0,096	n = 3	WT CTRL p = 0,017	Post-hoc Tuckey
		fmr1 KO	train	0,637 ± 0,068	n = 3		

Figure 16

16A	**Two-Way ANOVA**	**genotype*stimulation**					
	Jasplakinolide			F = 6,688		p < 0,001	df = 3,112
	CytochalasinD			F = 7,941		p < 0,001	df = 3,112
	HIV TAT pCof1			F = 20,035		p < 0,001	df = 3,112
	Legend			**Spine head dia.**	**n**	**Significance**	**Statistic test used**
	fmr1 WT	CTRL		0,50 ± 0,01	n = 15		
		stimu		0,59 ± 0,01	n = 15	WT CTRL p < 0,001	One-Way ANOVA Post-hoc Tuckey
		JPK during/after		0,63 ± 0,01	n = 15	WT CTRL p < 0,001	
		JPK after		0,61 ± 0,01	n = 15	WT CTRL p < 0,001	
		CyD during/after		0,48 ± 0,01	n = 15		
		CyD after		0,50 ± 0,01	n = 15		
		Cof1during/after		0,51 ± 0,01	n = 15		
		Cof1 after		0,50 ± 0,01	n = 15		
	fmr1 KO	CTRL		0,49 ± 0,01	n = 15		
		stimu		0,50 ± 0,02	n = 15	Cof1after p < 0,001	One-Way ANOVA Post-hoc Tuckey
		JPK during/after		0,52 ± 0,01	n = 15		
		JPK after		0,51 ± 0,01	n = 15		
		CyD during/after		0,50 ± 0,01	n = 15		
		CyD after		0,49 ± 0,01	n = 15		
		Cof1during/after		0,51 ± 0,01	n = 15	Cof1after p < 0,001	One-Way ANOVA
		Cof1 after		0,60 ± 0,02	n = 15	KOCTRL p < 0,001	Post-hoc Tuckey

Figure 17

17A	**Legend**			**mRNAs per µm²**	**n**	**Significance**	**Statistic test used**
	Profilin 1	cell body	0’	1,000 ± 0,098	n = 10		
			20’	0,781 ± 0,095	n = 10		
			40’	0,883 ± 0,076	n = 10		
			60’	0,747 ± 0,050	n = 10		
		nucleus	0’	1,000 ± 0,063	n = 10		
			20’	0,772 ± 0,116	n = 10		
			40’	1,052 ± 0,137	n = 10		
			60’	0,701 ± 0,082	n = 10		
		prox.dend.	0’	1,000 ± 0,211	n = 10		
			20’	0,584 ± 0,190	n = 10		
			40’	0,882 ± 0,175	n = 10		
			60’	0,873 ± 0,211	n = 10		
17B	Profilin 2	cell body	0’	1,000 ± 0,171	n = 10		
			20’	0,947 ± 0,105	n = 10		
			40’	0,970 ± 0,112	n = 10		
			60’	1,286 ± 0,146	n = 10		
		nucleus	0’	1,000 ± 0,162	n = 10		

			20’	1,072 ± 0,200	n = 10		
			40’	0,838 ± 0,172	n = 10		
			60’	0,808 ± 0,103	n = 10		
		prox.dend.	0’	1,000 ± 0,419	n = 10		
			20’	0,675 ± 0,165	n = 10		
			40’	1,074 ± 0,408	n = 10		
			60’	1,297 ± 0,295	n = 10		
17C	Cofilin 1	cell body	0’	1,000 ± 0,180	n = 10		
			20’	1,292 ± 0,225	n = 10		
			40’	0,958 ± 0,066	n = 10		
			60’	1,207 ± 0,225	n = 10		
		nucleus	0’	1,000 ± 0,134	n = 10		
			20’	1,833 ± 0,309	n = 10	0’ p = 0,016	One-Way ANOVA Post-hoc Tuckey
			40’	0,814 ± 0,130	n = 10	0’ p = 0,002	
			60’	0,890 ± 0,090	n = 10	20’ p = 0,005	
		prox.dend.	0’	1,000 ± 0,538	n = 10		
			20’	3,071 ± 0,750	n = 10		
			40’	2,594 ± 0,812	n = 10		
			60’	2,358 ± 0,540	n = 10		
17E	**Two-Way ANOVA**						
	genotype*stimulation			F = 1,106		p = 0,352	df = 3,72
	Legend			**Spine head dia.**	**n**	**Significance**	**Statistic test used**
	fmr1 WT	CTRL		0,600 ± 0,024	n = 10		
		20’		0,580 ± 0,009	n = 10	40’ p = 0,005	One-Way
		40’		0,510 ± 0,009	n = 10	CTRL p < 0,001	ANOVA Post-
		60’		0,491 ± 0,007	n = 10	CTRL, 20’ p < 0,001	hoc Tuckey
	fmr1 KO	CTRL		0,583 ± 0,015	n = 10		
		20’		0,558 ± 0,013	n = 10	60’ p = 0,033	One-Way
		40’		0,526 ± 0,016	n = 10	CTRL p = 0,019	ANOVA Post-
		60’		0,505 ± 0,007	n = 10	CTRL p = 0,001	hoc Tuckey
	Legend			**mRNAs per µm²**	**n**	**Significance**	**Statistic test used**
17F	Profilin 1	cell body	0’	1,000 ± 0,136	n = 15		
			20’	0,832 ± 0,081	n = 15		
			40’	0,855 ± 0,074	n = 15		
			60’	1,092 ± 0,093	n = 15		
		nucleus	0’	1,000 ± 0,162	n = 15		
			20’	0,807 ± 0,105	n = 15		
			40’	0,662 ± 0,053	n = 15		
			60’	1,071 ± 0,178	n = 15		
		prox.dend.	0’	1,000 ± 0,124	n = 15		
			20’	0,919 ± 0,150	n = 15		
			40’	0,820 ± 0,110	n = 15		
			60’	1,341 ± 0,184	n = 15		
17G	Profilin 2	cell body	0’	1,000 ± 0,086	n = 15		
			20’	1,419 ± 0,259	n = 10		
			40’	1,045 ± 0,100	n = 15		
			60’	1,048 ± 0,166	n = 10		
		nucleus	0’	1,000 ± 0,138	n = 15		
			20’	1,601 ± 0,325	n = 10		
			40’	1,135 ± 0,197	n = 15		

			60’	0,843 ± 0,085	n = 10
		prox.dend.	0’	1,000 ± 0,147	n = 15
			20’	1,090 ± 0,212	n = 10
			40’	1,013 ± 0,159	n = 15
			60’	0,918 ± 0,211	n = 10
17H	Cofilin 1	cell body	0’	1,000 ± 0,083	n = 15
			20’	1,331 ± 0,163	n = 15
			40’	1,535 ± 0,195	n = 15
			60’	1,136 ± 0,116	n = 15
		nucleus	0’	1,000 ± 0,102	n = 15
			20’	1,397 ± 0,165	n = 15
			40’	1,450 ± 0,143	n = 15
			60’	1,216 ± 0,140	n = 15
		prox.dend.	0’	1,000 ± 0,205	n = 15
			20’	0,973 ± 0,170	n = 15
			40’	0,743 ± 0,132	n = 15
			60’	0,517 ± 0,064	n = 15

9.2 List of abbreviations

ABP	Actin-binding protein
aCSF	Artificial cerebrospinal fluid
ADF	Actin destabilizing factor
ADP	Adenosine di-phosphate
AMPAR	Alpha-amino-3-hydroxy-5-methyl-4-isoxazolepropionic acid receptor
ANOVA	Analysis of variance
Arp2/3	Actin related protein 2/3
ATP	Adenosine tri-phosphate
CA	*cornu ammonis*
CamKIIß	Calcium/calmodulin-dependent protein kinase II beta
Cof1	Cofilin 1
cLTD	Chemically-induced long-term depression
cLTP	Chemically-induced long-term potentiation
CNS	Central nervous system
CPEB	Cytoplasmic polyadenylation element binding-protein
CTRL	Control
Cy2/Cy3	Cyanine 2, Cyanine 3
DHPG	Dihydroxyphenylglycine
DIV	Days *in vitro*
DNA	Deoxyribonucleic acid
E.coli	*Escherichia coli*
E-LTD	Early long-term depression
E-LTP	Early long-term potentiation
eGFP	Enhanced green fluorescent protein
MYR-eGFP	GFP fused to the myristoylation site of LCK protein tyrosine kinase
ERK	Extracellular signal-regulated kinase
F-actin	Filamentous actin
FISH	Fluorescence *in vitro* hybridization
FMRP	Fragile X mental retardation protein 1
FRAP	Fluorescence recovery after Photobleaching
FXS	Fragile X Syndrome
G-actin	Globular actin
GFP	Green fluorescent protein
Gp1 mGluR	Group 1 metabotropic glutamate receptor

HBSS	Hanks balanced salt solution
HRP	Horse reddish peroxidase
IP3	Inositol triphosphate 3
KH domain	hnRNP-K-homology domain
KO	Knockout
L-LTD	Late long-term depression
L-LTP	Late long-term potentiation
LIMK	LIM kinase
LTD	Long-term depression
LTP	Long-term potentiation
mGluR	Metabotropic glutamate receptor
mRNA	Messenger ribonucleic acid
N-WASP	Wiskott-Aldrich Syndrome protein
NB^-/NB^+	$Neurobasal^-$, $Neurobasal^+$ medium
NMDAR	N-methyl-D-aspartate receptor
P0, P14, P120	Postnatal day 0, 14, 120
p38 MAPK	p38 mitogen-activated protein kinase
PAK	Serin/threonine-protein kinase
PCR	Polymerase chain reaction
PFA	Paraformaldehyde
Pfn	Profilin
Pfn1	Profilin 1
Pfn2a	Profilin 2a
Pfn3	Profilin 3
Pfn4	Profilin 4
PIP_2	Phosphatidylinositol-4,5-biphosphate
PLC	Phospholipase C
PSD	Postsynaptic density
PTP	Protein tyrosine phosphatase
PVDF	Polyvinylidene fluoride membrane
RBP	RNA-binding protein
RGG Box	Arginine glycine glycine box
ROCK	Rho-associated protein kinase
SDS-PAGE	Sodium dodecyl sulfate polyacrylamide gel electrophoresis
SEP	Super-ecliptic pHluorin
SEP-GluR1	SEP fused to the N terminus of glutamate receptor 1
shRNA	Short hairpin RNA

SIM	Structured illumination microscopy
SSH1	Slingshot phosphatase
STED	Stimulated emission depletion microscopy
UPS	Ubiquitin proteasome system
UTR	Untranslated region
WAVE	WASP-family verprolin-homologous protein
WT	Wildtype